A SEARCH FOR GAMMA-RAY EMISSION AT ENERGIES GREATER THAN 10^{14}eV FROM CYGNUS X-3 AND EIGHT OTHER CANDIDATE SOURCES

by

David Clarke Prosser B.Sc.

Submitted in accordance with the requirements
for the degree of Doctor of Philosophy

The candidate confirms that the work submitted is his own and that appropriate credit has been given where reference has been made to the works of others

The University of Leeds
Department of Physics

December 1991

ABSTRACT

The discovery of cosmic rays with energies greater than 10^{14}eV has posed a question that has not, as yet, been answered: where are particles accelerated to such high energies? A possible answer to this question came in 1983 with the claim made by Samorski and Stamm of an excess number of cosmic rays from the direction of Cygnus X-3. This result was then confirmed by Lloyd-Evans et al. (1983). The excess was taken to be gamma-rays as the galactic magnetic fields result in charged particles being greatly deflected. These claims led to the birth of PeV gamma-ray astronomy and the building of numerous instruments designed to search for point sources of PeV gamma-ray emission. One such instrument was the GREX extensive air shower array built at Haverah Park which began collecting data in March 1986.

This thesis describes the GREX array and the methods of analysis used to reconstruct the size and arrival direction of the incident cosmic rays from the detected air showers. The methods used to search for potential point sources are then described. These methods have been applied to data recorded by the GREX array between 6 March 1986 and 18 December 1990. Particular attention has been paid to Cygnus X-3 and 8 other candidate sources. No evidence for steady, periodic or sporadic emission has been found for any of the 9 potential sources. In addition, an all-sky survey has failed to discover any unknown point sources of emission in the Northern sky. Observations made by other groups of Cygnus X-3 and the 8 other candidate sources at 10^{12} and 10^{15}eV are discussed.

Cassiday et al. (1989) claimed to have observed an excess of cosmic rays from Cygnus X-3 with energies greater than $5x10^{17}$eV. A claimed confirmation of this result was made by the Akeno group (Teshima et al. 1990). A search for emission of $5x10^{17}$eV cosmic rays from Cygnus X-3 has been made using data from the Haverah Park 12km^2 array and is described in this thesis. The upper limit to the flux from Cygnus X-3 in this search is significantly lower than the claimed flux, even during periods of contemporaneous observations.

PERSONAL CONTRIBUTION OF THE AUTHOR

The operation of both the Haverah Park 12km^2 and GREX arrays and the subsequent data analysis have been made possible following the efforts of a large collaboration. The results presented in this thesis have come from the work of numerous people over many years. Here the specific contributions made by the author are outlined.

On first joining the group I worked on searching the 12km^2 data base for evidence of neutral emission from Cygnus X-3 at energies above 5x10^{17}eV. I investigated the pointing accuracy and angular resolution of the 12km^2 array by studying events which had triggered both it and GREX during the period of simultaneous operation of the two instruments. I then made a search of the 12km^2 data set for evidence of emission from Cygnus X-3. A description of this work can be found in Chapter 5.

I then concentrated on analysis of GREX data. I determined the dependence of the angular resolution of the GREX array on core location, showing that the use of a common core in sub-array comparisons led to an overestimate of the angular capabilities of the array (see Chapter 2). I also studied the possibility of using the timing capabilities of individual detectors for diagnostic purposes. I became responsible for the routine analysis of the data recorded by the GREX array. This involved ensuring the general validity of the data, fault finding and investigating specific events such as the June/July 1989 radio flare of Cygnus X-3. I assisted the development of the azimuthal and equal exposure source search methods.

After it was discovered that the co-ordinates of detector 12 used in the analysis were incorrect I completely redetermined the shower front curvature parameterisation (see Chapter 2) and the angular resolution of the array (see Chapter 3). The group moved from performing data analysis on an AMDAHL mainframe to SUN workstations and I investigated potential computer and compiler dependent aspects of the analysis code. I then reanalysed almost 5 years of GREX data with the new curvature

parameterisation and searched for point sources of emission (see Chapter 4 for Cygnus X-3 and Chapter 6 for other sources). Finally I parameterised the effective area of the GREX array (see Chapter 2) to obtain upper limits to the flux from the candidate sources.

CONTENTS

List of Figures and Tables

Chapter 2

Chapter 3

Chapter 4

Chapter 5

Chapter 6

CHAPTER 1

INTRODUCTION

1·1 Discovery of Cosmic Rays

The birth of cosmic ray studies is generally taken to be the balloon flights made by Viktor Hess in 1912. It had been known from the turn of the century that the amount of ionizing radiation observed at sea-level was greater than could be explained by the natural radioactivity of surrounding material and it was believed that there existed some unknown, ground-based, gamma-ray source. Hess, in his balloon ascents, attempted to measure the expected decrease in ionization with increasing altitude. However, despite an initial drop, the ionization was seen to increase greatly. Hess concluded that the radiation was extra-terrestrial and further flights at night and during solar eclipses convinced him that the Sun was not the source.

It was believed that the radiation, christened 'cosmic rays' by Millikan, consisted of extremely penetrating gamma-rays. This idea was challenged when, in 1927, Clay began to collect evidence for a variation in the cosmic ray intensity with terrestrial latitude. The Earth's magnetic field acts as a filter of charged particles and a vertical particle requires greater energy to reach the equator, where the field lines are perpendicular to the direction of travel, than is required to reach higher latitudes. The 'latitude effect' was finally confirmed by Clay (1932) and, independently, by Compton (1932) when they showed that the intensity of observed cosmic rays at sea-level decreased towards the equator where the intensity was 16% lower than at a latitude of 46° (North or South). This proved that the radiation consisted of charged particles of energies 3×10^{9}–2×10^{10}eV as the lower energy particles could not reach the equator. Further geomagnetic experiments the following year (carried out by Johnson (1933) and Alvarez and Compton (1933)) demonstrated that more particles arrived from West of the zenith than from the East which showed that the particles were positively charged.

In 1938 the cosmic ray spectrum was greatly extended with the discovery of Extensive Air Showers (EAS). Auger was studying small showers seen when a cosmic ray particle passed through a sheet of material and produced secondaries that could simultaneously trigger detectors placed 1m apart horizontally. Great care was taken to ensure that the number of accidental coincidences unrelated to showers was kept to a minimum but the number of showers recorded appeared to be too high. Auger et al. (1939) separated the detectors by up to 300m and still the number of coincident events was much greater than would have been expected from accidental triggers. This led to the idea of extensive air showers where a primary particle hits the atmosphere and produces a large number of secondary particles. The great surprise was the high energies the primaries must possess. Auger measured densities in his detectors of 10 particles m^{-2} and, assuming that the whole space between detector separated by 300m is filled at this density, a shower would contain 10^6 particles. These particles were thought to be mainly electrons and positrons. Auger had no way of measuring the particle energies and so he assigned an energy to each of 10^8eV. This is roughly the energy in air below which electron energy loss is dominated by ionization and so may be thought of as a lower limit. The resulting energy of the initial, primary particle would therefore be at least 10^{14}eV.

The principle of using widely spaced detectors to record showers and therefore high energy primaries is still used today and the work in this thesis is based on the ability to detect EAS. In fact, owing to the low flux of high energy cosmic rays ($\sim 10^{-4}$ $m^{-2}s^{-1}sr^{-1}$ with energy greater than 10^{14}eV) it is impractical to attempt to detect the primaries directly with satellite or balloon borne experiments as is done at lower energies and so the detection of EAS is the only method of studying high energy primaries. The secondary and tertiary particles produced in an air shower travel in a disc perpendicular to the direction the primary would have taken if it had not interacted and so by noting the time differences between the triggering of widely spaced detectors the primary direction can be determined.

The discovery of EAS raised a question that has as yet remained unanswered: where in the Universe can the primary particles acquire such large energies? The vast majority of low energy cosmic rays were shown to be positively charged, protons or heavier nuclei, and it was assumed that this was also the situation at energies of 10^{15}eV or greater. Rather than being observed emanating from a number of point sources PeV($\equiv 10^{15}$eV) cosmic rays are seen to be incident at the Earth with a high degree of isotropy (there are no anisotropies greater than ~0·1%). This can be explained by considering the highly irregular magnetic fields of, on average, ~3μG that are known to pervade the galaxy. Any charged particle that travels through the galaxy will experience this magnetic field and so be deflected. A proton in a magnetic field of 3μG will have a gyroradius, given in parsecs (pc), of

$$\text{Gyroradius (pc)} = \frac{\text{E (eV)}}{3\text{x}10^{15}}$$

Thus a 10^{15}eV proton will have a gyroradius of ~0·3pc which is smaller than the distance to the nearest stars. The sources of cosmic rays will presumably be many parsecs distant and so by the time the particles reach the Earth their irregular paths through the galaxy will have robbed them of any directional information. At higher energies the gyroradii become comparable with the thickness of the galaxy (300pc at ~10^{18}eV) and the distance of the Earth from the galactic centre (10kpc at ~$3\text{x}10^{19}$eV). It is unlikely that the galactic magnetic field could trap particles with energies greater than ~10^{19}eV as the Larmor radii become greater than the size of the galaxy. In the 1950's it was felt that the highest energy cosmic rays could point back to their source and so many large arrays were built, including a 12km^2 array at Haverah Park near Leeds, to detect them. Whereas these arrays have been successful in determining the primary energy spectrum up to 10^{20}eV there has been rather less success in determining the sources of cosmic rays. The main problem has been a lack of events due to the extremely low flux at these energies. Also nothing is known of the composition of high

energy cosmic rays. The gyroradii values given above are for protons: a heavily charged nucleus will have a much reduced gyroradius e.g. a 3×10^{19}eV iron nucleus (z=26) will have a gyroradius of ~400pc as compared to 10kpc for a proton of the same energy. Thus, if iron nuclei made up the bulk of cosmic rays with energy greater than 10^{17}eV the expected anisotropies would not be so great if the sources were galactic.

The failure of these experiments to discover significant anisotropies meant that prior to the 1980's there was no firm experimental evidence to distinguish between the many theories of 10^{15}eV cosmic ray origin. However, the last decade has seen an interest in the neutral component of the cosmic ray flux and this thesis will describe the search for neutral particles from astronomical sources in two distinct energy ranges: 10^{14}–10^{16}eV and $>10^{17}$eV.

1·2 The Search for Sources of Neutral Emission

1·2 a) Observations at PeV Energies

In 1972 a huge flare of radio emission was seen from the low mass binary system Cygnus X-3 (Gregory 1972a). A Russian group (Vladimirsky et al. 1973) reported that a week after the radio maximum an excess of 10^{12}eV cosmic rays (observed by detecting the air-Čerenkov emission produced by relativistic secondary particles) was seen in the direction of Cygnus X-3. This object is located in the galactic plane at a distance of at least 8kpc from the Sun and so, from the arguments concerning the galactic magnetic fields above, this excess could not be due to protons and must be due to neutral particles that were not deflected. Neutrons cannot survive over a distance of 8kpc at this energy without decaying so Cygnus X-3 was taken to be a source of 10^{12}eV gamma-rays. The same group reported a similar excess of events after a radio flare in 1980 (Fomin et al. 1981). The mechanism thought most likely to produce gamma-rays was curvature radiation emitted by electrons moving in the magnetic fields of the system.

Cygnus X-3 subsequently became an object of extreme interest for cosmic ray astrophysicists as here was both a possible site for the acceleration of particles to large energies and a method of observing further sites. In the 10 years following 1972 confirmation had been obtained of the original 10^{12}eV observation (Danaher et al. 1981, Lamb et al. 1982, Dowthwaite et al. 1983) and reports had been made of emission at energies of ~10^{8}eV (Lamb et al. 1977), although the latter result has been disputed by the COS-B collaboration (Hermsen et al. 1987). In 1983 Samorski and Stamm reported an excess of cosmic rays from Cygnus X-3 at energies greater than $2x10^{15}$eV (Samorski and Stamm 1983a). Their experiment, at Kiel in Germany, consisted of 28 scintillation counters of $1m^2$. 13 detectors were placed on a 3m grid with the rest at distances of up to 100m. This array, or telescope, had an angular resolution of 1°. Their observations, made between March 1976 and January 1980, showed 31 events in a bin 3° wide in declination (δ) and 4° in right ascension (α) centred on Cygnus X-3 when 14·4 events were expected. In addition, the X-ray emission of Cygnus X-3 is modulated with a period of 4·8 hours and when Samorski and Stamm looked for this period in the arrival times of events in the source bin they saw an enhancement at phase 0·2–0·3 relative to the X-ray minimum (using the van der Klis and Bonnet-Bidaud (1981) ephemeris).

This report had an obvious effect on people working with EAS arrays and many groups attempted to replicate the Kiel result. In late 1983 the Haverah Park group reported confirmation of the Kiel result (Lloyd-Evans et al. 1983). A small portion of the $12km^2$ array was used to study the (relatively) low energy showers of 10^{15} to 10^{17}eV. No highly significant overall excess was observed but a source bin larger than Kiel's had to be used, 9° in α and 6° in δ, as the Haverah Park array, not having been designed with point source searching in mind, used deep, water-Čerenkov detectors and the angular resolution was relatively poor (~3°). When the data were phase analysed using the 4·8hr X-ray modulation an excess was seen at a phase that was consistent with that reported by Kiel. PeV gamma-rays could not be explained by curvature radiation as

electrons would very rapidly lose energy though synchrotron radiation. Also, if gamma-rays are produced in a region of high magnetic field they are rapidly absorbed. Hence an alternative mechanism was proposed in which the collision of protons accelerated in the system with surrounding material produces neutral pions which can then decay into two photons (Porter 1983). A full review of observations made of Cygnus X-3 will be given in Chapter 4.

The search for point sources of PeV gamma-rays now appeared a much more promising way to discover the ultimate origins of cosmic rays than looking at the highest energy events and so a large amount of effort was put into building arrays that would have a high resolution at PeV energies. One such array was GREX (Gamma-Ray EXperiment) which was built at Haverah Park. GREX (more fully described in Chapter 2) became operational in 1986 with 32 detectors of 0·8m^2 placed on 30 and 50m grids. The majority of this thesis will describe the analysis of five years of data recorded by GREX and the searches made in the data for point sources.

1·2 b) Observations at Energies Greater Than $5x10^{17}$eV

Despite the shift in emphasis towards PeV energies work at the highest energies was not abandoned and several groups have continued to make observations. The 'Fly's Eye' group, from the University of Utah, claimed to have seen an excess of extensive air showers from the direction of Cygnus X-3 with energies above $5x10^{17}$eV (Cassiday et al. 1989). At these high energies the effect of time dilation is such that a significant number of neutrons would be able to travel from Cygnus X-3 to the Earth without decaying. Hence a flux of neutrons, as an alternative to a gamma-ray flux, was an additional possibility.

This was the first claim of a point emitter at these energies and, if true, would pose a serious question to theorists working on the production mechanism of high energy cosmic rays. Whereas models exist in which particles can, with difficulty, be accelerated in compact systems such as Cygnus X-3 to PeV energies there are no models that can

produce higher energies within such systems.

Data recorded by the Haverah Park 12km^2 array between 1974 and 1987 were analysed by the author to attempt to evaluate the Fly's Eye claim. Details of this analysis and its results can be found in Chapter 5 (see also Lawrence et al. 1989).

1·3 Development of Extensive Air Showers

1·3 a) Photon Initiated Showers

An idea of the development of an extensive air shower can be gained by considering the interaction of a 10^{15}eV photon incident on the atmosphere. The photon will undergo its first interaction after traversing a thickness of ~50gcm^{-2} of atmosphere, which corresponds to a height of ~20km above sea-level. In the field of a nucleus (most likely oxygen or nitrogen) the photon can produce an electron/positron pair. The nucleus takes very little energy from the photon but it is required to balance momentum. The major energy loss for the electrons (and positrons) is the bremsstrahlung process in which a high energy photon is emitted when the electron is accelerated in the Coulomb field of an atom. The energy loss is given by:-

$$\frac{dE}{dx} = -\frac{E}{X_0}$$

where X_0 is the radiation length and is defined as the distance over which the electron will lose $(1 - {}^1/_e)$ of its energy i.e. ~63%. In air this radiation length is 37gcm^{-2} which is approximately the same distance as the mean free path (at high energies) for electron/positron pair production (λ_{pp}) (actually $\lambda_{pp} = {}^9/_7\, X_0$).

It can now be seen how an electromagnetic cascade could build up from a combination of pair production and bremsstrahlung. Photons will produce electrons and positrons which will then radiate further photons. This continues with the total number of elements in the cascade doubling and the average energy halving with each ~25gcm^{-2}

of atmosphere traversed.

This multiplication does not continue indefinitely. When the electrons and positrons reach a critical energy (E_c), which is, in air, 84MeV, they lose more energy through ionization than they do through bremsstrahlung and so the supply of photons decreases. Also, below 20MeV, the main energy loss for photons is by Compton collisions with electrons rather than by pair production. The maximum of a cascade initiated by a 10^{15}eV photon takes place after ~16 radiation lengths which will be at a depth of ~600gcm^{-2} (i.e. a height above sea-level of ~5km) and will consist of order 10^6 particles. The cascade then decays exponentially.

Although the electromagnetic cascade is the most important element in the development of photon initiated air showers there are additional processes that take place. There are two mechanisms for producing muons: photoproduction and μ^+/μ^- pair production. Any photon with energy greater than 1GeV can interact with a nucleon to produce pions. This interaction has a very small cross section: ranging from 1·5mb at 10^{10}eV to 2·4mb at 10^{15}eV (Stanev et al. 1985). The cross section for μ^+/μ^- pair production is 2μb at 10^{15}eV which is vastly lower than the cross section for electron/positron pair production (0·5b) and obviously the number of muons produced directly by this process will be small.

Charged pions can decay ($\pi^{\pm} \rightarrow \mu^{\pm} + \nu_{\mu}$) with a rest lifetime of 2·6x10^{-8}s. However, the highly relativistic speeds with which they travel means that the pions have a much increased lifetime and if the pion energy is greater than ~5x10^{10}eV the probability of interaction is greater than the probability of decay. Charged pion-nucleon interactions occur which are similar to photon-nucleon interactions, i.e.

$$\pi^- + p \rightarrow \pi^+ + n + N\pi$$

but with a mean free path of 120gcm^{-2}. The pions continue to interact in this way until their energy is degraded to ~5x10^{10}eV when decay becomes more likely than interaction

and they form muons. Muons are two orders of magnitude more stable than charged pions and have a rest lifetime of $2{\cdot}2\times10^{-6}$s after which they decay to electrons

$$\mu^{\pm} \rightarrow e^{\pm} + \nu_{\mu} + \nu_{e}$$

The muons, like the pions, are highly relativistic and so many can reach sea-level without decaying. They also have a large interaction mean free path ($>10^{5}$gcm^{-2}) and so the decay of charged pions to muons is effectively the end of this chain of development.

Owing to the extremely high energies of the particles involved in an air shower the resultant products of any interaction (e.g. electron/positron pairs, bremsstrahlung photons) will be produced in a tight cone about the original direction of travel. However, the shower does develop a lateral structure and, for the electromagnetic cascade, this is the result of the Coulomb scattering of electrons. The root mean squared angle (θ_{rms}) through which an electron of energy E will be scattered after traversing a thickness x is given by:-

$$\theta_{rms} = \frac{E_s}{E}\sqrt{\frac{x}{X_o}}$$

where E_S is a constant of 21MeV. For an electron at the critical energy passing through one radiation length the r.m.s. angle will be 0·25 radians. This leads to a characteristic scattering length called the Molière unit (R_O) which is the lateral distance an electron at the critical energy will travel in one radiation length. At sea level R_O has the value of 79m. This value increases with increasing temperature and decreasing pressure.

That Coulomb scattering is the dominant factor in producing the spread of particles can be seen by considering the pair-production opening angle and the angle with which bremsstrahlung photons are produced. Both the latter angles are of the same order and, at the critical energy, are $\sim6\times10^{-3}$ radians compared with 0·25 radians for Coulomb scattering.

The way in which the density of the electrons and positrons in a shower vary as the distance from the shower core increases has been determined by Nishimura and Kamata (1952) with modifications made by Greisen (1956). The lateral distribution function (NKG function) relates the electron density (ρ) to the distance from shower core (r):-

$$\rho(r) = \frac{N}{R_0^2} c(s) \left[\frac{r}{R_0}\right]^{s-2} \left[\frac{r}{R_0} + 1\right]^{s-4.5}$$

where N is the number of particles in the shower and c(s) is a normalising constant weakly dependent on s. S is defined as the shower age and is a measure of the shower's development. When the shower is at maximum its age is 1. Showers with s<1 have not reached maximum development and are often called 'young' while those with s>1 are past maximum and are 'old'. When only one particle remains in the shower s=2.

The lateral distribution function is rather steep. A vertical shower initiated by a 10^{15}eV photon will have an age, at sea level, of s~1·3 i.e. past maximum and a c(s) of 0·45 (Greisen 1956). At 1m from the shower core the density will be ~800 particles m^{-2}. At one Molière unit from the core the density falls to ~5 particles m^{-2}. As the age of the shower increases the lateral distribution becomes flatter.

1·3 b) Proton Initiated Showers

Of course the majority of air showers observed are not initiated by photons but instead by protons or heavier nuclei. Amazingly these hadron initiated showers are very similar to photon showers in many respects but with a few important differences.

The mean free path of a 10^{15}eV proton in air is ~60gcm^{-2} (cf. ~50gcm^{-2} for a photon of similar energy) and the interaction that occurs between the incoming proton (p_i) and either a proton (p_t) or neutron in the target nucleus produces numerous pions plus more exotic particles such as kaons, hyperons and nucleon-antinucleon pairs:-

$$p_i + p_t = p_i + p_t + N\pi\ (+ K + \Lambda + \ldots.)$$

The primary particle will retain ~50% of its energy in the collision. The rest of the energy is shared between pions (45%) and other particles (5%).

The incident proton leaves the first interaction (possibly changed to a neutron through charge exchange) with half its original energy and can go on to interact further. The atmosphere has a thickness of ~1030gcm^{-2} at sea-level and so a 10^{15}eV proton with a mean free path in air of 60gcm^{-2} would undergo ~17 collisions before reaching sea-level. The proton-air cross section decreases with decreasing proton energy resulting in an increase in the mean free path and, as the proton is losing half its energy in each interaction, the number of collisions will be slightly reduced from 17.

In each interaction more pions are produced with the number formed (N_π) being given roughly by:-

$$N_\pi = 2{\cdot}7\ E^{0{\cdot}25}$$

where E is the total energy available for pion production (~0·5 the incident nucleon energy) measured in GeV. Therefore it is expected that the first collision of a 10^{15}eV proton would produce of order 100 pions with equal numbers of each type (π^+, π^-, π^o). The exact multiplicity of pions produced is unknown as accelerator experiments cannot achieve the large energies observed in early EAS collisions and there is no way to observe these collisions directly.

Neutral pions are extremely unstable having a rest lifetime of ~10^{-16}s and so, even at highly relativistic energies, decay is more likely than interaction. The most probable decay mode is

$$\pi^o \rightarrow \gamma + \gamma$$

which occurs 99% of the time. Each of these two photons can now initiate an electromagnetic cascade by producing an electron/positron pair as described above. At each interaction of the primary more neutral pions will be produced and so the final electromagnetic cascade will consist of many cascades produced along the shower axis. Hillas (1987a) has shown by Monte Carlo simulations that despite the differences in cascade production between photon and proton initiated showers there is very little difference in the resulting lateral distribution of electrons at sea level. The simulations show that on average it is expected that photon showers will be slightly younger than proton showers.

Vastly more charged pions will be produced in a proton initiated shower as the proton/nucleon cross section is ~200 times higher than the photon/nucleon cross section at energies greater than a few GeV. These pions, after interacting, decay into muons which have a high probability of reaching the ground. Calculations have shown that a proton shower should have at least 10 times the number of muons at sea-level that a photon shower contains.

Owing to their large mass muons undergo negligible Coulomb scatter. The lateral distribution of muons observed results from their angle of emission and the height at which they are produced. The majority of detected muons in a proton shower are produced ~6–7km above sea level. They have a transverse momentum of ~0·4GeV/c and energy 10^{10}–10^{11}eV which results in an opening angle of up to 2·5°. This corresponds in a distance from the shower axis of ~300m on the ground.

1·3 c) Higher Energies

As the energy of the primary particle increases so does the depth in the atmosphere of the maximum. The higher the initial energy the more radiation lengths will have to be traversed before the average energy of particles in the shower falls to the critical energy. For a gamma-ray initiated vertical shower of ~5×10^{19}eV the shower maximum will be close to sea-level. Also the number of particles in the shower increases.

1·4 Study of Point Sources Post-1983

The observation and confirmation in 1983 of Cygnus X-3 as a source of PeV gamma-rays promised a quick answer to the problem of cosmic ray sources. It was felt that new instruments would be able to utilise Cygnus X-3 as a 'standard candle' and then a whole range of new sources would be discovered. This early promise has not been borne out and today there is much confusion and controversy surrounding PeV gamma-ray astronomy.

The largest disappointment has been Cygnus X-3. No group has seen evidence for long term emission from this object despite the fact that instruments are now more sensitive and would easily have detected emission at the level claimed in the original detections. It almost appears that after initiating the search for point sources Cygnus X-3 switched off! There have been numerous reports from many groups of transient signals often modulated with the 4·8hr period. However, the reports (described in Chapter 4) do not come together to produce a consistent overall picture and serve to highlight one of the major problems in the field. Quite often groups will impose numerous cuts on their data to produce a signal and it is not always clear that these cuts have been accounted for when a final reckoning of the statistical significance of the claim is made. Also, there is no current consensus on what cuts should be made to enhance a signal. It was initially felt by some that as the electromagnetic cascade in a proton shower is continually fed by new photons as the primary interacts lower in the atmosphere proton showers would develop later than photon showers of the same energy. For this reason cuts were made in the shower age, s, to only look at old (photon) showers. This proved successful in some cases, including the original Kiel report ($s>1\cdot1$). However, some groups have found an age cut unnecessary, e.g. the Haverah Park confirmation of the Kiel report, and, as described above, simulations by Hillas have shown that photon showers should, if anything, be younger than equivalent proton showers.

In a similar way the question of muon content in gamma-ray initiated showers is far from clear cut. It is expected that proton initiated showers will be muon rich compared to photon showers and so selecting events with few muons should help reject background events. Samorski and Stamm (1983b) reported that the muon content of Cygnus X-3 showers was ~80% of that in normal showers which is in contradiction with theory which would suggest that the ratio of muons in photon showers to muons in proton shower should be, at most, 10%. The 'CYGNUS' array at Los Alamos reported (Dingus et al. 1988a) two bursts from Hercules X-1 during 24 July 1986 in which the muon content of signal showers was no different from the bulk of showers. In contrast to these results some groups have been successful in applying muon cuts (e.g. Kifune et al. 1986) on Cygnus X-3, but once again there is a lack of consensus.

The possibility exists of course that 'photon showers' are being initiated by some new particle or that the photoproduction cross section increases at high energies explaining why photon showers look different to what is expected. This would not explain the fact that different groups obtain results only after making different, and often contradictory, cuts. The picture is therefore far from clear.

The situation with Cygnus X-3 at 10^{18}eV is also rather confused. The original detection by the Fly's Eye group (Cassiday et al. 1989) was confirmed by the Akeno group (Teshima et al. 1990) but observations by the Haverah Park group showed no effect. Even in the confirmation by the Akeno group problems exist in that there is no agreement on the energy spectrum, 4·8hr modulation or exact part of the sky in which an excess was observed (see Chapter 5 for full details).

Despite the lack of any overwhelming success in detecting PeV gamma-ray sources more telescopes are being built around the world with improved sensitivity. This means that it will be possible to monitor sources almost continuously making the detection of transient effects more likely. Also many results so far presented are of very low statistical significance close to the sensitivity of the detectors. If new arrays with improved sensitivity fail to see any signals it will appear that groups in the past have

been misled by statistical fluctuations.

This thesis will describe searches made for PeV and 10^{18}eV point sources of neutral particles using data collected at Haverah Park with emphasis on the methods employed to try and avoid the problems inherent in looking for small signals in a large background.

CHAPTER 2

THE GREX ARRAY

2·1 Introduction

The Haverah Park confirmation of the original Kiel Cygnus X-3 detection had chiefly relied on the object's 4·8 hour periodicity as the D.C. excess observed was only at the 1·7σ level. The angular resolution attainable was limited to ~3° by the use of deep water-Čerenkov detectors with slow rise times (~60ns). At the flux reported by the Kiel group for Cygnus X-3 ($7{\cdot}4\times10^{-14}$ photons $cm^{-2}s^{-1}$ above 2×10^{15}eV) a strong D.C. signal was not expected with the angular resolution available. To continue observations of point sources at PeV energies a new array was built at Haverah Park.

To obtain a 4σ excess in less than 6 months from a source with the flux reported for Cygnus X-3 an array of 100m radius operating with 80% on-time efficiency requires an angular resolution of less than 1°. Ultimately the angular resolution obtainable is limited by the width of the shower front. Fluctuations in the times recorded by a single detector are the result of the detector timing resolution and the fact that the finite area of the detector means that the detector does not necessarily trigger on the leading edge of the shower. At ~40m from the shower core the thickness is ~6ns for particle densities of $1{\cdot}6m^{-2}$ (Lambert and Lloyd-Evans 1985). This spread in times at 40m gives an angular resolution of 1° at best. Obviously the timing resolution of the detectors must be much smaller than this to give the desired angular resolution. Therefore, the first requirement for an array designed to observe point sources of PeV gamma-rays is that it consists of detectors with 1ns or less timing resolution.

Also, as the flux of cosmic rays is low at PeV energies, it is desirable to cover as large an area as possible. However, the detectors must not be too widely spaced otherwise the threshold energy will be too large. It was these constraints (with additional economic limitations) that led to the design adopted for GREX at Haverah Park.

This chapter will describe the GREX array and outline the analysis performed on the data recorded by the array. Areas in which the author did not make a direct contribution are described in brief. However, the reanalysis of the shower front curvature performed by the author is described in detail.

2·2 The GREX Array at Haverah Park

2·2 a) GREX Detectors

The GREX array was build in 1985/1986 with 32 individual detectors (Brooke et al. 1985). An additional 4 detectors were added in May 1989 to increase the effective area of the array at low energies (Bloomer et al. 1990a). Each detector is of the same basic design (Figure 2·1) containing 0·84m^2 of 76mm thick NE 102A plastic scintillator with a decay time of ~3ns. The scintillator is viewed from beneath by a fast, 7cm diameter photomultiplier tube (PMT) operating at ~2·1kV. Originally Philips XP2312B PMTs were used, but in the new detectors, and where old tubes have had to be replaced, EMI 9821B tubes are used as Philips are unable to supply the original type of tube. Both types of PMT have rise times of ~2·5ns. At high densities signals can be produced directly by particles passing through a PMT and hence tubes are held beneath the scintillator to ensure that spurious pre-pulses are not recorded.

Within the detectors the scintillator and PMT are housed in a light tight box which is painted black internally. This stops reflected light reaching the tube and thus improves the light pulse risetime. A sheet of aluminized foil was placed on top of the scintillator to reflect upward going light back towards the PMT. This was found to produce a 60% increase in the light yield without degrading the rise time (West 1988). The PMT is held at a distance of 600mm from the scintillator which results in the light path from a corner of the scintillator to the tube being 1·47 time longer than from the centre of the scintillator. Ideally the light paths should be of the same length. However, increasing the distance of the tube from the scintillator would result in a further reduction in the amount

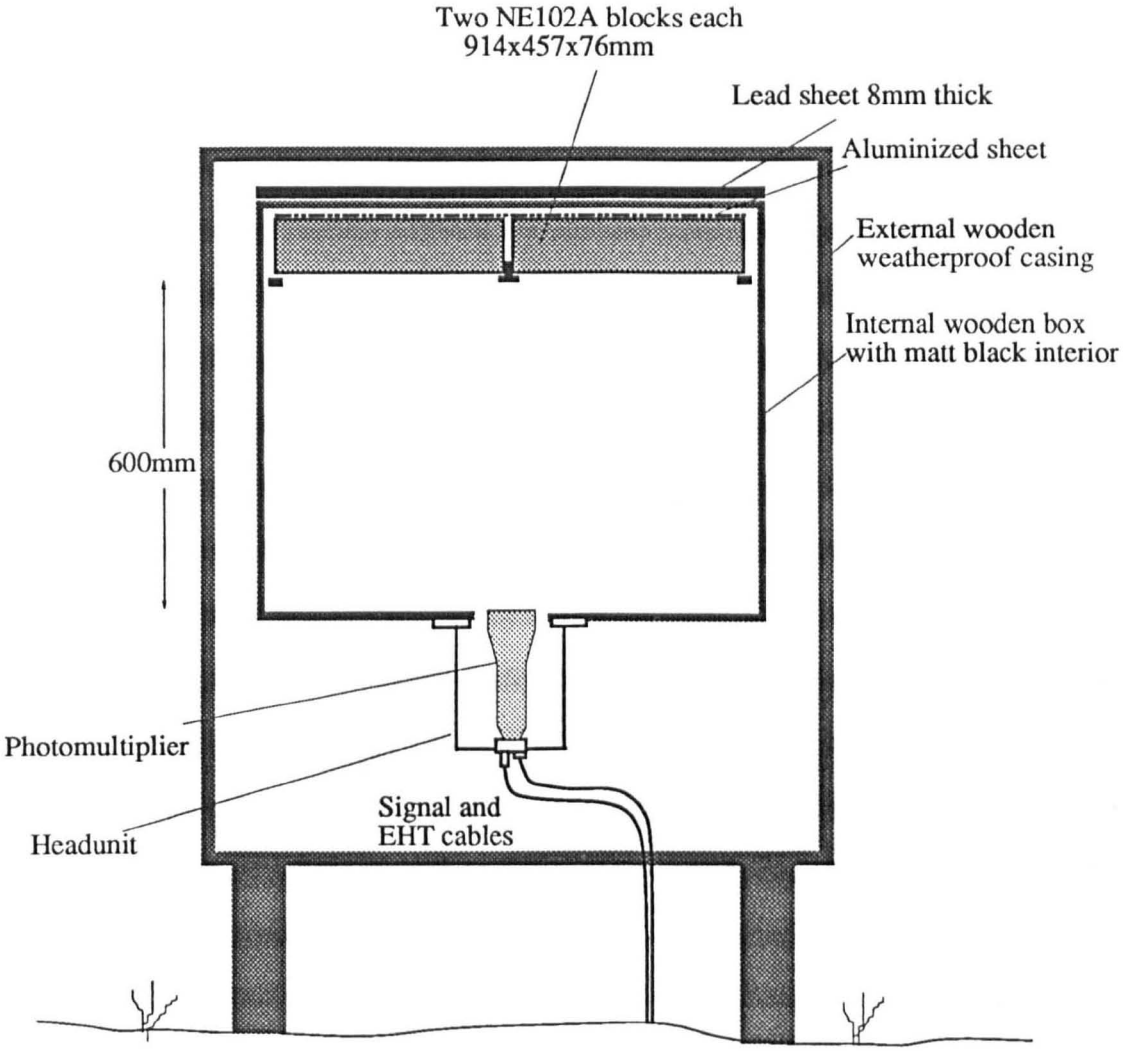

Figure 2·1 Cross-section of a standard GREX detector

of light reaching the tube and so 600mm was chosen as a compromise. At low densities the detectors had a timing resolution of 0·9±0·1ns (Lambert and Lloyd-Evans 1985).

In June 1987 an 8mm (~1·4 radiation lengths) sheet of lead was placed above the scintillator of each detector. As a consequence of the Rossi transition effect the lead causes the materialisation of prompt gamma-rays in the shower front and absorbs late, low energy particles. The timing of the detectors is therefore improved as they are more likely to sample the leading edge of the shower front. The effect of the lead on the angular resolution of the array is discussed in Chapter 3.

The detectors are distributed on 30 and 50m grids (Figure 2·2). This spacing, together with the trigger conditions described below, gives a threshold energy of ~10^{14}eV and a median energy of ~10^{15}eV. The array is 53° 58' N and 1° 38' W and is ~200m above sea-level. There are two pairs of side-by-side detectors (15, 16 and 25, 32) which can be used to investigate the timing resolution of detectors. The signal from each detector is passed to the central electronics (housed at 15 and 16) via buried high bandwidth Aerialite 363 cables.

Housed at the centre of the array (near detectors 15 and 16) is a 40m^2 muon detector operated by the University of Nottingham. The detector consists of 16 shielded liquid scintillator tanks having a threshold muon energy of ~300MeV (Barley et al. 1990).

2·2 b) Conditions for Triggering

Signals from the detectors are fed into two LeCroy voltage discriminators and, after passing though a 20ns delay cable, an ADC. One discriminator is set to ~10mV which is the voltage produced by a single vertical muon passing through the scintillator (the 'D2' level) while the second is set at one third this value (the 'D1' level). If the D1 level is reached then the TDC for that detector starts counting. If the D2 level is reached a 1μs coincidence window is opened. The window is longer than the total time taken for a shower to sweep across the array and for the signals to travel to the central electronics

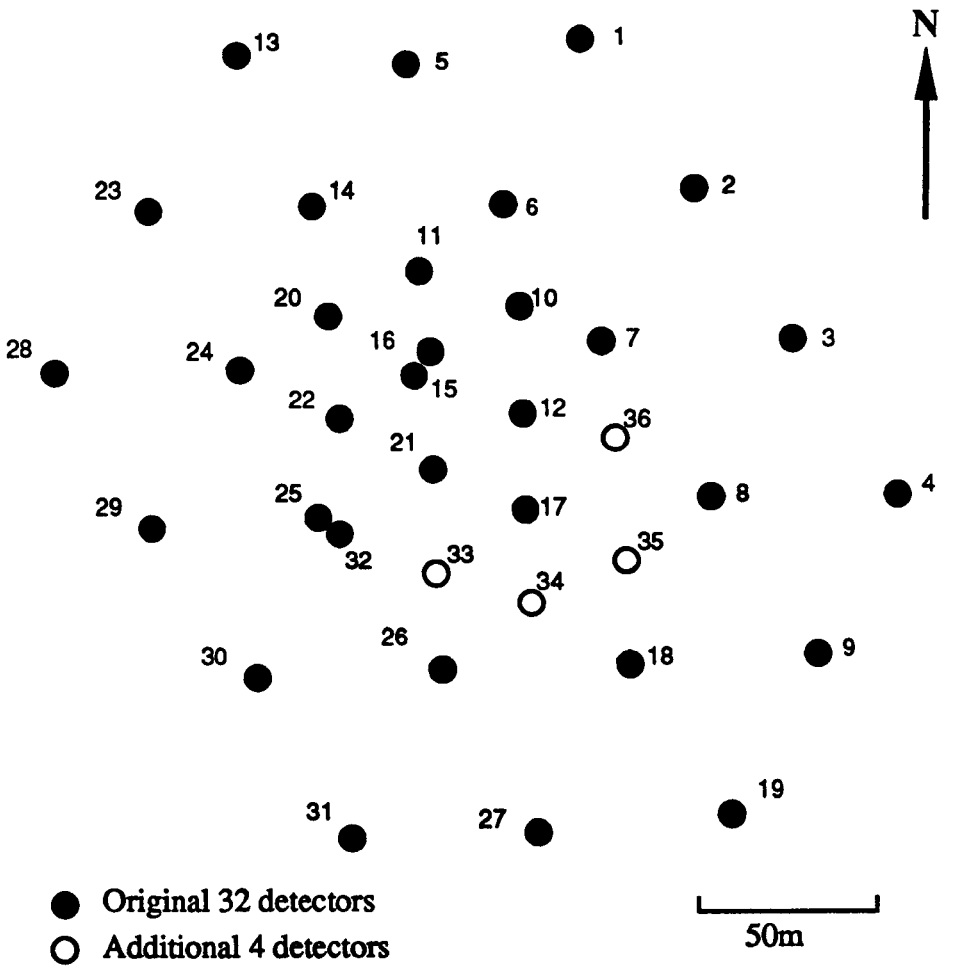

Figure 2·2 The layout of the GREX array showing the positions of the original 32 detectors and the 4 additional detecors added in May 1989

so allowing detectors at opposite ends of the array to form part of the trigger. A coincidence unit sums all the D2 logic outputs and discriminates at five times the single detector level. This is the event trigger (five or more detectors, each with one particle) and if the condition is satisfied a common pulse is produced which opens a second window of 1μs. All individual detector times are recorded relative to this common pulse with a resolution of 1ns. The five detectors that formed the trigger will therefore have negative times as they came before the trigger. The absolute time of the trigger is also recorded to 1ms accuracy from a quartz clock. The clock is synchronised every hour using a radio timing signal. For historical reasons the absolute time is recorded as the number of 30 seconds having elapsed since 16:40 BST on 21/03/63.

If no trigger is received within 1μs of a detector reaching the D1 level all the TDCs and ADCs are cleared. It takes 1μs to reset all the channels and so for each spurious D1 there is a 2μs dead time. There is an additional dead time which occurs after an event has been observed. The times and densities of each triggered detector have to be read out and recorded and, until the TDCs and ADCs are cleared, no further events will be accepted. Originally a North Star 8-bit computer was used which required up to 1·2s to read an event. This was replaced in November 1987 by a 16-bit Uman which reduced the dead time per event to 350–840ms. From March 1989 a 32-bit VME controlled GPIB fast transfer system has brought the dead time down to 2ms per event. The array currently triggers at ~0·3Hz. Each event consists of 252 bytes of data and is recorded on magnetic tape for subsequent analysis.

2·3 Analysis of Events

Once the data have been recorded at Haverah Park they are taken to Leeds for analysis. The raw ADC counts are converted into densities. As the transit times of signals through the PMTs, the Aerialite cables and the discriminators have previously been measured, a recorded time can be corrected to give the precise time that the shower

front was incident on the detector. Three main pieces of information are obtained for each event: the shower core position, shower size and the original arrival direction.

An initial, trial core position is found from the centre of gravity of the square of the densities recorded at each of the triggered detectors. A plane is fitted to the four detectors with the largest densities which gives an initial arrival direction. An improved core position can now be found. Taking the centre of gravity core an estimate of the size of the shower can be made. For any core position and shower size the lateral distribution function can be used to predict the density at each of the detectors. The goodness of fit parameter, χ^2, is calculated by comparing the observed detector densities with those predicted. The core position is moved so as to minimise χ^2 and the predicted densities recalculated for the new core position. This process is repeated iteratively until the minimum of χ^2 is found or a maximum number of steps is reached. At each iteration a new estimate of the shower size is made. The minimum of χ^2 is rather flat which, together with the computing time limit on the number of iterations possible, results in a final core position that is accurate to ~7m (Idenden 1991). A measure of the shower size is the density at 50m from the shower core, S(50). The primary energy (E) in eV of a shower at 20° to the vertical is given by:-

$$E = 6{\cdot}4 \times 10^{14} \, . \, S(50)^{0{\cdot}8}$$

where S(50) is in particles m^{-2} (Bloomer 1990). Showers incident on the array from other inclinations will have passed through different depths of atmosphere and so showers with the same S(50) but different inclinations will not have the same primary energy. Therefore, to obtain the primary energy of a shower the S(50) is normalised to 20°. This specific density/energy relationship is dependent on detector type and array geometry and so is unique to the GREX array.

To find an accurate arrival direction for each of the events the shape of the shower front must be taken into account. As a result of the lateral scattering of particles in the

shower the shower front is non-planar. For a given density the time that the shower front lags behind a plane front increases with increasing distance from the shower axis. Also, at a given distance the time lag decreases with increasing density. The curvature of the shower front as seen with GREX has been parameterised in terms of density, distance from the shower axis and size of shower (see section 2·4). For each detector density and distance from the shower core (in the shower plane) a predicted time delay is obtained and subtracted from the observed detector time. A plane is found by performing a weighted fit to the resultant reduced times. This is a two stage process. It is first assumed that all the detectors are at the same height (a reasonable first approximation) and a χ^2-like statistic in which the observed times are compared to the predicted times is analytically minimised (Bloomer 1990). The uncertainties in the times used to fit the plane are not constant and vary with density and distance from the core. The timing uncertainties have been parameterised by comparing the times recorded in side-by-side detectors and these uncertainties give the weights for each time. Once a direction has been found the second stage of the process is to perturb the predicted times by a small about to take into account the differences in height of the detectors and repeat the analytical calculation with the new times.

Once again this two stage process can be repeated iteratively. If the fit is particularly bad the most deviant detector is dropped and a new plane fitted. The entire iterative process continues until the latest direction found is within $6\text{x}10^{-5}$ radians of the previous direction, the number of iterations exceeds the maximum allowed (50) or the number of detectors used in the fit falls below 5 owing to deviant detectors being dropped.

2·4 Curvature of the Shower Front

2·4 a) Parameterisation of the Shower Front Curvature

The shower front curvature seen by the GREX array depends not only on the

intrinsic curvature due to the lateral scattering of particles in the atmosphere but also on the design and spacing of the GREX detectors. Close to the shower core the particle density is high and so a detector will trigger on the leading edge of the shower disc. As the distance from the shower core increases the particle density becomes less and the thickness of the shower front increases and so it becomes much more likely that a detector will trigger on a particle further into the shower disc. This exaggerates the curvature of the shower front. For this reason a unique parameterisation of the curvature as seen by GREX was determined. The method (more fully described in Bloomer 1990) was to fit a plane to three detectors triggered by a shower and then measure the time difference between the recorded times at the other triggered detectors and the expected, plane times. The time differences for a large number of showers were binned in density bands. For each band the time delay (Δt) was plotted against core distance (r). The logarithms of the resulting gradients ($d(\Delta t)/dr$) were plotted against the logarithms of the densities (ρ). A linear relationship was found between $\ln (d(\Delta t)/dr)$ and $\ln(\rho)$ and the gradient and intercept of the line obtained. As the addition of 8mm lead sheets to each detector affects the way in which the array responds to the shower front the above procedure was performed twice: on showers recorded before and after the addition of lead.

It was found that the curvature of the shower front could be described by the equations:-

$$\Delta t = r \exp\{-0{\cdot}25\ln(\rho) - 1{\cdot}45\} \qquad \text{(unleaded array)}$$

$$\Delta t = r \exp\{-0{\cdot}29\ln(\rho) - 1{\cdot}51\} \qquad \text{(leaded array)}$$

where the expected time delay, Δt, is expressed in ns, the distance from the shower core, r, is in metres and the density, ρ, at that distance is in particles m^{-2}.

To achieve this parameterisation showers were selected which fell within 10m of detector 16 and triggered the inner 30m ring detectors (10, 11, 12, 20, 21 and 22). A

plane was then fitted to detectors 11, 12 and 22. This method has suffered owing to an error made in surveying the array. After the array was built it was professionally surveyed to determine the co-ordinates of each detector (Garner and Davey 1985). It was discovered in September 1990 that the reported co-ordinates of detector 12 differed from its actual position by ~4·3m. The reported position of detector 12 lies on one of the nodes of the 30m grid. However, to avoid a ditch detector 12 was built close to, rather than on, the node. It appears that the survey reported the co-ordinates of where detector 12 ought to be rather than where it actually is. This error is significant considering the prominent part detector 12 played in determining the parameterisation of the shower front curvature.

The erroneous nature of the original curvature for the unleaded array can be seen in Figure 2·3. The first plot (a) shows the mean time difference between observed and predicted times as a function of core distance for ~15000 detector triggers. Ideally these time differences should be zero at all distances. However, in reality there is a discrepancy of almost 2ns at 80m. With this curvature, detectors within ~35m of the shower core have predicted times that are systematically too small whereas at greater distances the predicted times are too large. The second plot (b) shows the mean time differences for individual detectors. Once again it would be expected that the means should be scattered about zero. As stated above the recorded times are corrected to allow for the signal transit time though cables, etc. If one of these delays had been incorrectly measured for a detector it would result in a mean time difference offset from zero. However, Figure 2·3b shows a systematic shift which, together with Figure 2·3a suggests a problem with the parameterisation.

The original method of parameterisation had been limited statistically by the small sub-set of showers used. Assuming that the relationship between time lag, density and core distance is correct the values of the gradient and intercept can be changed and the effect on the distribution of mean time differences with distance can be observed. The aim is to make the deviations as close to zero as possible at all distances. In this method

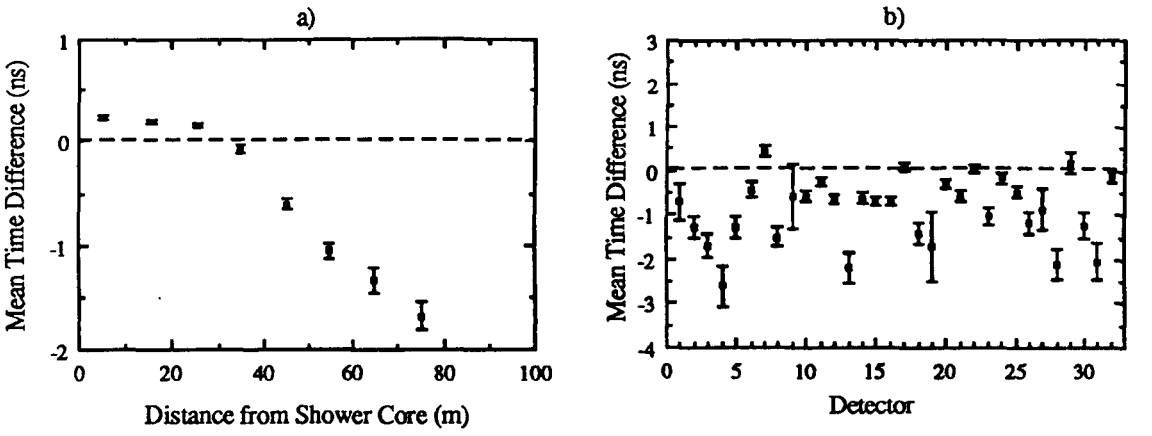

Figure 2·3 The mean time differences between observed and predicted detector times are shown in a) as a function of detector distance from the shower core and in b) for individual detectors. Showers have been analysed using the original unleaded curvature.

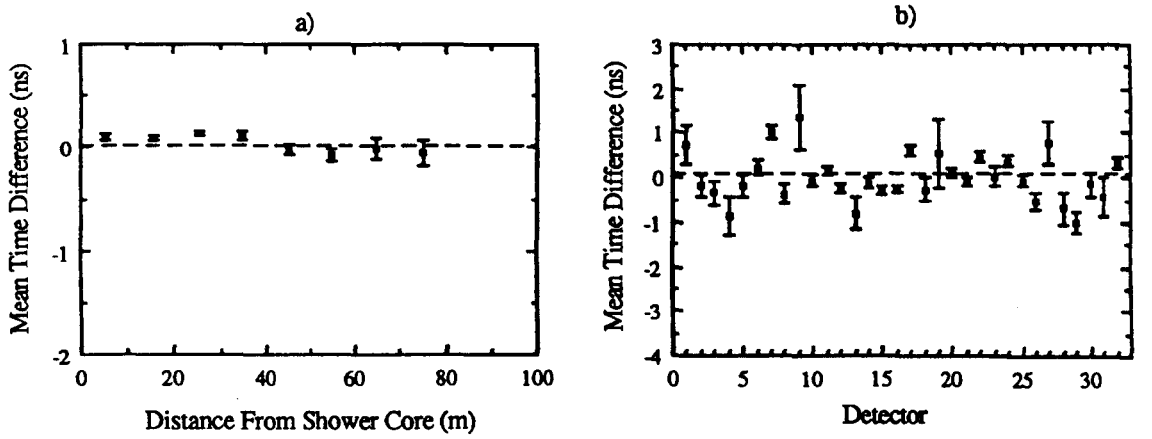

Figure 2·4 The same as in Figure 2·3 but with showers analysed using an improved shower front curvature parameterisation deduced after correcting the co-ordinates of detector 12.

no restriction need be made on which detectors are triggered or where the core fell (provided that the shower was within the array). This makes it possible to use many more detector times.

The new parameterisation is in the same form as that used previously with the exception that there is now a distinction made between showers of different sizes. Originally the curvature was assumed to be independent of S(50), the density at 50m. However, it was found that the deviations of the mean time differences from zero could be reduced (and therefore the parameterisation improved) by having two S(50) bands. Separate curvature parameterisations were found for showers with S(50) less than 2 particles m^{-2} and those with S(50) greater than 2 particles m^{-2}. Setting the boundary density at 2 particles m^{-2} splits the data into two approximately equal parts. The curvature, as seen by the unleaded array, is given by:-

$$\Delta t = r \exp\{-0{\cdot}12\ln(\rho) - 1{\cdot}53\} \qquad S(50) < 2 \text{ particles } m^{-2}$$

$$\Delta t = r \exp\{-0{\cdot}23\ln(\rho) - 1{\cdot}73\} \qquad S(50) \geq 2 \text{ particles } m^{-2}$$

The results of this can be seen in Figure 2·4. The showers used are the same as in the previous figure (giving ~15000 detector times). The distribution of mean time difference against core distance (a) is much improved, being almost flat. This was the best that could be achieved by manipulating the coefficients. Also the plot of individual detector mean differences (b) shows an improvement with the means now scattered about zero. The two S(50) bands were chosen somewhat arbitrarily and it may be fruitful to investigate the relationship between shower size and curvature more closely to achieve a parameterisation that more accurately describes showers.

Figure 2·5 shows a comparison between the original form of the parameterisation and new form described above. The NKG function (described in section 1·3a) was used to determine the expected density for a range of core distances. A shower age of 1·3 was used as this is approximately the age at sea-level of a 10^{15}eV proton initiated shower.

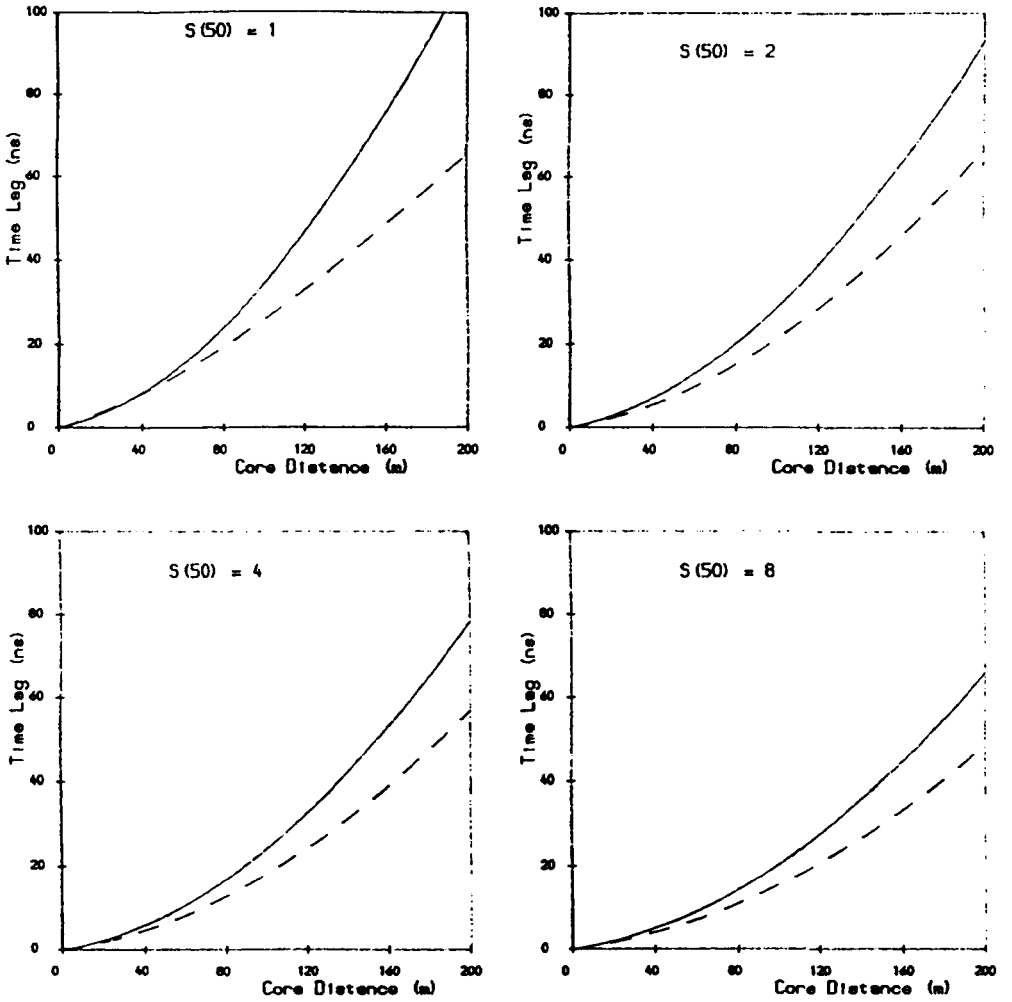

Figure 2·5 Time lag behind a plane front as a function of core distance for the original (solid line) and new (dashed line) forms of the shower front curvature parameterisation for the unleaded array. The four plots are for values of S(50) of 1, 2, 4 and 8 particles m^{-2}. Although core distances of up to 200m have been shown showers will only be able to trigger detectors over a limited range e.g. a shower of S(50) = 1 will trigger detectors out to 50m.

The four plots shown cover a range of shower sizes. In all cases the upper curve is the original parameterisation i.e. the new parameterisation consistently predicts a smaller time lag of the shower front behind a plane front. At 80m the time difference between the two parameterisations is ~4ns for an S(50) of 1 particle m^{-2}.

The effect of the new curvature was investigated by obtaining arrival directions for ~5000 events using both the old and new curvatures. Figure 2·6 shows the distribution of space angle differences between directions found for these showers using the two parameterisations. The resulting r.m.s. space angle shift between the arrival directions was 1·2°, with 34% of showers being shifted by more than 0·5° and 15% by more than 1°.

2·4 b) Use of Distant Detectors

In the original analysis of GREX events detectors had only been used to find the shower arrival direction if they were within 80m of the shower core. The time lag of the shower front behind a plane had not been determined with sufficient accuracy at distances greater than 80m. A new curvature that appeared to accurately predict the times out to 80m offered the possibility of relaxing this constraint and thus increasing detector multiplicity.

Figure 2·7 shows the mean time difference against distance distribution using the new parameterisation with no cut on the distance of a triggered detector from the shower core. With the condition that the shower core must fall within the array the furthest a detector can be from the core is ~250m. As can be seen the mean time difference is within ±0·5ns out to 120m. The mean times for distances greater than 200m have not been plotted as there are very few triggers beyond this distance.

Removing the distance cut has two advantages which result from the the increased detector multiplicity. Firstly more showers are analysed. As described above the direction finding algorithm will drop 'bad' detectors if they have highly deviant times. The algorithm will only continued if sufficient detectors (5 or more) remain; otherwise

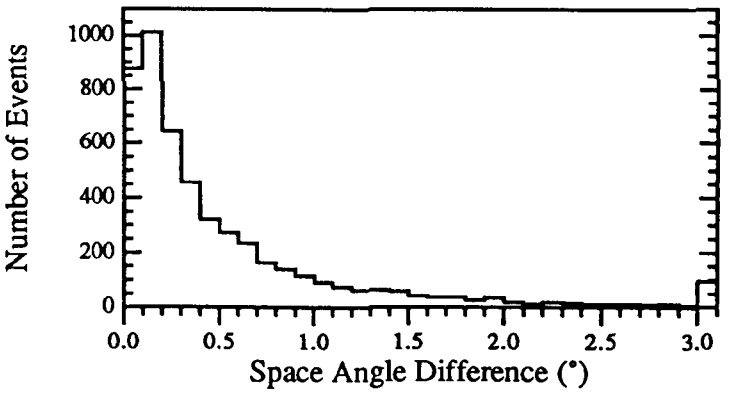

Figure 2·6 Space angle difference between arrival directions found for 5000 showers using the original unleaded curvature parameterisation and the new parameterisation. 34% of showers have directions shifted by >0·5° and 15% by >1°

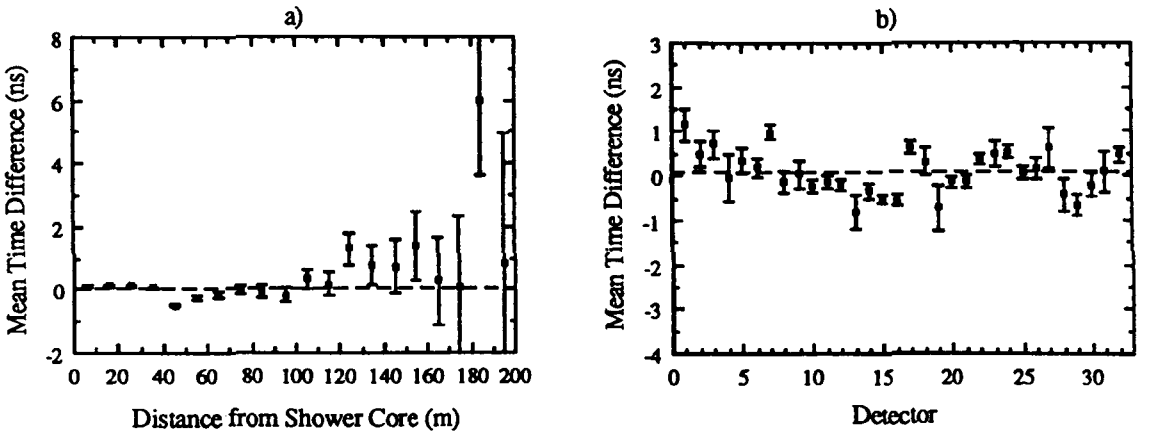

Figure 2·7 The mean time differences between observed and predicted detector times are shown in a) as a function of detector distance from the shower core and in b) for individual detectors. Showers have been analysed using the new unleaded curvature and with no cut made on detectors greater than 80m from the shower core.

the shower is discarded. Obviously it is less likely for a shower to be discarded due to the dropping of a detector if there are more detectors to begin with. Performing an analysis with no cut made on detector distance results in an ~20% increase in the number of showers analysed. The second advantage is that using more detector times should result in improved arrival directions.

This advantage can be illustrated by considering a single shower. Figure 2·8 shows an event recorded on 24/10/86. In part a) a detector was used if it had a density>1·25 and was within 80m of the shower core. A direction was found by using the 8 detectors passing this selection criteria (two of which were side by side). As the fit was not considered to be good enough the worst detector was dropped, in this case detector 12, and a new direction found. This process was repeated with detectors 22 and 21 being dropped until a final direction was found with zenith angle (θ) = 21° and azimuth angle (ϕ) = 43°. Part b) of Figure 2·8 shows the same event but with the distance cut removed. In this case 10 detectors were selected. The only detector to be dropped was 31 and a direction of θ=20°, ϕ=114° was found. The space angle difference between the arrival directions the two analyses produced for the same shower was 48°! An analysis by eye suggests that it is the time of detector 31 which is spurious and that by restricting detectors to be within 80m a grossly incorrect direction was derived. This is an extreme example: less than 1% of showers have directions shifted by more than 5°. However, it illustrates how using more detectors will make it more likely that 'rogue' times are caught.

2·4 c) The Curvature for the Leaded Array

As stated above the addition of 8mm sheets of lead to each detector increased the probability of detectors triggering on the leading edge of the shower front. Therefore, a separate parameterisation of the curvature is required for the leaded array. The same procedure performed on showers recorded by the unleaded array was followed for events recorded by the leaded array. Figure 2·9 shows the effects of using the original

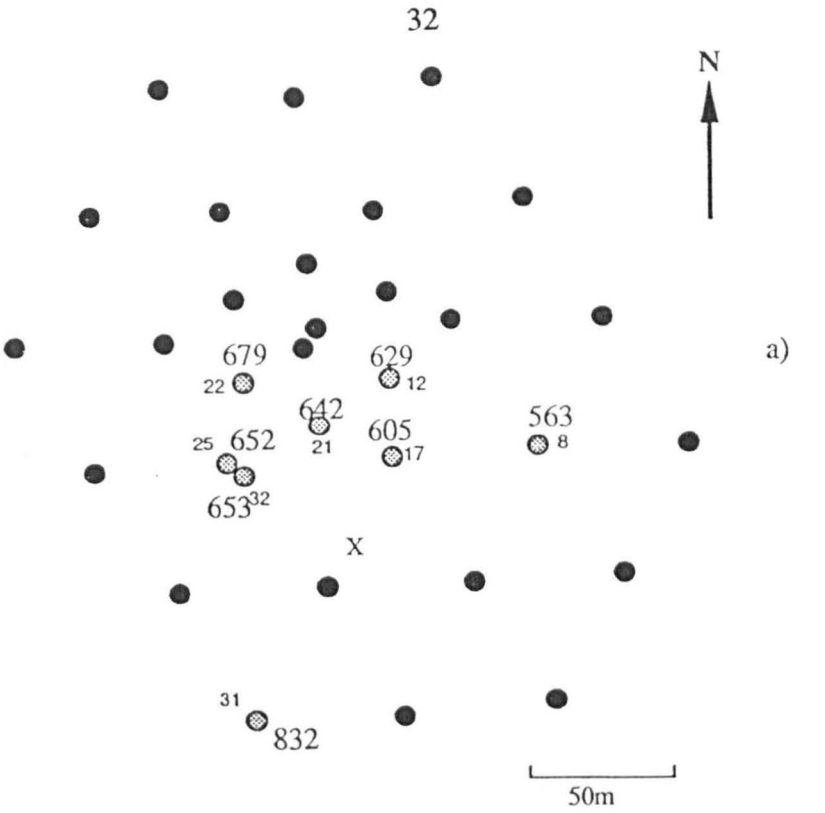

⊗ Detectors used in fit with trigger times in ns

X Core Position

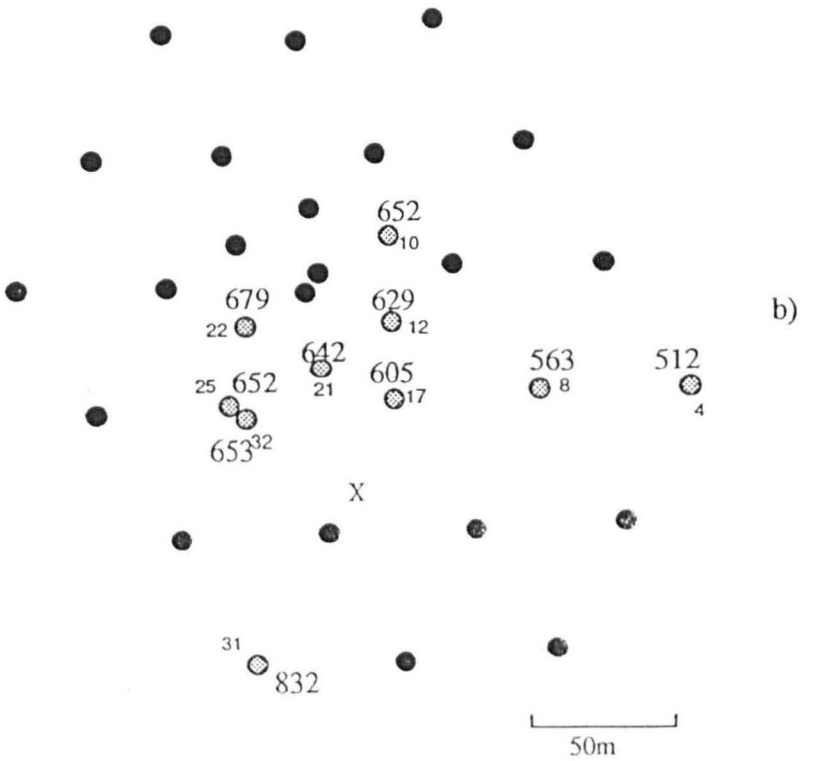

Figure 2·8 Analysis of an event recorded on 24/10/86. Part a) shows the triggered detectors that were within 80m of the shower core (in the shower plane). Part b) shows all the triggered detectors.

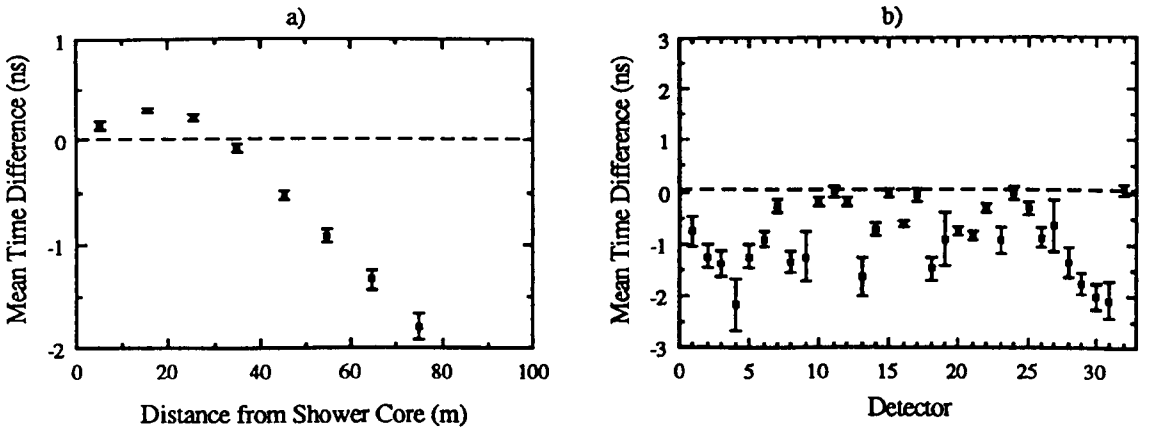

Figure 2·9 The mean time differences between observed and predicted detector times are shown in a) as a function of detector distance from the shower core and in b) for individual detectors. Showers have been analysed using the original leaded curvature

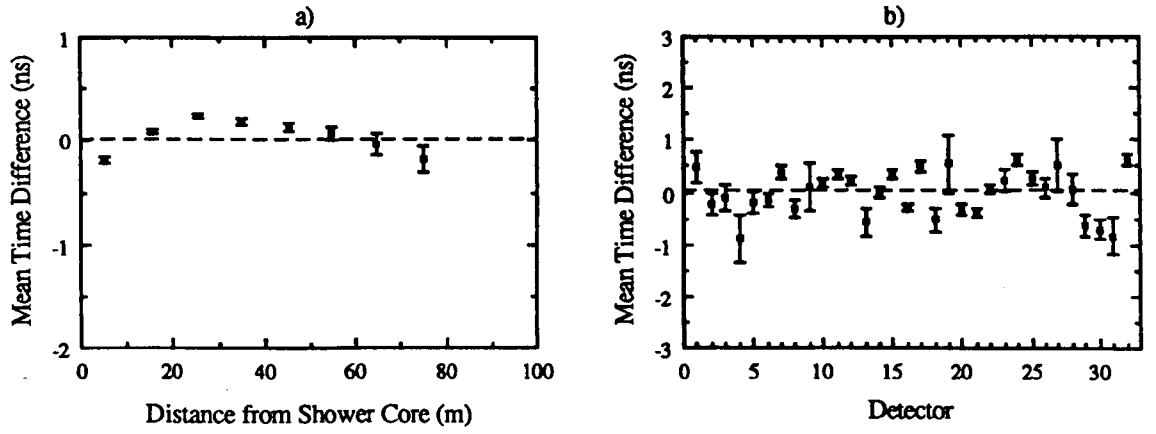

Figure 2·10 The same as in Figure 2·9 but with showers analysed using an improved shower front curvature parameterisation deduced after correcting the co-ordinates of detector 12.

parameterisation of

$$\Delta t = r \exp\{-0{\cdot}29\ln(\rho) - 1{\cdot}51\}$$

with which showers had been analysed. The same problems are seen in the plot of mean time difference against core distance (a) that were evident for the unleaded array. With increasing core distance the old parameterisation increasingly fails to predict accurately the shower front arrival times at detectors. At 80m there is a 2ns difference between the observed and predicted times. Also, for the individual detectors there is a marked tendency for the predicted times to be larger than those observed (b). A few detectors, e.g. 7, 10, 11, do have mean time differences around zero. These detectors are mainly in the centre of the array and are more likely to be near the shower core, where the curvature was reasonably well described, than detectors towards the array perimeter.

In the same way as for the unleaded array it was found that the curvature seen by the leaded array could be more accurately described by using two shower size bands. The resultant parameterisation can be described by the following equations:-

$$\Delta t = r \exp\{-0{\cdot}22\ln(\rho) - 1{\cdot}85\} \qquad S(50) < 2 \text{ particles m}^{-2}$$

$$\Delta t = r \exp\{-0{\cdot}21\ln(\rho) - 1{\cdot}77\} \qquad S(50) \geq 2 \text{ particles m}^{-2}$$

Figure 2·10 shows the same showers as in Figure 2·9 but analysed with the new curvature description. The results are not ideal as the time differences are not all zero. Again a further investigation of the effect of shower size on shower front curvature could prove profitable. However, this was the best that could be achieved by manipulating the coefficients of the parameterisation and is an improvement on the original with the mean time difference never getting beyond ±0·25ns at distances less than 80m (a). In addition, the individual detector means are now scattered about zero (b).

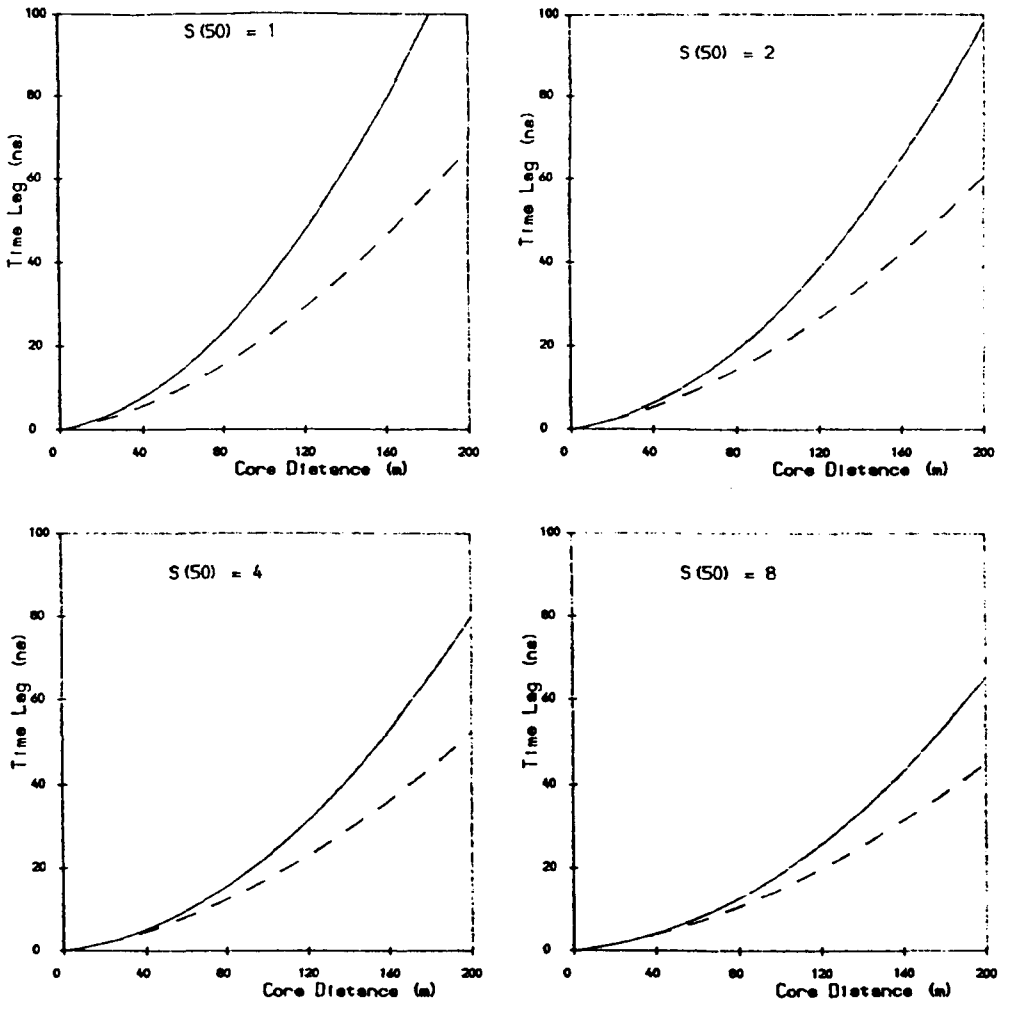

Figure 2·11 Time lag behind a plane front as a function of core distance for the original (solid line) and new (dashed line) forms of the shower front curvature parameterisation for the leaded array. The four plot are for values of S(50) of 1, 2, 4 and 8 particles m^{-2}

The differences between the old and new parameterisations for the leaded array are shown in Figure 2·11. As before, the NKG function has been used with a shower age of 1·3 to determine the particle density as a function of distance from the shower core. Again the new parameterisation consistently describes a flatter shower front, although for larger showers there is very little difference below 40m.

The distribution of space angle differences between arrival directions calculated for 5000 events using both the original and new parameterisations is shown in Figure 2·12. The spread in the distribution is noticeably less than for the unleaded array (Figure 2·6) with an r.m.s. space angle difference of 0·5°. In this case 23% of comparison showers are shifted by more than 0·5° and only 2% by more than 1°.

Once again the fact that the curvature can be accurately described below 80m makes an investigation of the curvature beyond 80m worth while and opens up the possibility of using more distant detectors. An analysis of showers using all triggered detectors is shown in Figure 2·13. The curve is within ±0·5ns to at least 120m. Beyond 120m there is a greater scatter of means but the small number of detectors triggered at these distances results in poor statistics, as can be seen by the large errors.

2·5 Timing Stability of the GREX Array

The mean difference between the times observed by a detector and the times predicted by the parameterisation of the shower front curvature can provide a large amount of information. As has been seen the limitations of the original shower front curvature parameterisation were highlighted by the mean time differences. However, the time differences also provide an indication of the stability of the array. Correcting the time recorded at the central electronics to give the time at which the shower hit a detector requires knowledge of the transit time of the PMT, recording electronics and connecting cable. If any of these times change then the change will be seen (if it has not been accounted for) in a shift of the mean time difference. Figure 2·14 shows the mean time

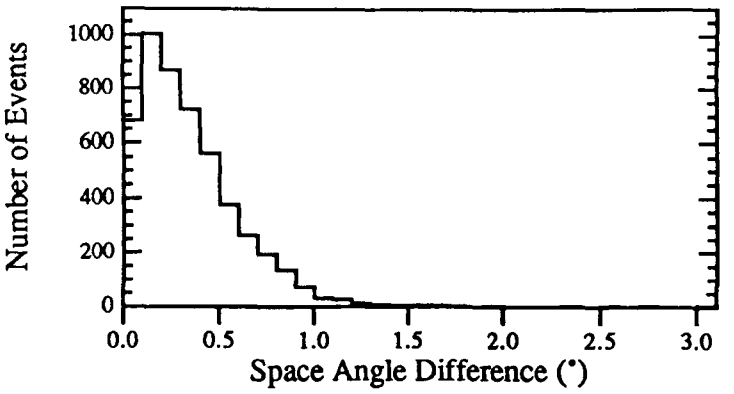

Figure 2·12 Space angle difference between arrival directions found for 5000 showers using the original leaded curvature parameterisation and the new parameterisation. 23% of showers have directions shifted by >0·5° and 2% by >1°

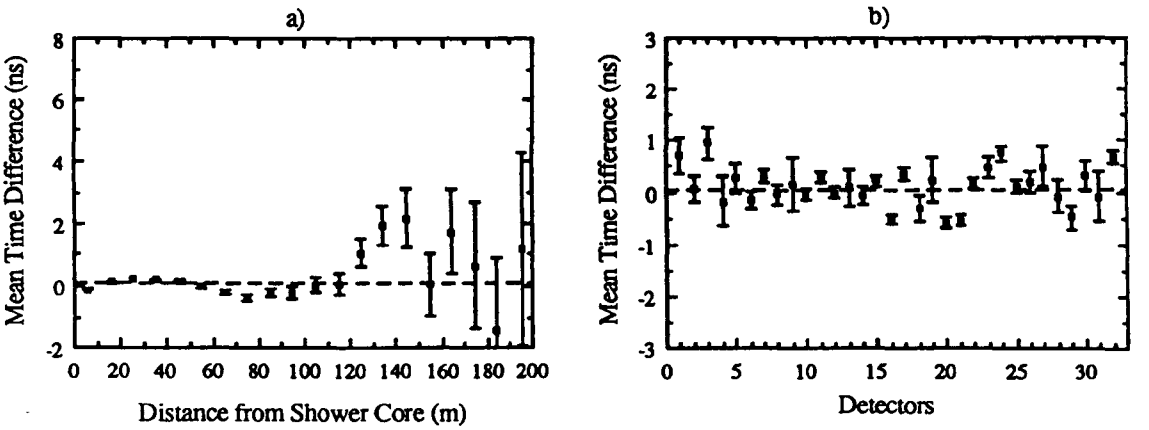

Figure 2·13 The mean time differences between observed and predicted detector times are shown in a) as a function of detector distance from the shower core and in b) for individual detectors. Showers have been analysed using the new leaded curvature and with no cut made on detectors greater than 80m from the shower core.

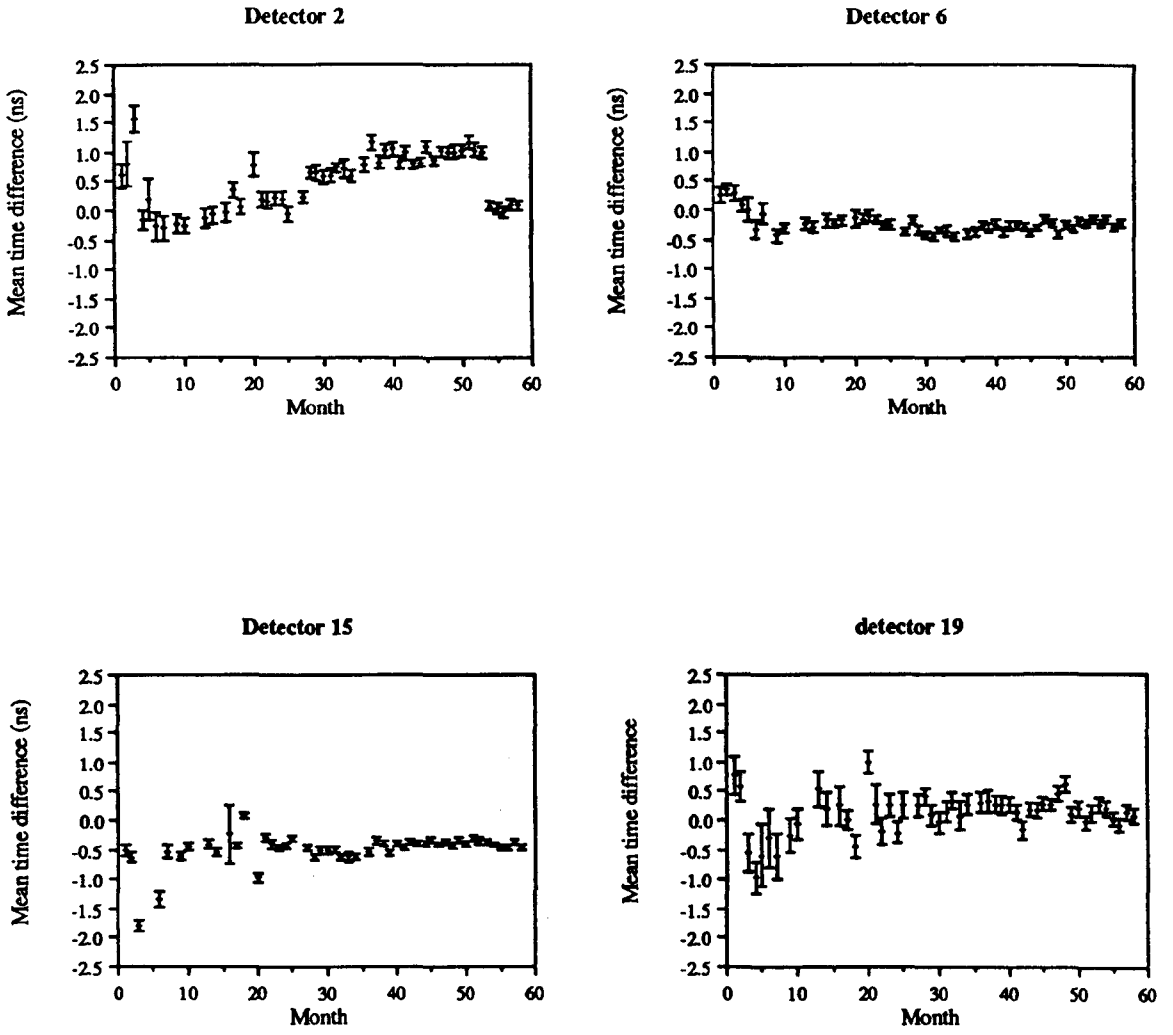

Figure 2·14 The mean time difference between observed and predicted detector times for 4 detectors as a function of time from March 1986 to December 1990

difference between observed and predicted times for four typical detectors as a function of time from the start of the data set. The best, detector 6, shows an overall stability of ±0·2ns over three years. Not all detectors are this stable. Detector 2 suffers a long term drift of over 1ns with a sudden jump at July 1990. This jump was the result of the transit time of the PMT being remeasured and found to be different from the value used by 1·5ns. Detector 19, on the edge of the array, is the furthest detector from the centre and so is not triggered as often as the others shown here.

The overall stability of the GREX array compares well with other instruments for which this information is known. The HEGRA array at La Palma suffers detector delay shifts of between 1 and 3ns per day (Karle 1991). The cables connecting detectors to the recording apparatus are not buried and are therefore exposed to the Sun and hence diurnal temperature variations. The detectors of the JANZOS experiment in New Zealand experienced a slow timing drift of between 2 and 4ns in the first two years of operation (Spencer 1990). The SPASE array at the South Pole is of a similar design to GREX. For the period February 1990 to March 1991 detectors in SPASE were stable to ±0·1ns at worst (Johnson 1991). This is better than GREX (and especially impressive considering the hostile working environment). However, a direct comparison cannot be made as detectors are used at GREX at much greater distances from the shower core than are used at SPASE.

Knowing that the array is very stable and that detector delays can be measured to approximately ±0·1ns using extensive air showers opens up the possibility of correcting the arrival times to remove the small systematic errors that appear to exist. It would be possible to correct the detector times by the amount that the mean times deviate from zero. This has not been tried on GREX data but could prove interesting and should be attempted.

2·6 Effective Area of the GREX Array

If the core of a shower falls beyond the boundary of the GREX array the accuracy with which the core position can be determined is much lower than if the core falls within the array. For this reason only showers that fall within the array are used in attempts to search for point sources. This places a geometric constraint on the area of the GREX array. However, the array is not equally sensitive over this area. Consider a small vertical shower. If the shower hits the array in a region of high detector density (e.g. near detector 15, see Figure 2·2) the shower may trigger 5 or more detectors. If, however, it falls in a region of low detector density (e.g. between detectors 26 and 27) the same shower will probably not be able to trigger 5 detectors. Therefore, the effective area for small showers is less than the geometric area. Also, showers that do not come from the zenith will see a reduced, projected area. To determine the flux of gamma-rays from a source the effective area must be known.

A simple way to determine the effective area of an extensive air shower array is to throw simulated showers at the array and observe whether or not the array is triggered. This has been done using a Monte Carlo simulation program developed by D. Idenden. For a given zenith angle and shower size 10000 showers (N) were thrown inside the array boundary and the number (N_T) that triggered the array noted. The effective area (A_{eff}) is then given by:-

$$A_{eff} = \frac{N_T}{N} A_{proj}$$

where A_{proj} is the full geometric area projected to the zenith angle of the incoming showers. A_{proj} is given (in m^2) by:-

$$A_{proj} = 36113 \cos\theta.$$

This process was repeated for a range of zenith angles and shower sizes. Also, it was performed for all 4 array eras (i.e. switch on, ADC attenuation*, addition of lead to the detectors and the addition of 4 detectors). Figure 2·15 shows the effective area as a function of shower size and zenith angle for two array eras: era 3 (a) and era 4 (b). It was found that there was no significant difference between the results obtained for the first three eras.

As can be seen, for each zenith angle the effective area is zero for very small showers. As the shower size increases the effective area rises until an energy is reached such that all showers of that energy (or above) will trigger the array. An interesting effect is observed in the transition between zero and total projected area. For small showers (i.e. ln(S(50)) between -1·0 and 0·0) the effective area at high zenith angles is larger than that at low zenith angles despite the fact that the projected area is smaller at high zenith angles. As the zenith angle increases, the projected separation between detectors decreases and it therefore becomes easier to trigger the array. Also, it should be noted that the effective area for small showers is larger in era 4 than in the previous eras. This is due to the 4 detectors that were added to the array in May 1989.

The effective area of the GREX array may be parameterised by:-

$$A_{eff} = \frac{1}{2\pi} (x - \sin x) \, . \, A_{proj}$$

where x (in radians) is given by:-

$$x = \frac{\ln(S(50)) - L(\theta)}{U(\theta) - L(\theta)} \, . \, 2\pi$$

L is the value of ln(S(50)) at which the effective area begins to rise from zero. If ln(S(50)) is less than L then x=0. U is the point at which the effective area reached the maximum projected area. If ln(S(50)) is greater than U then x=2π. Both L and U are functions of S(50) and are given by:-

*when the detector saturation density was increased form 20 particles m^{-2} to 45 particles m^{-2}.

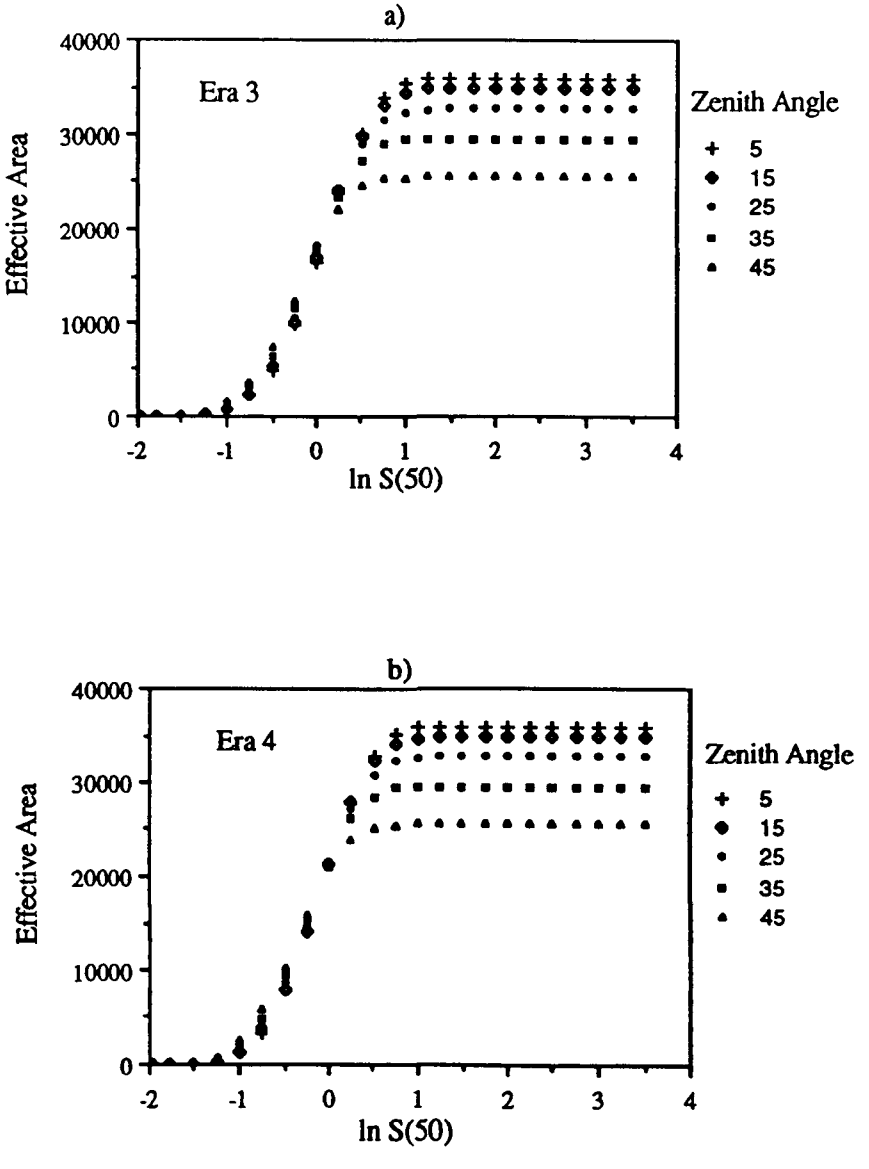

Figure 2-15 The effective area (m^{-2}) of the GREX array as a function of simulated shower size and zenith angle. The two graphs shown are for a) era 3 (32 leaded detectors) and b) era 4 (36 leaded detectors). There are no significant differences between the first 3 eras.

Era	L	U
1-3	-1·99 + 0·85 cosθ	0·22 + 1·04 cosθ
4	-2·42 + 1·11 cosθ	0·19 + 0·93 cosθ

This parameterisation gives values of the effective area (in m^2) which agree with the values from simulation to better than 1% for $S(50) > 0{\cdot}7m^{-2}$ ($\ln(S(50)) > -0{\cdot}35$).

A method of testing the parameterisation is to calculate the integral flux of cosmic rays as measured by the GREX array. The integral flux (I) above a certain energy (E) is given by:-

$$I(>E) = \left(\frac{N_E}{\sum_i A_i\Omega_i}\right)\left(\frac{N_E\,\beta}{t}\right)$$

where N_E = Number of events

β = dead time factor

t = on-time

$\Sigma A_i\Omega_i$ = sum of (effective area x solid angle) per event.

For events restricted to within 40° of the zenith $\Omega_i = 1{\cdot}47\pi$. There is a certain dead time associated with each detector triggering, as described in section 2·2b. However, this is insignificant when compared to the dead time following an array trigger when the times and densities from all the detectors are read and recorded. It is this dead time that must be taken account of. The dead time factor, β, is given by:-

$$\beta = \frac{1}{1 - g\tau}$$

where g is the observed trigger rate and τ the dead time. Table 2·1 gives the observed rate and dead time factor as a function of array epoch.

Figure 2·16 shows the integral primary cosmic ray background spectrum with

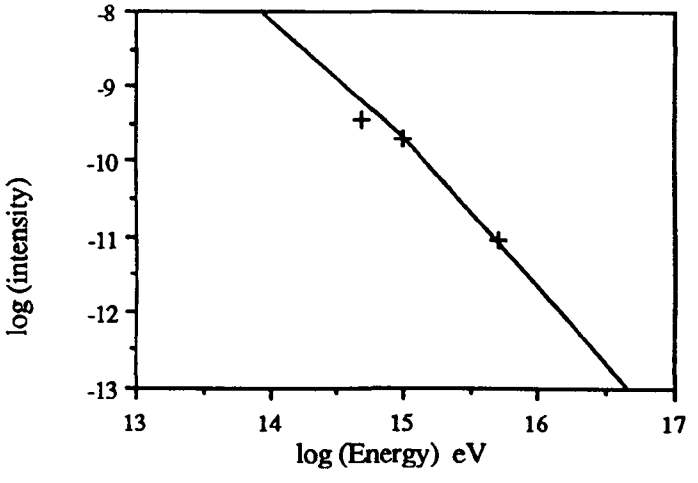

Figure 2·16 The integral primary spectrum (in cm^{-2} s^{-1} sr^{-1}) of cosmic rays is shown with three values (denoted by crosses) of the flux derived from measurements made by the GREX array.

three values of the integral flux calculated from measurements made with the GREX array. As can be seen the calculated points are in good agreement with the accepted spectrum and so give confidence in the effective area parameterisation.

Date	Computer system	Dead time	Observed rate (min^{-1})	β
06/03/86-28/06/87	North Star	1·2s	10	1·25
28/06/87-23/11/87	North Star	1·2s (lead)	12	1·32
23/11/87-15/03/89	Uman	~350ms	15	1·10
15/03/89-18/12/90	Fast Transfer	~2ms	18	1·00

Table 2·1 The recording electronics, array dead time, observed event rate and dead time factor (β) as a function of epoch for the GREX array.

2·7 Conclusions

The original method of parameterising the shower front curvature of events recorded by the GREX array relied heavily on detector 12. The subsequent discovery that this detector had been inaccurately surveyed led to a reassessment of the parameterisation. This reassessment showed that the curvature could be improved. However, of order 40 million showers had already been analysed using the old curvature and reanalysis would only be worth while if the new curvature made a significant difference.

For the unleaded array the r.m.s. angle shift between directions found using the old curvature and directions found for the same showers using the new curvature was 1·2°. For the leaded array the shift was 0·5°. As the angular resolution of the array is ~1° the importance of the change in curvature is rather marginal, especially for events recorded by the leaded array. However, there are additional considerations. Firstly the new curvature parameterisations mean that there is no need to exclude from the analysis

detectors that are more than 80m from the showers core. This results both in ~20% more showers being analysed and the possibility of more times being used in individual showers giving more accurate arrival directions. Secondly, in the original analysis a cut was made so that events that fell without the array were not analysed. However, the test for whether events were within the array boundary was incorrectly implemented with the result that some events that fell within the array were not analysed and some that fell without were analysed. 10% of all showers fell inside the array but were flagged as having fallen outside and so not analysed,while 2·5% fell outside but were flagged as falling inside and analysed. Correcting this mistake would result in a net 7·5% increase in the number of showers analysed. Finally the recent availability of more powerful computers meant that a reanalysis would take less than two weeks to perform.

The possibility of increasing the data set and improving the arrival directions has led to the entire GREX data set being reanalysed by the author with the new curvature descriptions and using all triggered detectors.

CHAPTER 3

ANGULAR RESOLUTION AND SOURCE SEARCHING

3·1 Introduction

To search for point sources of PeV gamma-rays two characteristics of the instrument used must be determined: the angular resolution and the absolute pointing accuracy. The angular resolution determines the size of solid angle into which a point signal will be spread by the array. This region should be centred on the source position. However, systematic errors in the reconstruction of arrival directions could lead to the signal being shifted and hence missed in a source search. Knowing the absolute pointing accuracy of the array is therefore essential.

At optical energies there are numerous objects of known position and magnitude that can be used to verify the angular resolution, pointing accuracy and calibration of an optical instrument. X-ray and low energy gamma-ray detectors can be tested on the ground using man-made beams of X-rays and gamma-rays to determine the angular resolution. Then, after deployment, observations of an astronomical object of known intensity which acts as a 'standard candle' can be made, providing information on the angular resolution, pointing and sensitivity of the instrument.

These conventional methods cannot be used to check an extensive air shower array. There exists no man-made source of PeV gamma-rays and, as of yet, no steady source has been found which could act as a standard candle. Therefore, indirect methods must be used to determine both the angular resolution and pointing accuracy of an array. This chapter will describe the methods adopted to determine the capabilities of the GREX array. Also some of the methods used by other groups will be described.

Once the angular resolution of an array is known attempts can be made to search for point sources of emission. The final section of this chapter will outline the methods used to search the GREX data set.

3·2 Angular Resolution and Absolute Pointing of the GREX Array

3·2 a) Sub-Array Comparisons

One of the most common methods of assessing the angular resolution of an extensive air shower array makes use of showers that trigger a large number of detectors. The triggered detectors are split into two subsets and a primary arrival direction found for the shower using each subset. This method had been used for the GREX array (Bloomer et al. 1990b). Detectors 7, 14, 16, 25 and detectors 6, 15, 17, 24 form two equivalent, concentric, 50m sub-arrays (see Figure 3·1). Showers were selected that fell within 50m of the central detectors and within 40° of the zenith and triggered all eight of the sub-array detectors. Two arrival directions were obtained for each shower, one from each of the four detector sub-arrays, and these directions compared.

In a similar way detectors 10, 15, 20, 21 and detectors 11, 12, 16, 22 make-up two 30m sub-arrays. The same comparison of showers (restricted in this case to within 30m of the central detectors) was performed. For the 30m and 50m grids the difference in sub-array directions was parameterised in terms of S(50) (i.e. shower size). In addition, it was found that there existed a zenith angle dependence for 30m showers.

This procedure was performed using data from each of three of the eras of the lifetime of the array, i.e. the original configuration of 32 detectors (post-18/2/86), after the attenuation of detector signals to the ADCs (15/9/86) and after the addition of an 8mm lead sheet to each detector (29/6/87). Attenuating the signal to the ADCs increased the detector particle saturation density from $20m^{-2}$ to $45m^{-2}$. This increased the accuracy with which the core position could be found and so it was expected that the angular resolution would improve. The addition of a sheet of lead to each detector was also expected to improve the angular resolution (see Chapter 2). The sub-array comparisons showed that the angular resolution of the GREX array did improve following the above modifications.

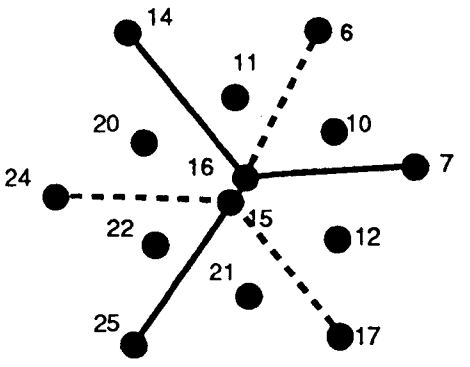

Figure 3·1 The central portion of the GREX array showing the detectors which make-up two, equivalent, four detector sub-arrays. The outer detectors are 50m from the central detectors, 15 and 16.

Chapter 2 described the reevaluation of the shower front curvature following the discovery that detector 12 had been incorrectly surveyed. It was expected that the new parameterisation of the curvature would result in an improved angular resolution. Also, detector 12 is part of one of the 30m sub-arrays. With only four detectors in each sub-array, mistaking the position of one of the detectors by ~4m has a large effect on the ability to reconstruct a shower arrival direction. Therefore, the author has reassessed the angular resolution of the GREX array using his new parameterisation of the shower front curvature, with the correct co-ordinates of detector 12.

The reassessment was performed using the same procedure as had been originally carried out. Showers were selected from each era which fell within the boundary of the ring of sub-array detectors, had zenith angles less than 40° and triggered all the sub-array detectors. Table 3·1 shows a comparison between the original analysis and the current analysis. The mean space angle difference between the arrival directions obtained by the sub-arrays is given as a function of array epoch and sub-array base line. The original values are taken from Bloomer et al. (1990b).

	50m		30m	
	old	new	old	new
Original array	1·55°±0·02°	1·47°±0·03°	2·10±0·02°	1·67±0·02°
Post-ADC change	1·46°±0·01°	1·26°±0·02°	1·96±0·02°	1·49±0·02°
Leaded array	1·16°±0·02°	1·04°±0·02°	1·73±0·02°	1·11±0·01°

Table 3·1 The mean space angle difference between directions obtained using two, four detector sub-arrays is shown as a function of array epoch and sub-array base line. 'Old' refers to the work of Bloomer et al. (1990b) and 'new' to the current work.

As can be seen there is an improvement in all cases. The improvement is particularly marked for the 30m sub-arrays where the mean space angle difference drops by ~30%. The major reason for this improvement is, of course, the correct positioning

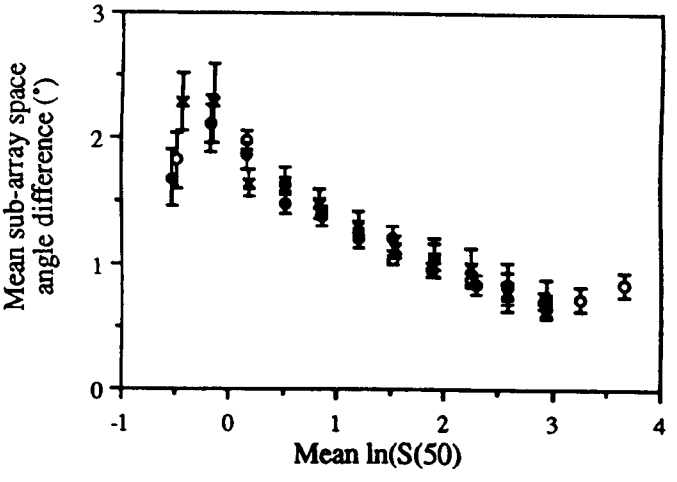

Figure 3·2 The mean space angle difference between arrival directions derived using the 30m sub-arrays as a function of ln(S(50)). Three zenith angle bands are shown: 0-22° (open circles), 22-30° (solid circles) and 30-36° (crosses). The data were recorded in the second array era (particle saturation density = $45m^{-2}$, no lead shielding).

of detector 12.

One curiosity of the original analysis had been the dependence of angular resolution on zenith angle for the 30m grid but not for the 50m grid. Figure 3·2 shows the mean space angle difference for the 30m sub-arrays as a function of mean ln(S(50)) for showers recorded during the second era (i.e. detector saturation density 45 particles m^{-2} and without lead shielding on the detectors). The data have been split into three zenith angle bands and there is no evidence for a significant zenith angle dependence. This was also found to be the case for the other array eras. It would appear that the dependence found originally was an artifact arising from the incorrect co-ordinates given for detector 12.

The improvement in angular resolution with increasing S(50) seen in Figure 3·2 is expected. As the size of the shower increases the mean particle density at the triggered detectors will also increase. Sampling the shower in an area of high density makes it more likely that the trigging particle will be at the leading edge of the shower front. This means that the derived arrival direction is more likely to coincide with the actual arrival direction. Figure 3·3 shows the mean space angle difference against ln(S(50)) for all array eras. The relation between the space angle difference and ln(S(50)) is linear over almost the entire range of S(50). The angular resolution appears to flatten for very large showers ($S(50)>20m^{-2}$). These showers will have a large number of saturated detectors and so the core position may not be known very accurately. This will result in an angular resolution that is worse than would be expected by extrapolating from smaller showers.

The error in the position of detector 12 resulted in there being a significant difference between the angular resolution obtained by the 30m and 50m grids. This led to a complicated system of classifying events according to which detectors had been triggered. Approximately 40% of all analysed showers failed to fit into any of the classifications and so were not used in source searching. It can be seen from Figure 3·3 that following the current analysis of the angular resolution the difference in the

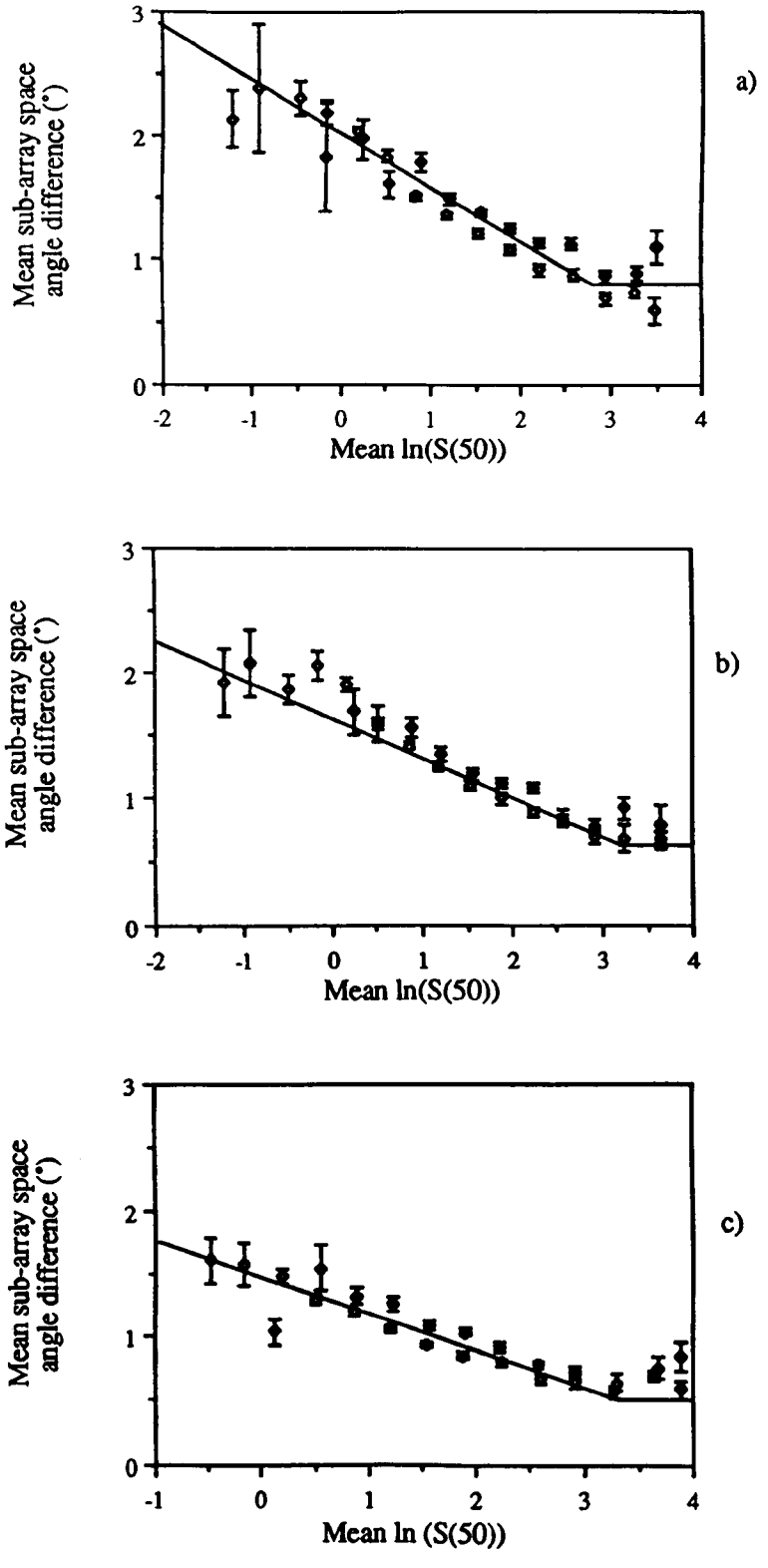

Figure 3-3 The mean space angle difference between arrival directions as a function of ln(S(50)) for both 30m (open squares) and 50m (solid squares) sub-arrays. Results for showers recorded with a) the original GREX configuration, b) after the increase in particle saturation density and c) after the addition of lead shielding are shown. Also shown are the parameterisations used to obtain the angular resolution.

dependence on S(50) between the 30m and 50m sub-arrays is small. This may appear to contradict Table 3·1 where the 50m sub-array comparisons produce significantly smaller mean space angle differences. However, the 30m sub-arrays, having detectors that are on average closer to the shower core, will see smaller showers that the 50m sub-arrays. As explained above the angular resolution decreases for smaller showers and it is these showers that produce the effect seen in Table 3·1.

As no evidence has been found for either a zenith angle dependence or a large difference between 30m and 50m sub-arrays the mean space angle has been parameterised only in terms of ln(S(50)) for each of the array eras. The space angle difference is given by:-

		minimum
Original array	$\psi = -0{\cdot}43 \ln(S(50)) + 2{\cdot}00$	$0{\cdot}71^\circ$ $(S(50)>20{\cdot}1)$
Post ADC-change	$\psi = -0{\cdot}31 \ln(S(50)) + 1{\cdot}65$	$0{\cdot}65^\circ$ $(S(50)>25{\cdot}2)$
Leaded array	$\psi = -0{\cdot}29 \ln(S(50)) + 1{\cdot}48$	$0{\cdot}50^\circ$ $(S(50)>29{\cdot}4)$

If the space angle difference obtained is smaller than the minimum value then it is set to the minimum. This allows for the flattening seen for larger showers. The parameterisation can be seen in Figure 3·3.

3·2 b) Effect of Shower Core Position on Angular Resolution

The above method of determining the angular resolution of the GREX array does not take into account the uncertainty in the core position. The core position is found using the densities in all the triggered detectors and this core is used by both sub-arrays. The condition that all the sub-array detectors must be triggered results in a core position for each shower that has been found using at least 8 detectors. Each sub-array has only 4 detectors and so the angular resolution found above may be an over estimate. Obviously an empirical determination of the effect of using the high multiplicity core is desirable.

For 595 showers that triggered the 50m sub-array the core position was reanalysed twice, once for each sub-array. The method used for finding the core was the same as for the routine analysis (i.e. χ^2 minimisation of the difference between the particle densities recorded at detectors and the densities predicted by the lateral distribution function: see section 2·3). However, the detectors used were restricted to only the four in each sub-array.

Figure 3·4 shows the distribution of distance between the 50m sub-array cores. The mean core shift is (18·5±0·5)m. As both sub-arrays are identical it is assumed that the uncertainty in each sub-array core position can be added in quadrature. This gives a core position uncertainty for each four detector sub-array of ~13m. Idenden (1991) gives the error in the core position to be ~7m. This is an average value and will include events with high detector multiplicity which have smaller core position uncertainties. Therefore, Figure 3·4 is not inconsistent with Idenden's result. Extreme core differences may be the result of the core finding routine falling into a local minimum of χ^2 and being unable to find the true minimum.

An arrival direction was then found for each shower using each sub-array with the core found by that sub-array. Figure 3·5 shows the space angle difference distribution for the 50m sub-arrays using both a common core analysis and an independent core analysis for the same data set. Using independent cores causes an appreciable shift in the distribution. For the unleaded array the mean space angle difference increase from 1·42°±0·05° to 1·62°±0·04°. After lead was added to the detectors the space angle difference increased from 1·19°±0·02° to 1·42°±0·03°. It should be noted that the set of showers used in this analysis was different to that used to obtain the values in Table 3·1. Also, the effect of using independent cores was investigated before the new parameterisation of the shower front curvature was determined. This analysis has not been repeated on reanalysed showers but it is assumed that the increase, a factor of ~1·2, will be the same.

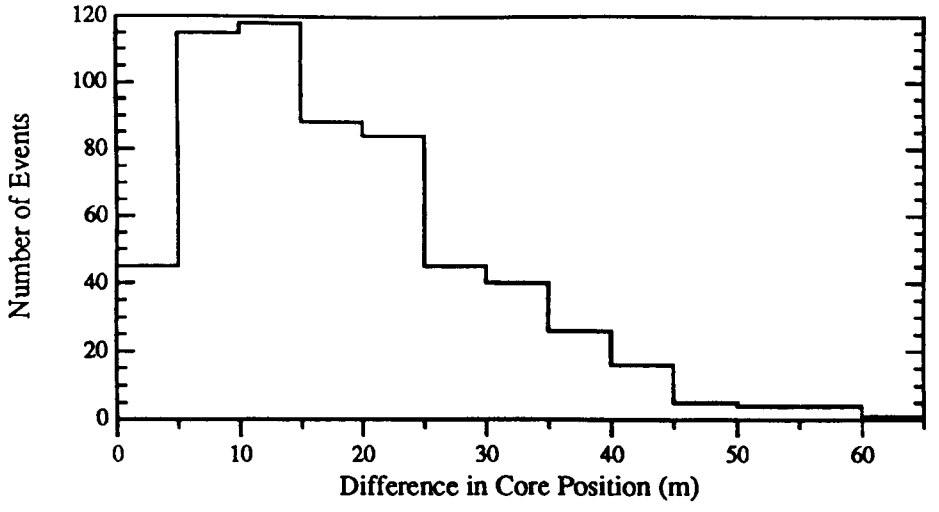

Figure 3·4 The distribution of differences in core position using two, four detector, 50m sub-arrays.

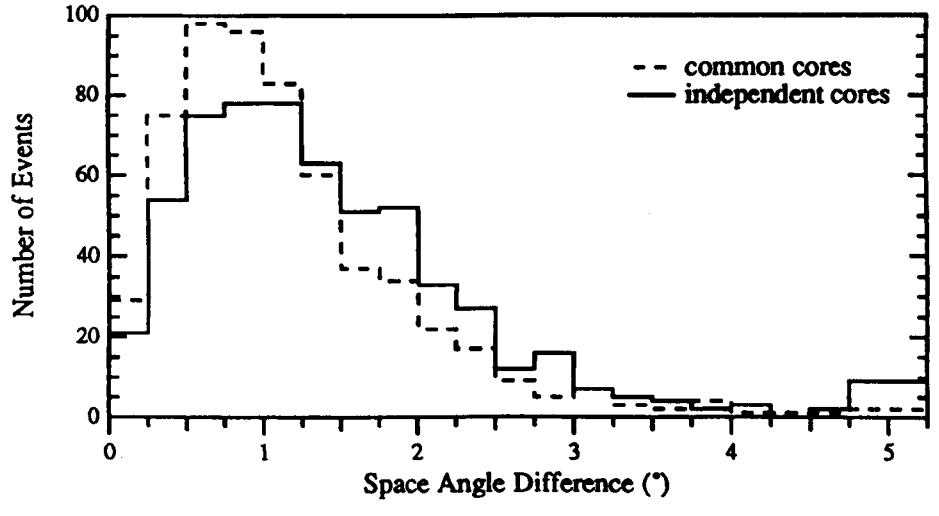

Figure 3·5 The space angle difference between arrival directions obtained from two 50m sub-arrays. The difference between using a core common to the sub-arrays (dashed line) and an independent core for each sub-array (solid line) is shown.

3·2 c) Optimum Bin Size for Source Searching

The parameterisation described in 3·2a gives the mean space angle difference in arrival directions obtained by two sub-arrays as a function of shower size. To obtain the optimum bin size for source searching what is required is the one dimensional uncertainty in the arrival direction (i.e. the uncertainty in zenith angle or declination). Assuming the angular resolution function is Gaussian, the one dimensional width for a set of four detectors (σ) is related to the mean space angle difference (ψ) by:-

$$\psi = \sigma \times 1{\cdot}77.$$

All analysed showers have at least five detectors used in the reconstruction of the primary arrival direction and the mean detector multiplicity is ~8. Hence, the above parameterisations are underestimates and to account for this the values of the width are divided by a factor of $\sqrt{2}$. In addition, the width must be multiplied by the factor 1·2 obtained by using independent core positions in the sub-array comparisons.

For point source searching a source bin is required that will maximize the source signal to background noise ratio. For a circular bin the signal to noise ratio is optimised when the bin ratio is $1{\cdot}6\sigma$. A bin of this size will contain ~70% of the signal. Therefore, the sizes of the circular bins used for source searching are given by:-

$$\text{bin size} = (\psi \times 1.2 \times 1.6) / (1{\cdot}77 \times \sqrt{2}).$$

To take advantage of the change in angular resolution with increasing energy the data are split into three energy bands. The size of the search bin for each energy band is given by the above equation with the value of ψ appropriate for the lower energy limit in the band. The values of S(50) used to determine the bin sizes are 0·5, 2 and 8m^{-2}. Table 3·2 shows the angular resolution and radii of resultant circular sources for the GREX array as a function of array era and energy.

Era	Lower S(50) limit (m^{-2})	Mean space angle difference (ψ°)	Radius of circular bin (r°)
Original array	0·5	1·03	1·65
	2·0	0·82	1·31
	8·0	0·53	0·85
Post-ADC change	0·5	0·84	1·35
	2·0	0·69	1·10
	8·0	0·48	0·77
Leaded array	0·5	0·76	1·21
	2·0	0·61	0·98
	8·0	0·42	0·67

Table 3·2 The angular resolution and resulting radius of the circular on-source search bins for the GREX array as a function of shower size and array era.

3·2 d) Absolute Pointing Accuracy of the Array

The pointing accuracy of the GREX array has been studied by comparing the arrival directions obtained by GREX with those obtained from other, independent, instruments operated simultaneously. Chapter 5 describes the $12km^2$ air shower array that was in operation at Haverah Park until 1987. Comparisons between the $12km^2$ array and GREX show no systematic differences in the arrival directions of showers that triggered both arrays (see Chapter 5 for more details).

In addition, a tracking detector has been built at the centre of the GREX array. PLASTEX consists of two 6-plane stacks of limited streamer tubes (Chan et al. 1990). Muons can be tracked though the stacks and the arrival directions determined. A shower arrival direction is then obtained from the muon directions. Preliminary work has shown that absolute arrival difference between PLASTEX and GREX is less than 0·2° (Catalano and Linsley 1991). However, this result was obtained using the old curvature parameterisation for GREX and the incorrect position of detector 12.

3·3 Additional Methods Employed by Other Groups

Although sub-array comparisons are still the most widely used method of determining the angular resolution of an extensive air shower array some groups have used additional methods to confirm the sub-array comparison results.

In 1957 Clark suggested that it would be possible to observe the shadows of the Sun and Moon. The small angular size of both objects, ~0·26° in radius, and the poor angular resolution of air shower arrays means that a large number of events have to be recorded to produce a significant result. The latest generation of large arrays has made this possible.

The CYGNUS group have observed a deficit of 1800 showers within 2° of the Sun and Moon on a background of ~93000 events (an ~6σ deficit)(Alexandreas et al. 1991a). From the decrease in deficit with distance from the Sun and Moon centres this group have derived an angular resolution of 0·75°. The HEGRA group reported (Karle 1991) a 3·3σ deficit within two bins of radius 0·65° centred on the Sun and Moon (1680 events on, 1820 off). These results give the groups concerned confidence in their estimates of the angular resolution and the absolute pointing. This method has the advantage of being a true astronomical observation.

Unfortunately this is not a method that can be used for GREX. Neither the Sun nor the Moon rise very high in the sky at the latitude of GREX (at best, for a few days per month, the Moon transits at ~35° from the zenith) and so the counting rate is very low. A 3σ deficit would require 2500 counts in a bin of radius 1° centred on the Sun and the Moon. At the current GREX trigger rate this would take approximately a further five years of observing.

Despite the absence of an unequivocal source of PeV gamma-rays one group has used observations of Hercules X-1 to determine the angular resolution of their instrument. The Ooty group reported (Gupta et al. 1990) four episodes of burst emission from Hercules X-1 observed in 1986 modulated with a period of 1·2357701s.

They claim to observe 26 events between phases of 0·1 and 0·4 when 3 are expected. Assuming this excess represents a true signal the group have looked at the dependence of excess number of showers on bin size (Gupta and Tonwar 1991). They obtain an angular resolution of 1·6°±0·4° which agrees well with their value of ~1·5° derived from sub-array comparisons.

A third method has been used at the South Pole for the SPASE array. A small Čerenkov light detector with an aperture of 1·5° in diameter was run simultaneously with the air shower array (Walker et al. 1991). 372 showers that triggered both SPASE and the Čerenkov detector had directions close to the pointing direction of the detector. An estimate of the angular resolution and pointing accuracy of SPASE was obtained by comparing the reconstructed arrival directions with the pointing direction of the Čerenkov detector. This method has the advantage of requiring relatively few events to produce a significant result. Also, unlike the Moon and Sun shadowing method, it has no geographical restriction.

3·4 Source Searching

The basic method of searching for point sources of PeV gamma-ray emission is to compare the number of events recorded in a bin centred on the potential source with the number recorded in equivalent regions of the sky. If the candidate object is a source then an excess number of counts should be observed in the on-source bin as the gamma-rays will add to the isotropic background. A measure of the significance of the signal observed is given by Li and Ma (1983) as:-

$$S = \sqrt{2}\left\{ N_{on} \ln\left[\frac{1+\alpha}{\alpha}\left(\frac{N_{on}}{N_{on}+N_{off}} \right) \right] + N_{off} \ln\left[(1+\alpha)\left(\frac{N_{off}}{N_{on}+N_{off}} \right) \right] \right\}^{\frac{1}{2}}$$

where N_{on} and N_{off} are the total counts in the on-source and off-source regions respectively and α is the ratio of the on-source observation time to the off-source

observation time. The excess observed is then an 'S standard deviation result'. In the absence of a signal the significance, S, is distributed as a Gaussian with zero mean and unit width.

Two distinct variations of the on-source/off-source method have been employed to search the GREX data set for point sources. Both these variations are described below. In both cases the on-source and off-source collecting times are equal but the off-source collecting area (Ω_{off}) is greater than the on-source collecting area (Ω_{on}). α becomes $\Omega_{on} / \Omega_{off}$.

3·4 a) Azimuthal Method

In this method a shower falling within a circular bin centred on the zenith and azimuth of the source at the shower arrival time is considered an on-source event. The radius of the bin is derived from the angular resolution as described in section 3·2c. If the shower is not within the on-source bin, but within a strip of sky 360° in azimuth centred on the source zenith and of width equal to the diameter of the on-source bin then the event is an off-source event (see Figure 3·6). If the shower falls without the strip it is discarded.

Obviously, the off-source region is much larger than the on-source region. Each off-source event is weighted by the ratio of the width of the on-source bin at the event zenith to (360 - width) (see Figure 3·7). The further the off-source event falls from the centre of the on-source bin in zenith the smaller the weight.

A second weighting is required to correct for the azimuthal asymmetry of the array. As a source rises and sets it passes though a limited range in azimuth, whereas the background is taken from 360° in azimuth. Consider the case of a source transiting in the South and an array with an azimuthal asymmetry that results in more showers being accepted from the South. The source would not pass into the shower poor region of the North, but the background strip would include this area. This would result in an underestimate of the background.

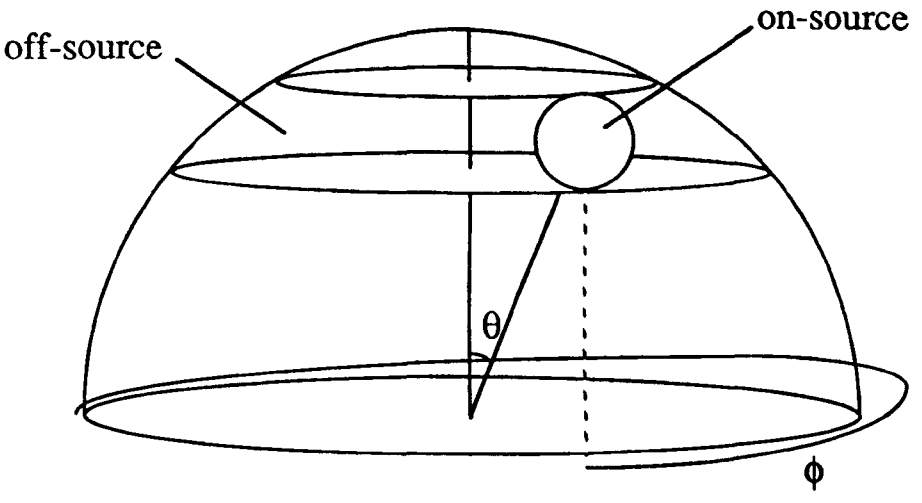

Figure 3·6 The on-source and off-source regions in the azimuthal method. The on-source region is a circular bin in zenith (θ) and azimuth (ϕ) centred on the source. The off-source region is a strip in azimuth centred on the zenith of the the source.

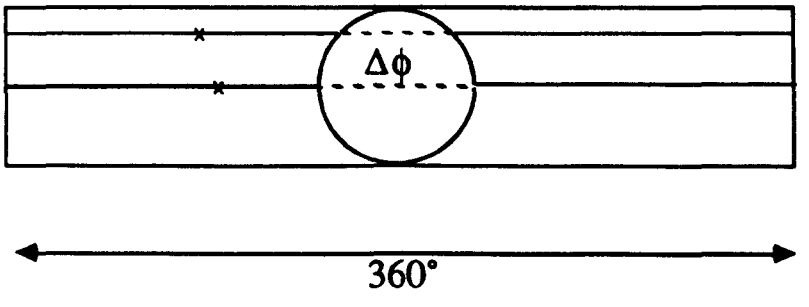

$$\text{weight} = \frac{\Delta\phi}{360 - \Delta\phi}$$

Figure 3·7 The weighting of off-source events to account for the much larger off-source area. $\Delta\phi$ is the width of the on-source bin at the zenith of the off-source event.

The azimuthal distribution of showers recorded by the GREX array has been found for different shower sizes, zenith angles and array eras. In addition to the three eras described in section 3·2a the fourth era formed following the addition of four new detectors in May 1989 was included. These extra detectors do not affect the angular resolution of the array, but do alter the azimuthal distribution of the array. For each era/energy/theta angle range the Fourier coefficients of the first and second harmonics of the azimuthal distribution have been found.

Figure 3·8 shows the magnitude and phase of the first harmonic of the azimuthal distribution as a function of energy. As can be seen the peak in the distribution shifts from the South at low energies to the North at higher energies. The GREX array has an ~3° slope toward just west of North. This means that the projected area of the array is greater when viewed from the North than from the South. This should result in an excess of showers from the North. However, the slope of the array also means that the inter detector spacing appears smaller from the South so making the array easier to trigger. At low energies the apparent closeness of the detectors as seen from the South outweighs the increased area as seen from the North and so the azimuthal distribution peaks in the South. As the energy increases the difference in detector spacing becomes less and less important and so the area effect dominates. Although Figure 3·8 shows the first harmonics for the azimuthal distribution over all eras and zenith angles the same basic effect is, in general, seen in each era and zenith band.

With the azimuthal distribution known each off-source event can be weighted by the ratio of the azimuthal acceptance at the source azimuth to the acceptance at the off-source event azimuth.

The major disadvantage of this method is that it cannot be used when a source passes very close to the zenith. If the angular distance between the source position and the zenith is less than the bin size then the background area goes to zero.

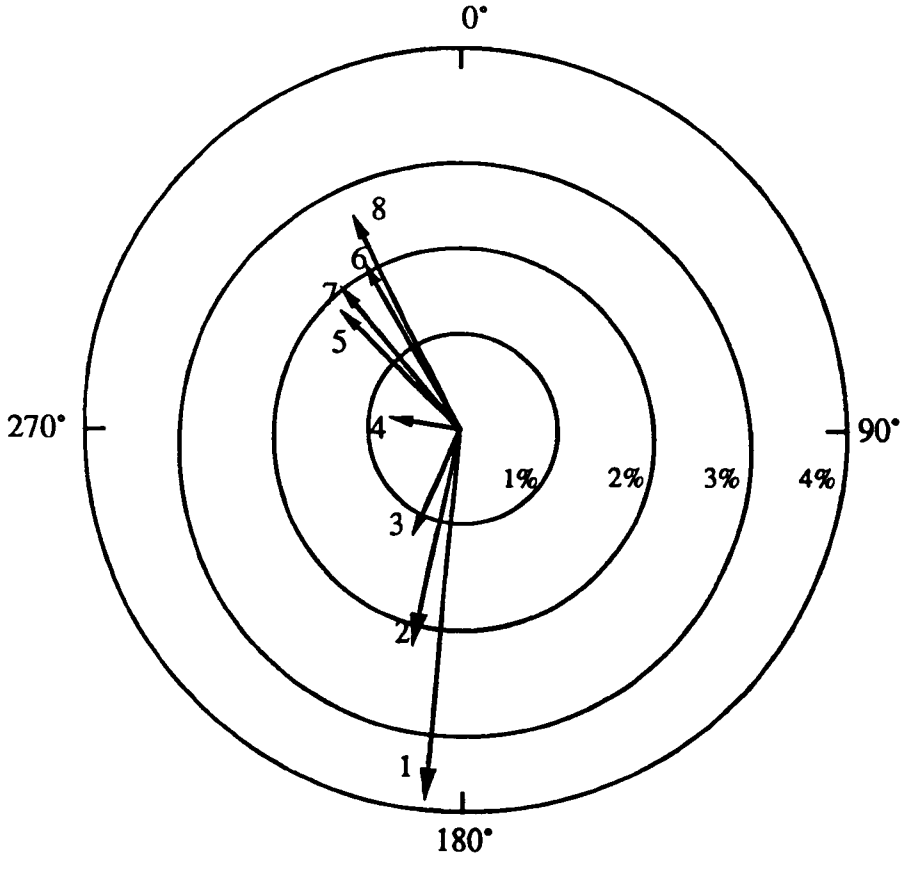

Figure 3·8 The magnitude and phase of the first harmonic of the azimuthal distribution of the GREX array as a function of energy. The distribution has been summed over all array eras and zenith angles. North is at 0° and the radial scale gives the amplitude of the harmonic as a percentage of the total distribution. The mean S(50) in each band is:- 1=0·38, 2=0·70, 3=1·12, 4=1·86, 5=3·08, 6=5·19, 7=8·81, 8=17·83 m^{-2}

3·4 b) Equal Exposure Method

In this case events are binned in right ascension and declination rather than zenith and azimuth angle. The on-source region is a square bin in right ascension and declination centred on the position of the candidate source. The size of the bin is such that it contains the same solid angle as the corresponding bin in the azimuth method. The background is obtained from a number (n) of bins of the same size and centred on the same declination as the on-source bin but shifted in right ascension. Half the bins lead the on-source bin in right ascension and half trail behind. The background is taken to be the mean of these off-source bins. Decreasing the uncertainty in the background estimate increases the sensitivity of the array to a source. As the uncertainty in the background is proportional to $1/\sqrt{n}$ it is desirable to make the number of bins as large as possible.

It is essential that the exposure of each bin is the same. If, for example, the array was switched off after the source bin had risen but before all the trailing off-source bins had risen the background would be underestimated. This would probably not lead to a systematic error over a large number of days, but would be important for single days. To avoid this the condition is made that all the bins should spend the same amount of time above the 'horizon'. The horizon is taken to be 40° from the zenith as showers with zenith angle greater than 40° are not included in source searching. However, ensuring equal on-time is not sufficient to ensure equal exposure. The count rate of GREX per unit solid angle is found to vary as $\cos^7\theta$ and so a bin at a large zenith angle will see fewer showers in a given period of time than a bin of the same size at a smaller zenith angle. In this case the two bins could have equal on-times but different exposure. To overcome this problem the 'equal exposure' method was developed by Idenden (1991) wherein sidereal days were only accepted if the exposure in all the bins was equal i.e. all bins were exposed to the same region of sky for the same period of time.

As stated above the accuracy of the background estimate increases with bin number. However, the larger the number of bins the more likely it is that a day will be rejected due to unequal exposure as the array must run uninterrupted for a longer period.

As a compromise six off-source bins were used in source-searching with three bins on either side of the source bin.

The major problem with this method is the small number of events used to determine the background. For a typical source each off-source bin might contain ~5 events per sidereal day. In a search for sporadic emission periods are considered interesting if the number of on-source events is high compared to the background. However, with an uncertain estimate of the background this excess could be the result of a downward fluctuation of the background rather than an increase in the number of on-source events. By comparison the background estimate in the azimuthal method is derived from ~200 events per sidereal day and so the azimuthal method is preferred in searches for short term sporadic emission. However, the azimuthal method is more susceptible to systematic errors (e.g. in the weighting for the azimuthal asymmetry of the array) and so care must be taken when using it in searches for long term emission.

3·5 Conclusions

The current work has simplified the angular resolution parameterisation used for the GREX array. It has been shown that there is no longer any differences between the 30m and 50m baseline sub-arrays and that there is no zenith angle dependence for the 30m sub-arrays. These effects were almost certainly the result of using the incorrect co-ordinates for detector 12. The capabilities of the GREX array had, therefore, been underestimated, especially for showers that triggered the 30m grid. The angular resolution has been improved by using an improved parameterisation of the shower front curvature and the number of events that can be used for source searching has doubled. This has resulted in a signal to noise improvement of ~45% so increasing the sensitivity of the array to point sources.

Two methods of source searching have been described. The azimuthal method offers a novel way of reducing the uncertainties in the estimation of the background rate.

Candidate sources have been searched for using both methods (except for those that pass too close to the zenith for the azimuthal method). The background estimates of the two methods are virtually independent of each other and so offer a check that neither method is affected by systematic errors. Results using these methods are described in the next chapter and in Chapter 6.

CHAPTER 4

CYGNUS X-3

4·1 Introduction

Cygnus X-3 must rank as one of the most widely observed astronomical objects. Since its discovery in 1966 as an X-ray source it has been searched for in almost all energy ranges from radio wavelengths to 10^{18}eV gamma-rays. Despite this interest, Cygnus X-3 still remains a mysterious object with our knowledge of its true nature based more on conjecture than established fact.

In 1983 Samorski and Stamm claimed that Cygnus X-3 was an emitter of PeV gamma-rays. This was the first claim made for a point source of gamma-rays at this energy and it, together with the confirmation by Lloyd-Evans et al. (1983), initiated a large scale effort to search for further point sources. As part of this effort the GREX extensive air shower array was built at Haverah Park specifically for the search for point sources of PeV gamma-rays.

In this chapter the history of observations of Cygnus X-3 will be reviewed with emphasis placed on the validity of observations at TeV and PeV energies. Also details will be given of a search of the 5 year GREX data set for evidence of emission from Cygnus X-3 at 10^{15}eV.

4·2 Observations of Cygnus X-3 Below TeV Energies

Cygnus X-3 was first discovered in X-rays during a rocket flight (Giacconi et al. 1967) and then radio emission was observed 5 years later in the course of a survey of X-ray sources (Braes and Miley 1972, Hjellming et al. 1972). The radio source was point-like, situated at coordinates α_{1950} = 20h 30min 37·63s ± 0·03s, δ_{1950} = +40° 47' 12·5" ± 0·5". On 2 September 1972 Cygnus X-3 flared at radio wavelengths when the

flux rose by a factor of 10^3 to ~20Jy in a matter of hours and then declined to the quiescent level over a few days (Gregory et al. 1972b). A series of three flares of decreasing intensity were then observed from the 19 to 27 September (Aller and Hodge 1972). A large scale radio event of this type is seen from Cygnus X-3 approximately once a year (Johnston et al. 1986).

The flare of 1972 enabled an estimate to be made of the distance to Cygnus X-3. The mass and velocity of the material between Cygnus X-3 and the Earth were derived from the amount of hydrogen absorption in the 21cm radio signal. This gave a lower limit to the distance of 11kpc. This limit has decreased to 8kpc as the distance of the Sun to the galactic centre has been revised (Bonnet-Bidaud and Chardin 1988).

Such large scale variations as seen in the radio output have never been observed at X-ray energies. The X-ray intensity does vary by as much as a factor of 10, but this is a gradual variation over a time scale of weeks (Bonnet-Bidaud and van der Klis 1985). This variability has given rise to a number of claims of periodicity with periods of order 30d. Subsequent, more extensive observations have failed to confirm these reports.

However, one X-ray periodicity of Cygnus X-3 has been established. Observations made at 10keV revealed a 4·8hr periodicity (Brinkmann et al. 1972, Parsignault et al. 1972, Sandford and Hawkins 1972). The shape of the light curve varies from cycle to cycle, but when averaged over several cycles it is stable for years. The light curve is characterised by a gradual rise followed by a sharp decrease (van der Klis and Bonnet-Bidaud (1989)). Variations are seen in the average shape of the light curve during periods (lasting for up to a few weeks) of increased X-ray flux (van der Klis and Bonnet-Bidaud (1981)). Following analysis of 15 years of X-ray observations van der Klis and Bonnet-Bidaud (1989) have determined that the 4·8hr period is lengthening slowly at a rate of $\sim 10^{-9} ss^{-1}$.

There is no strong evidence for a 4·8hr modulation of the radio signal. However, it has been suggested (Molnar et al. 1984) that the low-level radio emission observed is formed by the superposition of a series of small flares produced with a period near the

4·8hr X-ray period.

Cygnus X-3 lies almost exactly on the galactic plane and, at 8kpc, is on the far side of a spiral arm. The material in the spiral arm causes a decrease in the visible part of the spectrum of at least a factor 1000 or ~8 magnitudes and consequently Cygnus X-3 is extremely difficult to observe optically. However, a faint object has been reported at the radio position (Weekes and Geary 1982).

At infrared wavelengths the extinction of Cygnus X-3 due to material in the intervening spiral arm is less than 1·5 magnitudes and so the source reappears. The 4·8hr X-ray modulation is clearly observed at ~2μm with the same phasing and shape as is seen at X-ray energies (Becklin et al. 1974). Superimposed on the 4·8hr modulation are irregular, three fold flares of a few minutes duration (Mason et al. 1986). Additional observations have been made at 0·9μm which also show the 4·8hr periodicity (Wagner et al. 1989).

There appears to be no correlation between radio flares, infrared flares and periods of increased X-ray flux.

Gamma-ray observations in the range 30-5000MeV have been carried out using balloon borne and satellite experiments. One of the first balloon flights in 1972 had indicated a 3·5σ excess from Cygnus X-3 (Galper et al. 1975). However, subsequent flights by the same group in 1974 and others (McKechnie et al. 1976) failed to substantiate this claim and placed an upper limit to the flux above 70MeV significantly lower than the claimed flux. Also the first observations made with the SAS-2 satellite at energies >100MeV failed to detect emission (Fichtel et al. 1975).

A second period of observations with SAS-2 did detect a 4·5σ excess of gamma-rays with energy >35MeV from Cygnus X-3 modulated with the 4·8hr period (Lamb et al. 1977). However, observations made later with the COS-B satellite over 7 years failed to confirm this result despite having accumulated ~70 times more events then the SAS-2 experiment in the Cygnus X-3 region (Hermsen et al. 1987). The COS-B group maintain that the SAS-2 observations are consistent with the background

as measured by COS-B and so no point source need be invoked. Also they believe the 4·8hr modulation to be spurious. However, Fichtel et al. (1987) argue that source variability could explain the discrepancy in the results.

The status of Cygnus X-3 as a low energy gamma-ray source should soon be clarified with results from the Gamma Ray Observatory (GRO). This satellite, which is currently observing, covers a wide range of gamma-ray energies from 100keV to 30GeV (Schönfelder 1990). It is ten times more sensitive than any previous experiment and should provide an accurate estimate of the background in the Cygnus X-3 region.

4·3 Observations of Cygnus X-3 at TeV Energies

4·3 a) Steady and Period Modulated Emission

A 10^{12}eV cosmic-ray has insufficient energy to initiate an extensive air shower able to trigger an array of detectors at ground level, even at mountain altitudes. However, ground based observations can be made by observing brief flashes of Čerenkov light. If a charged secondary particle in the shower has enough energy such that it travels through the atmosphere faster than the speed of light in air then Čerenkov light is produced. With many highly relativistic secondaries in the shower the amount of light produced in a pulse of ~5ns is great enough to be seen against the background light of the night sky. As the light is emitted along the direction of travel of the particles the primary arrival direction can be derived.

The first claimed detection of TeV gamma-rays was made by Vladimirsky et al. (1973). Two World War 2 searchlight mirrors of 1·5m aperture viewed by photomultipliers were used to collect the Čerenkov light. A 5σ excess of showers from Cygnus X-3 was observed with one of the mirrors on 8 and 9 September 1972 (i.e. just after the first detected massive radio flare). No signal was observed in the second mirror but this had a higher threshold energy and a steep spectral index was invoked to explain the discrepancy.

The group continued to observe Cygnus X-3 building up a data set over the next four years with a total on-time of ~200hr. The result was a net 3·9σ excess from the direction of Cygnus X-3. Assuming the excess to be a genuine signal they then used the data to derive a 4·8hr ephemeris which agreed with the X-ray ephemerides. Two narrow peaks of emission were observed, one of 5·4σ around phase 0·2 and one of 3·3σ at phase 0·8 (Figure 4·1a) (see Weekes 1988 review). However, it should be noted that Chardin and Gerbier in their critical review of 1989 suggest that with the signal optimization performed by the Crimean group (i.e. period, number of bins and origin of the first bin) a 3·0σ excess can easily arise from statistical fluctuations.

The early 1980's saw interest being shown in Cygnus X-3 at 10^{12}eV in other parts of the world. Observations made in mid-1980 at the Whipple Observatory on Mount Hopkins using a similar design of telescope to that used in the Crimean experiment showed an excess of 3·5σ between phase 0·6-0·7 (Weekes et al. 1981) using the van der Klis and Bonnet-Bidaud (1981) ephemeris (Figure 4·1b). Using two 11m diameter mirrors a group at the Jet Propulsion Lab (JPL), California observed a 4·2σ excess during August-September 1981 at phase 0·5-0·7 using the same 4·8hr ephemeris (Figure 4·1c) (Lamb et al. 1982). The third independent confirmation came when the Durham group reported a 4σ excess at phase 0·6-0·7 in more than 350 hours of observations made in 1981 and 1982 (Figure 4·1d) (Dowthwaite et al. 1983). The three experiments all gave integral gamma-ray fluxes of ~10^{-10} photons $cm^{-2}s^{-1}$ at energies greater than 1TeV.

Following the successful use of a small telescope at the Whipple Observatory a 10m imaging telescope was built. Rather than having a single photomultiplier tube to collect the light an array of 37 tubes was used to obtain an image of the Čerenkov flash. From simulations it was expected that the image produced by a gamma-ray initiated shower would be narrower than that produced by a proton initiated shower and so cuts could be made that rejected background events. Data recorded from Cygnus X-3 during October/November and November/December 1983 were phase analysed using the van

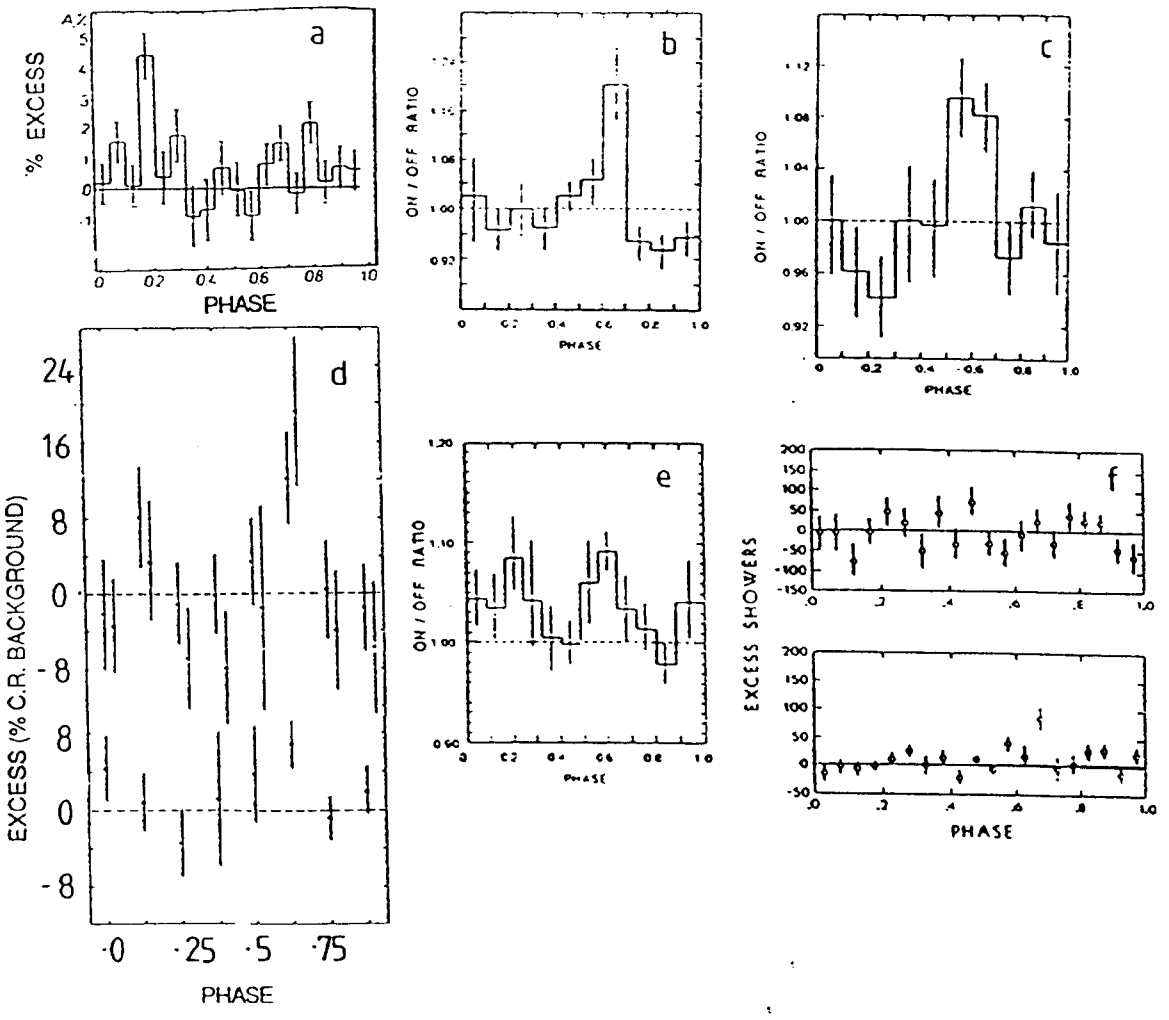

Figure 4·1 a-f) 4·8hr phase distribution reported by air-Čerenkov experiments. Except for a, all use the van der Klis and Bonnet-Bidaud (1981) X-ray ephemeris. a) Excess events expressed as a percentage for data recorded by the Crimea detector during 1972-1977 (Neshpor et al. 1979), b) On/off ratio of showers recorded by the Mount Hopkins experiment May-June 1980 (Weekes et al. 1981), c) On/off ratio of showers recorded August-September 1981 at JPL (Lamb et al. 1982), d) Percentage excess of showers recorded by the Durham group in 1981 and 1982 (Dowthwaite et al. 1983), e) On/Off ratio of showers recorded with the 10m telescope at Mount Hopkins in October and November 1983 (Cawley et al. 1985), f) Excess number of showers in the energy ranges 10-100TeV (upper plot) and 100-1000TeV (lower plot) recorded by the Fly's Eye, mid-1985 (Baltrusaitis et al. 1987). Presentation from Bloomer (1990).

der Klis and Bonnet-Bidaud (1981) ephemeris. A 4·4σ excess was seen in the phase range 0·58-0·67 and a 2·2σ excess in the range 0·17-0·25 (Cawley et al. 1985) for the October/November period (Figure 4·1e). During this time Cygnus X-3 was at ~30° when at phase 0·6 and ~60° at phase 0·2 so the threshold energy was greater at phase 0·2. It is not clear if the choice of 12 phase bins was made a priori or a posteriori. No enhanced emission was observed in the November/December data set which the Whipple group take to be evidence of the variability of Cygnus X-3.

For 4 months in mid-1985 the Fly's Eye group searched for gamma-rays from Cygnus X-3 (Baltrusaitis et al. 1987). The threshold energy of the Fly's Eye instrument was lowered to 10TeV. A 3·1σ excess was found in a bin 7°x7° centred on Cygnus X-3 for the energy range 100-1000TeV. When phase analysed with the van der Klis and Bonnet-Bidaud (1981) ephemeris a 3·9σ excess was seen in the phase bin 0·65-0·70 (Figure 4·1f). No evidence for D.C. or phase enhanced emission was found in the lower energy decade of 10-100TeV.

4·3 b) Possible 12·59ms Pulsar

On 12 September 1983 the Durham group observed an ~7 minute excess from the direction of Cygnus X-3 during a 6 hour observation period. During the burst, which corresponded to phase 0·625 in the 4·8hr X-ray period, 450 events were observed when ~373 were expected. This data set offered a sample of sufficient signal strength to make a search for the short periodicities typical of pulsars worthwhile. The Durham group searched for periodicity over the range 10ms to 50s (Chadwick et al. 1985a). The most significant peak observed was at 12·5908ms with a chance probability, accounting for the number of periods tested, of $3{\cdot}3\times10^{-3}$ (Figure 4·2a). Although not overwhelmingly significant in itself the Durham group offer two pieces of corroboratory evidence.

Firstly, if the periodicity is genuine it is expected that the fraction of phased events should follow the increase and decrease in the count rate during the burst. If the periodicity is a statistical fluctuation the fraction of phased events will be independent of

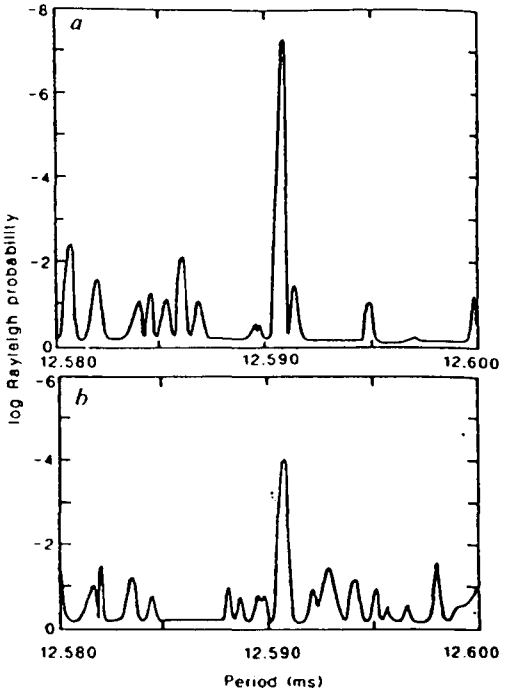

Figure 4·2 a) The chance probability of periodicity in the 450 events containing the count rate excess recorded by the Durham group on September 12 1983 as a function of trial period. b) The chance probability of periodicity as a function of trial period for events on October 2 1983 recorded at exactly the same phase in the 4·8hr cycle (Chadwick et al. 1985a)

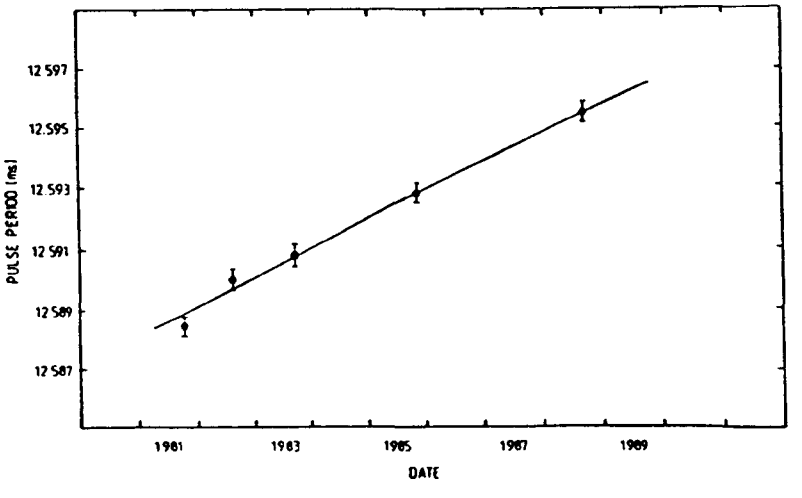

Figure 4·3 Variation of the period of the claimed pulsar in Cygnus X-3 in VHE gamma-ray measurements made by the Durham group between 1981 and 1988 (Brazier et al. 1990a)

the rate of events. A correlation was found between the periodicity power and counting rate during the 7 minute burst at a chance probability of $9{\cdot}5\times10^{-4}$. Secondly, the same periodicity (Figure 4·2b) was detected in one of seven similar observations made at phase 0·625 in the 4·8hr cycle with a probability of 0·0028 (allowing for the trials in looking in 7 data sets). This gave an overall significance claimed for the detection of 4×10^{-7}.

Since their original detection the Durham group have reanalysed their earlier data of 1981 and 1982 to search for the 12·59 periodicity and have made further observations. Brazier et al. (1990a) claim four significant detections of the pulsar between 1981 and 1988 in addition to the original 1983 detection. They also claim that the period of the pulsar is increasing with a period derivative of $(1{\cdot}9\pm0{\cdot}3)\times10^{-14}ss^{-1}$ (Figure 4·3).

The Durham claims are impressive with a large degree of self consistency within their data. However, to date, only one group has made a tentative confirmation of this result despite searches by many other groups. The Whipple, Haleakala and Gulmarg groups all report unsuccessful searches (respectively Fegan et al. 1989, Resvanis et al. 1987 and Bhat et al. 1990). The one tentative confirmation is by the Adelaide group using the novel high zenith angle technique (Gregory et al. 1990). If a Čerenkov detector observes at low elevations the threshold energy increases by a factor of ~100 to 0·1PeV, but this is accompanied by a much increased effective collection area. The Adelaide group found evidence at the 1% level for a periodicity at the period predicted by the Durham ephemeris during 5 days in August/September 1989. The high energy of this result implies that Northern hemisphere extensive air shower arrays with low threshold energies should search for the pulsar.

Further confirmation is required with greater statistical significance by additional groups before the existence of a pulsar in Cygnus X-3 can be confirmed.

4·3 c) Authenticity of the TeV Signal

Figure 4·1 shows the main claims of evidence for emission of TeV gamma-rays from Cygnus X-3. If these claimed detections are genuine then the overall picture that emerges is of highly variable emission, mainly around phase 0·6 of the X-ray 4·8hr cycle. As stated above, the existence of a short, pulsar periodicity remains unconfirmed.

However, there is no overwhelming piece of evidence for the emission of TeV gamma-rays from Cygnus X-3 and some critics (most noticeably Bonnet-Bidaud and Chardin (1988) and Chardin and Gerbier (1989)) have argued that the results reported are consistent with no signal. They point to a lack of long term D.C. excess from Cygnus X-3 and the reliance on the agreement in the position of the phase peak reported by different groups. They claim, however, that the phase agreement is rather superficial: Weekes et al. (1981) reported a 20% excess lasting for 30min, Lamb et al. (1982) a 6% excess for 1hr and Dowthwaithe et al. (1983) an 8% excess for ~30min, with all the results in the region of phase 0·6 (see Figure 4·1). The original Crimean detections showed the strongest effect at phase 0·2 (although with an additional, less significant peak at 0·8). Chadwick et al. (1985a) suggest that enhanced emission may occur for periods of less than 10min.

Of course one would like an unambiguous picture of emission at 10^{12}eV, but is it reasonable to expect such a picture to emerge? There are two main considerations. Firstly Čerenkov detectors can only be operated on clear, moonless nights and so the duty cycle for each detector is very low. This makes simultaneous observations at different sites rare. Cygnus X-3 is studied for small periods of time and if it is at all variable at TeV energies different observations will give different results. Secondly, could we expect Cygnus X-3 to be variable at TeV energies? It is surely unreasonable to expect the processes that accelerate charged particles to energies in excess of 10^{13}eV to be well regulated and constant.

4·4 Observations of Cygnus X-3 Above 0·1PeV

4·4 a) Steady and Period Modulation Emission

As the initial energy of the primary cosmic ray or gamma-ray increases the resulting extensive air shower penetrates deeper into the atmosphere. At 10^{14}eV an air shower is produced which can trigger an array at ground level. This section will detail observations made of Cygnus X-3 using extensive air shower arrays.

Some early attempts to detect an excess of gamma-rays from Cygnus X-3 with energies greater than 10^{14}eV had failed (e.g Fegan and Danaher 1981). The first claimed detection of gamma-rays with energies in the PeV region from Cygnus X-3 was made by Samorski and Stamm in 1983(a). Their air shower array at Kiel, West Germany, consisted of 28 scintillation detectors of $1m^2$ area separated by distances of up to 100m. The array had an angular resolution of ~1°. Showers recorded between March 1976 and January 1980 were binned into 90 bins of 4° in right ascension in a strip of declination 3° wide centred on Cygnus X-3. The age parameter (s) of each shower was measured and the data split into two groups - showers with $s<1{\cdot}1$ ('young') and showers with $s\geq1{\cdot}1$ ('old'). It was expected that gamma-ray initiated showers would develop earlier in the atmosphere and so a stronger signal would be seen in older showers ($s\geq1{\cdot}1$) (see section 1·4). For old events 31 showers were seen in the bin centred on Cygnus X-3 when 14·4 were expected. This was the greatest deviation from the expected background seen in any of the 90 bins. No effect was observed for young showers. The data set in which the excess was observed was then phase analysed with the 4·8hr modulation using the Parsignault et al. (1976) X-ray ephemeris (Figure 4·4a). The phase bin 0·3-0·4 contained 13 events when 1·44 were expected. A time averaged integral flux of $(7{\cdot}4\pm3{\cdot}2)\times10^{-14}$ photons $cm^{-2}s^{-1}$ was derived for energies greater than 2×10^{15}eV and $(1{\cdot}1\pm0{\cdot}6)\times10^{-14}$ photons $cm^{-2}s^{-1}$ for $E>10^{16}$eV.

In addition to measuring the age of each shower the Kiel array also measured the muon content. As described in section 1·3b it was expected from simulations that a

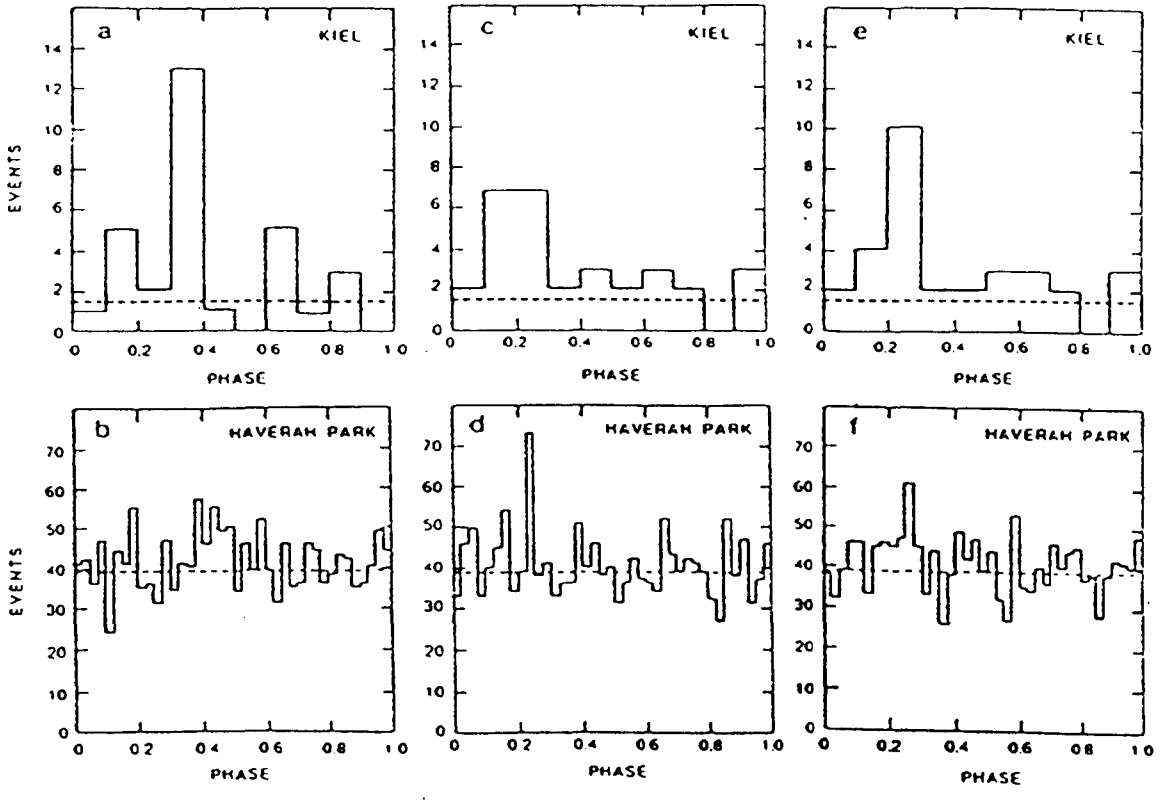

Figure 4-4 a-f) A comparison between the phase distribution of events recorded by the Kiel array between 1976 and 1980 and the Haverah Park array recorded between 1979 and 1982. a and b) analysed with the Parsignault et al. (1976) X-ray ephemeris. c and d) analysed with the van der Klis and Bonnet-Bidaud (1981) ephemeris. e and f) analysed with the Mason (1986) ephemeris. Taken from Bloomer (1990).

gamma-ray initiated shower would have a tenth of the muons that a hadron initiated shower produced. The Kiel result (Samorski and Stamm 1983b) showed that the muon content of showers from Cygnus X-3 was actually ~80% of the muon content of background showers.

The first confirmation of the Kiel result came from the $12km^2$ array at Haverah Park. This array, described in Chapter 5, consisted of a series of sub-arrays, any one of which could operate independently. Whereas the threshold energy of the entire array was $\sim 10^{17}$eV the sub-arrays triggered on showers of 10^{15} or 10^{16}eV depending on the sub-array base-line. Each sub-array was made up of four deep water-Čerenkov detectors with inherently slow rise times which limited the angular resolution to ~3°. Data recorded from 1979 to 1982 were analysed with a bin 9° in right ascension and 6° in declination centred on Cygnus X-3 being the on-source region. The background estimate was derived from the same 6° declination strip (Lloyd-Evans et al. 1983). For the data in the 10^{15}-10^{16}eV range a small, $1{\cdot}7\sigma$, excess was observed from Cygnus X-3 (1627 events on-source, 1559 off-source). In the higher energy range ($>10^{16}$eV) a $1{\cdot}3\sigma$ deficit was observed (397 on, 424 off). The age was not calculated for these showers and no information was known regarding the muon content.

When analysed with the Parsignault et al. (1976) ephemeris the low energy data did not show a significant excess (Figure 4·4b). However, analysis with the van der Klis and Bonnet-Bidaud (1981) ephemeris revealed 73 events in the 0·225-0·250 bin when 39·0 were expected (Figure 4·4d). The probability of seeing an excess of this size in one of 40 bins is $\sim 2{\cdot}8\times10^{-5}$. The integral photon flux above 3×10^{15}eV was calculated to be $(1{\cdot}5\pm0{\cdot}3)\times10^{-14}$ $cm^{-2}s^{-1}$. If the Kiel data are reanalysed with the van der Klis and Bonnet-Bidaud (1981) ephemeris the peak at 0·3-0·4 is replaced by a broad excess (14 on, 2·88 expected) between 0·1 and 0·3 (Chardin and Gerbier 1989) (Figure 4·4c). Better phase agreement is obtained if both data sets are analysed using the Mason (1986) ephemeris (Figures 4·4e and f). However, the significance of the main Haverah Park peak is reduced. Although both covering ~4 years the Kiel and Haverah Park

observations are not exactly contemporaneous as the Kiel observations began 3 years before those of Haverah Park. Therefore, the differences in the light curves could be the result of source variability. Against this, the presence of a narrow peak in the Haverah Park phasogram would suggest phase stability.

Weak evidence for variability of the phase of emission was found when the Haverah Park data set was extended to include observations made in 1983 and 1984 (Lambert et al. 1985). Using the van der Klis and Bonnet-Bidaud (1981) ephemeris no emission is seen around phase 0·25 in 1982 and 1983 and only a small peak is seen in 1984. The most significant peak in the 1984 data is around phase 0·6. The chance probability of observing the two peaks in the 1984 data set is 2·3%. This effect is lost if the Mason (1986) ephemeris is used (Bloomer 1990).

A third report came from the Akeno extensive air shower array in Japan (Kifune et al. 1986). The array consisted of 153x1m^2 scintillation detectors and 9x25m^2 muon detectors. The threshold energy was ~1PeV. A region of sky 20°x20° centred on Cygnus X-3 was searched for muon poor events between 1981 and 1984. 18 events were found with a muon content of at most 3% of that observed in 'normal' showers. No background estimate was given. When phase analysed with van der Klis Bonnet-Bidaud (1981) a broad excess is seen around phase 0·6 with a 0·2% probability of occurring by chance (Figure 4·5a). This result is of interest as, if genuine, it contradicts the Samorski and Stamm claim as an effect is only observed if a strong muon cut is imposed. Also, cutting in shower age does not affect the Akeno result.

The Plateau Rosa array consisted of four scintillator detectors at 3500m above sea-level. The high altitude and small dimensions of the array resulted in an exceptionally low threshold energy for an extensive air shower array (~10^{13}eV), although the angular resolution was rather poor at 5·5°. Initial observations between 1980 and 1983 showed a 2·8σ excess at phase 0·60-0·65 (Figure 4·5b) (Morello et al. 1983). Further observations up to 1987 did not increase the significance of this result (Morello et al. 1990).

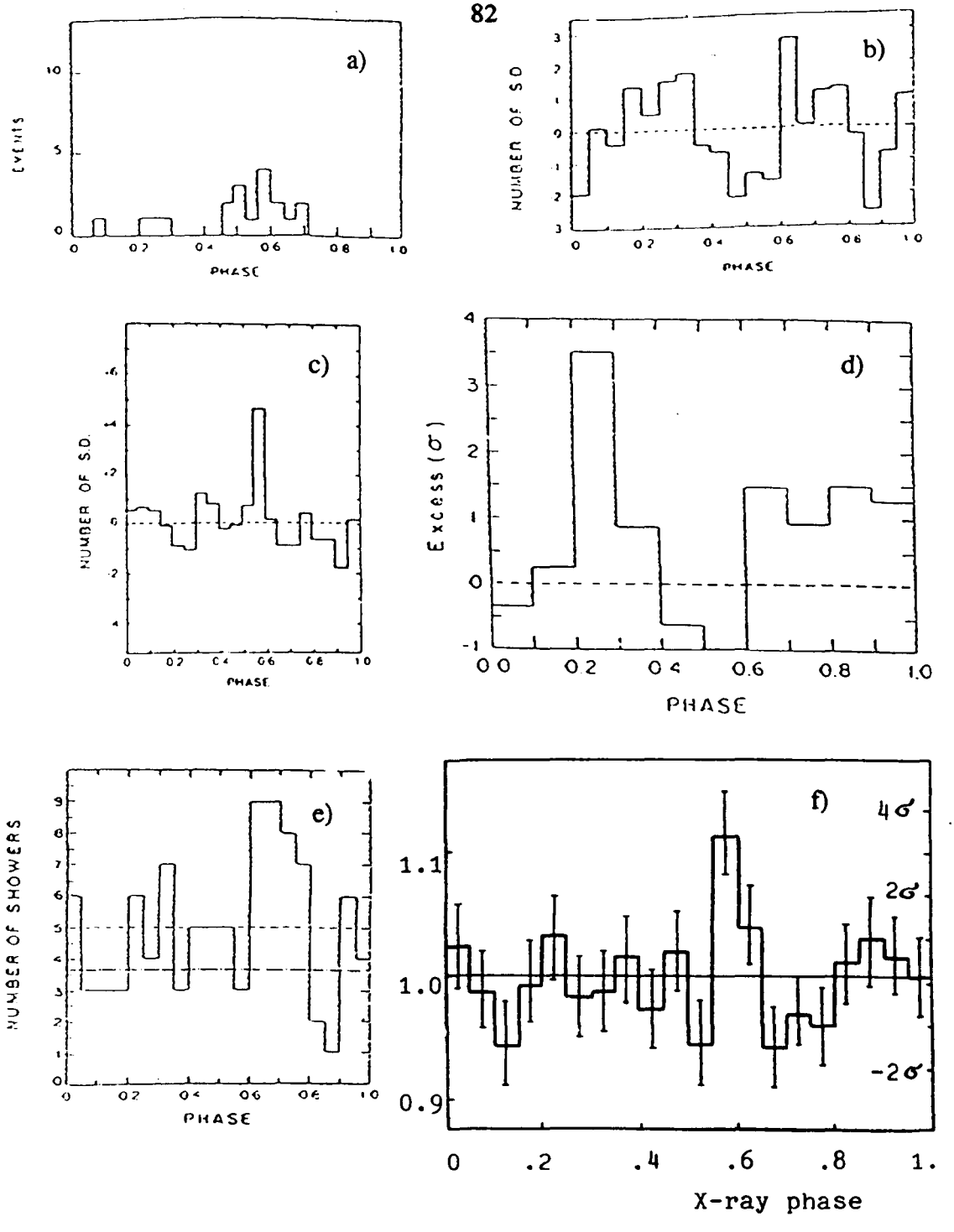

Figure 4-5 a-i) Phase distribution of PeV observations of Cygnus X-3. Except where stated, the van der Klis and Bonnet-Bidaud (1981) ephemeris has been used. a) Distribution of muon poor events recorded between 1981 and 1984 at the Akeno array (Kifune et al. 1986). b) The excess number of showers, expressed in standard deviations, recorded by the Plateau Rosa array in 1982 (Morello et al.1983) (Elsner (1980) ephemeris). c) Excess, in standard deviations of the 1976 and 1977 Gulmarg data (Bhat et al. 1986a). d) Excess, in standard deviations, of 1983 Fly's Eye data (Baltrusaitis et al. 1985a). Continued on next page.

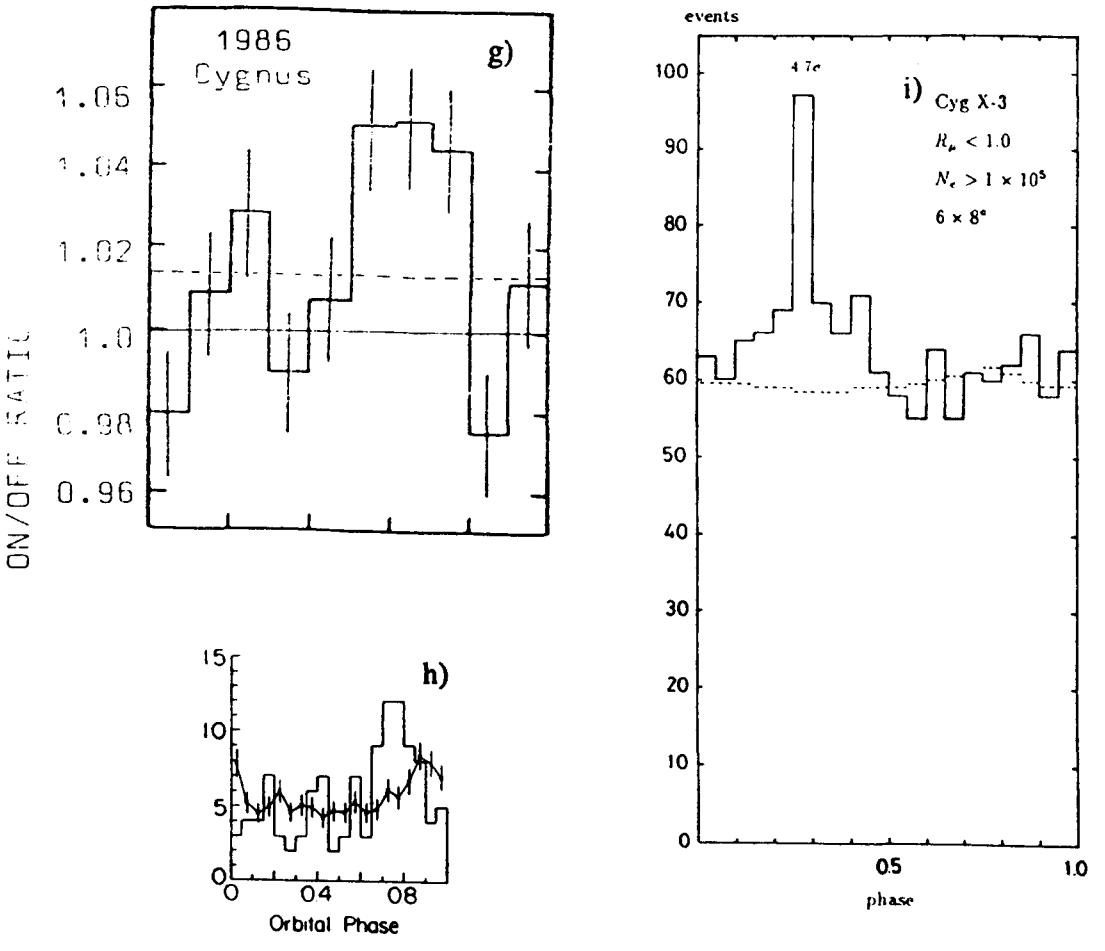

Figure 4·5 Continued from previous page. e) Number of showers of size $N_e > 5 \times 10^5$ and all ages recorded between 1984 and 1986 by the Ooty array (Tonwar et al. 1988). f) Excess (given in both on/off ratio and number of standard deviations) recorded in the first 250 days of operation of the Baksan array in 1984 (Alexeenko et al. 1985). g) On/off ratio of data recorded in 1986 by the Baksan array (Alexeenko et al. 1987b) (ephemeris not stated). h) Number of events with 0 or 1 muon recorded by the CYGNUS experiment in the 45 days following April 17 1986 (Dingus et al. 1988b) (Mason (1986) ephemeris). i) Number of events recorded by the Ōhya array in 4 years from 1986 (Muraki et al. 1991).

One of the simplest methods of observing extensive air showers was that used in Gulmarg, India. Two bare, uncollimated photomultiplier tubes were operated in coincidence to observe Čerenkov light with an acceptance angle of 0·5sr (Bhat et al. 1986a). For data recorded in 1976 and 1977 a broad excess of events was observed around right ascension 300°. When events from the Cygnus X-3 region were phase analysed (using the van der Klis and Bonnet-Bidaud (1981) ephemeris) a 4·5σ peak was found at phase 0·55-0·60 (Figure 4·5c). This produces a time averaged flux for E>500TeV of $(2{\cdot}6\pm0{\cdot}3)\times10^{-12}$ cm^{-2}s^{-1}, a flux that is over an order of magnitude greater than any subsequent measurements at this energy. An attempt to replicate the result in 1984 at the same site gave an upper limit to the flux of 8×10^{-14} cm^{-2}s^{-1}. The extremely high flux and the lack of controls on the background normally used in air-Čerenkov experiments have resulted in doubt being cast on this claim.

A second high energy air-Čerenkov experiment was performed by the Fly's Eye group (Baltrusaitis et al. 1985a). The Fly's Eye was operated with a threshold energy of 1PeV during 1983 and 1984. The 1983 data showed a 3·5σ excess at phase 0·2-0·3 of the 4·8hr period (using the van der Klis and Bonnet-Bidaud (1981) ephemeris) (Figure 4·5d). It is noted that most of the signal appears in a narrow peak 0·04 wide centred on phase 0·27. There is no evidence for emission in 1984. The observed phase peak is at the phase observed by the Kiel and Haverah Park experiments. However, as stated above, Lambert et al. (1985) reported that there was no evidence for emission (at any phase) in the Haverah Park data set for 1983 and some evidence for emission in 1984. These results therefore appear to be in conflict. The modes of operation of the two instruments are, however, different. The Haverah Park 12km^2 array observed Cygnus X-3 whenever it was above the detector horizon. The Fly's Eye only operated on clear, moonless nights, but the large acceptance of the instrument resulted in a high event rate. Therefore, the Fly's Eye was more sensitive to sporadic emission.

Data recorded between 1984 and 1986 by the 24 detector array at Ooty, Southern India, showed a D.C. excess from Cygnus X-3 (Tonwar et al. 1988). This was the first

claim since the original Kiel report that did not rely on the 4·8hr periodicity. An excess of 3·4σ (300 on-source, 247 off) was observed in 'old' showers (s>1·4) in the 4°x4° bin centred on Cygnus X-3. However, a 3σ deficit was observed in one of the background bins shifted in right ascension by 32° from the Cygnus X-3 bin but at the same declination. The data were split into 4 shower size bands and excesses of 3·1, 0·8, 0·2 and 3·8σ observed, for which a chance probability of 10^{-5} (allowing for trials) was claimed. However, in the lowest size band there is a background bin with an excess of the same size as in the on-source bin. The presence of deviations as large as in the on-source bin in those background bins shown in the 1988 paper (where the number of counts in only one third of the background bins are given) cast doubt on the significance of the claimed result. There was some evidence for a broad peak around 0·6-0·8 when the on-source data were phase analysed with the 4·8hr period (Figure 4·5e).

The Baksan group operating the 'carpet' array started collecting data in 1984. No D.C. excess was observed from Cygnus X-3 above $2x10^{14}$eV in eighteen months of observing. However, a 3·6σ peak was found at phase 0·55-0·60 when the data from the first 250 days of operation were analysed using the van der Klis and Bonnet-Bidaud (1981) ephemeris (Figure 4·5f) (Alexeenko et al. 1985). Over three days after the October 1985 radio burst the Baksan group observed an excess of 60·8 events on a background of 234·2 (Alexeenko et al 1987a). This corresponds to an integral photon flux of $(4·9\pm1·5)x10^{-12}$ $cm^{-2}s^{-1}$ above $2x10^{14}$eV. There was no evidence of phase enhanced emission during this post-radio burst period.

During 1986 the Baksan group observed an excess from Cygnus X-3 above 10^{14}eV of ~2·8σ (Alexeenko et al. 1987b). The majority of the signal was seen in the months of May, September, October and November. When phase analysed (the ephemeris used is not stated) a broad peak is observed in the range 0·5-0·8 (Figure 4·5g).

The CYGNUS experiment at the Los Alamos National Laboratory has found no evidence for steady emission of PeV gamma-rays from Cygnus X-3 since being

commissioned in April 1986. This group place an upper limit to the flux above 40TeV of $1{\cdot}9 \times 10^{-13}$ $cm^{-2}s^{-1}$ derived from data recorded up to May 1991 (Alexandreas et al. 1991b). However, there is evidence of a burst lasting 45 days starting on the 17 April 1986 and therefore overlapping with the period of enhanced emission seen at Baksan in May. A $2{\cdot}2^{\circ} \times 3{\cdot}0^{\circ}$ bin centred on Cygnus X-3 showed a small excess above the background when all showers were analysed (Dingus et al. 1988b). On average the CYGNUS detectors record 2·3 muons per shower. As gamma-ray initiated showers are thought to have 10% the muon content of hadron showers, showers with 0 muons were analysed separately. This greatly reduced the significance of the excess. The most significant peak (113 on a background of 77) was observed when showers with either 0 or 1 muon were analysed. When these showers were phase analysed (with the Mason (1986) ephemeris) a peak was seen between phases 0·65-0·85 with a probability of occurring by chance of 0·3% (not including the trials involved in looking at different muon cuts) (Figure 4·5h). There was no evidence of an excess during the period of September-November 1986.

The Haverah Park group, continuing to use small arrays of water-Čerenkov detectors, observed enhanced emission (of low statistical significance) at phases ~0·3 and ~0·7 following the October 1984 and October 1985 radio bursts (Eames et al. 1987a). The Akeno group reported 4 muon poor events (all with less than 10% of the number of muons in normal showers) in the region of Cygnus X-3 in the month following the 1985 radio flare when 0·4 such events were expected (Kifune et al. 1987).

There appeared to be a link between the emission of very high and ultra high energy gamma-rays from Cygnus X-3 and radio flares. Therefore the June and July 1989 bursts were greeted with a great deal of interest. However, except in one case, no significant emission was observed (see Fegan 1990 for review). The exception was the claim by Muraki et al (1991) for evidence of emission in data recorded by the array at Ōhya. This group claims a $4{\cdot}7\sigma$ excess on May 27 and $3{\cdot}4\sigma$ on June 16 1989. However, insufficient details are given in the claim to judge the credibility of this result.

In the same paper Muraki et al. claim a 4·7σ excess at phase 0·3 for data recorded over 4 years from 1986 (Figure 4·5i). A cut was made to look at muon poor showers. However, it is not certain if the muon cut used was applied a priori. Also sufficient inconsistencies exist within the paper to cast doubt on the validity of the result.

The extensive air shower array on Mount Hopkins, which is co-located with the 10m Čerenkov detector, searched for gamma-rays from Cygnus X-3 (energy greater than $4x10^{13}$eV) during the periods 2/87-6/87 and 10/87-6/88 (Gillanders et al. 1990). No evidence for D.C. emission was found. The Utah-Michigan array failed to detect D.C. emission from Cygnus X-3 ($E>2x10^{14}$eV) during 4/88-7/89 (Ciampa et al. 1990). The Tata group also failed to detect emission ($E>1·6x10^{15}$eV) in data recorded by the KGF array during 10/84-1/87 (Sinha et al. 1990). The Chicago air shower array, operating in 1989 with 49 of the planned 1089 detectors, places an upper limit to the flux above 0·1PeV from Cygnus X-3 of $4·3x10^{-13}$ $cm^{-2}s^{-1}$ (Krimm et al. 1990). Preliminary analysis of data recorded by CASA in 1991 produces an upper limit above $1·2x10^{15}$eV of $1·5x10^{-15}$ $cm^{-2}s^{-1}$ (Ong 1991).

4·4 b) Authenticity of the PeV Signal

The picture of gamma-ray emission from Cygnus X-3 at PeV energies is far from clear. The reports described above all share certain common features but there are still damaging contradictions between them. A signal was only observed in the original Kiel data by rejecting 'young' showers. It was believed by some at the time that photon initiated showers would be older than proton initiated showers. Similarly, Tonwar et al. (1988) had to impose a strong age cut to obtain a significant signal in their data. However, many other groups have obtained apparently significant signals without age cuts and simulations by Hillas (1987a) have shown that photon showers should be slightly younger than proton showers. Also, there are problems with the muon content of signal showers. Simulations have shown that number of muons in a photon shower should be at most 10% of that in a proton shower. The Kiel group found that their signal

showers had a muon content of 80% that of 'normal' showers. This is in contradiction with the 1986 Akeno claim, where an excess was observed in showers with muon contents less than 3% that of background showers. In addition the Akeno excess was not restricted to one age range. The CYGNUS group find their most significant result in showers with lower than ~50% the normal muon content but not as low as 10%.

The most frequently invoked piece of evidence for PeV gamma-ray emission from Cygnus X-3 is the fact that most groups claiming to observe a signal do so around phases 0·6-0·8 in the 4·8hr X-ray period. Figure 4·5 shows the phasograms produced by some of the groups claiming positive results. As can be seen there is a wide variety of signals, from narrow peaks of 0·05 of a cycle to broad excesses over almost a third of the X-ray period. Of course these results do not come from data recorded at the same time but cover over 10 years of observations. In a similar way to the TeV results the most favoured phase appears to have shifted from 0·2 to around 0·6 (although this change occurred ~4 years after that in the TeV range). The suggestion put forward above that the highly energetic processes producing TeV gamma-rays could not be expected to be constant obviously applies more strongly here.

Extensive air shower arrays are not limited in their duty cycles to clear, moonless nights in the same way as air-Čerenkov detectors are but can observe whenever Cygnus X-3 is above the detector horizon. For the past 4-5 years there have been sufficient arrays around the world to monitor Cygnus X-3 almost constantly with a certain degree of overlap between detectors. These detectors are all of greater sensitivity than the original Kiel array. During this time there have been no significant claims of steady, D.C. or pulsed emission of PeV gamma-rays from Cygnus X-3. The one thing that can be stated with confidence is that during the second half of the 1980's Cygnus X-3 was not a source of PeV gamma-rays at the fluxes claimed in the early 1980's.

4·4 c) Cygnus X-3 at Energies Above 10^{17}eV

The energy range over which Cygnus X-3 has been searched for was increased by 3 orders of magnitude with the report by the Fly's Eye group in 1989 (Cassiday et al. 1989). They claimed to observe an excess of showers from the region of Cygnus X-3 with energies above $5x10^{17}$eV. Observations made between 1974 and 1987 with the Haverah Park 12km^2 array failed to confirm the Fly's Eye result (Lawrence et al. 1989). However, both the Akeno (Teshima et al. 1990) and the Yakutsk (Glushkov et al. 1990) groups have obtained positive results from Cygnus X-3 at these energies. A full review of these observations is given in Chapter 5.

4·5 Observations of Underground Muons from Cygnus X-3

To try and eliminate the cosmic ray background proton decay experiments are built deep underground, often in mines. Despite stopping most particles, highly energetic muons or neutrinos can still pass though large thicknesses of rock and be detected. As a result of this, proton decay experiments have an astronomical offshoot. One of the most famous examples of this was the detection by two proton-decay experiments of neutrinos from SN1987A.

The first report of muons apparently coming from the direction of Cygnus X-3 came from the Soudan-1 proton-decay detector located underground at a depth equivalent to 1800m of water. At this depth a muon produced in the atmosphere requires at least 600GeV to reach the detector. Between September 1981 and November 1983 the detector recorded 780,000 single muon events (Marshak et al. 1985). Events were selected that fell within 3° of Cygnus X-3. Using the van der Klis and Bonnet-Bidaud (1981) ephemeris an excess of 60 events on a background of 285 was found in the phase range 0·65-0·90 (Figure 4·6a). This corresponds to a muon flux of $\sim 7x10^{-11}$ cm^{-2}s^{-1} for atmospheric muons of energy greater than 650GeV. This is approximately the observed flux of cosmic rays of 1TeV and above. However, a 1TeV

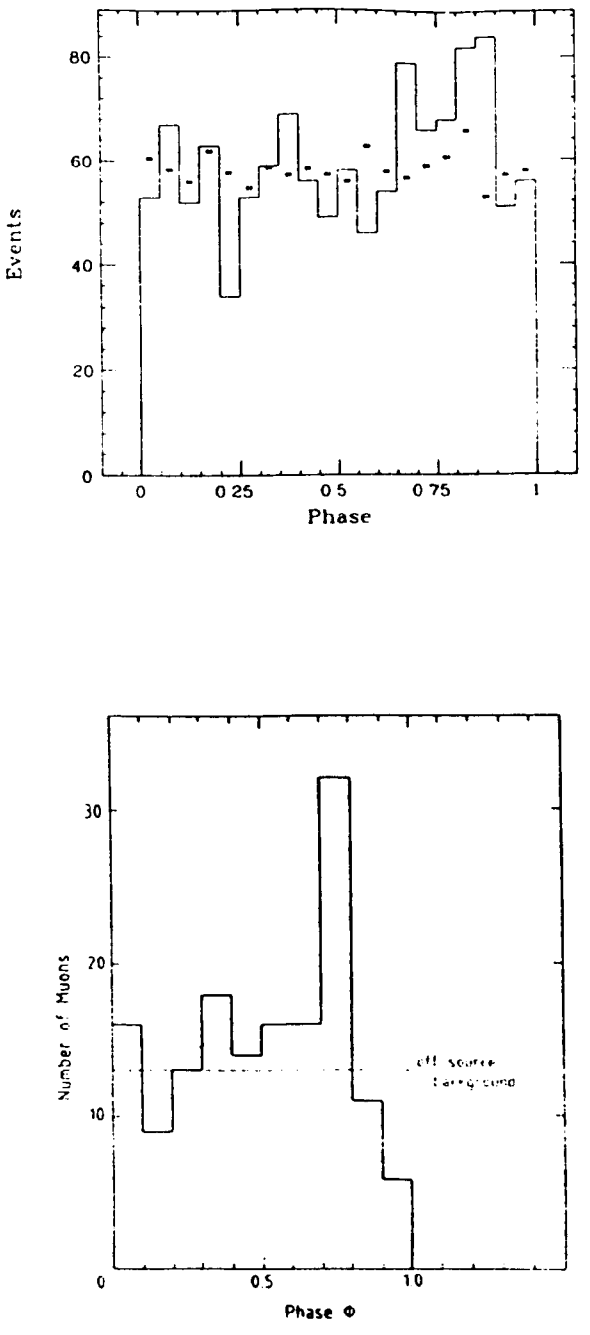

Figure 4·6 The phase distribution of underground muons analysed with the van der Klis and Bonnet-Bidaud (1981) ephemeris. a) shows results from the Soudan-1 experiment between 1981 and 1983 (Marshak et al. 1985). b) shows the results from 1982 to 1985 from the NUSEX experiment (Battistoni et al. 1985).

gamma-ray could not produce a 650GeV muon and so the Soudan-1 threshold energy implies more energetic primaries. Additional data up to 1989 continued to show a phased effect but with a lower significance than the original result (Johns et al 1990).

The NUSEX experiment located beneath Mont Blanc at a depth of 5000m water equivalent also gave a positive result. Being deeper than the Soudan-1 experiment it has a higher threshold energy of 5TeV. Events recorded between June 1982 and February 1985 that fell within a bin 10°x10° centred on Cygnus X-3 were phase analysed (Battistoni et al. 1985). The size of bin used was chosen to maximise the signal. 32 events were seen in the phase bin 0·7-0·8 when 13·0 were expected (Figure 4·6b). This is equivalent to a flux of $(2{\cdot}5\pm0{\cdot}5)\times10^{-12}$ cm^{-2}s^{-1} above 5TeV.

Against these observations are several negative results. The Frèjus experiment is similar to NUSEX and is located 80km away at a depth of 4800m water equivalent. Using the same analysis technique as the NUSEX group an upper limit to the flux of muons from Cygnus X-3 was obtained of $0{\cdot}8\times10^{-12}$ cm^{-2}s^{-1} for E>3TeV (Berger et al. 1986). This limit covers the period February 1984 to January 1986. An update of the NUSEX data (Aglietta et al. 1990) showed that no phase enhanced excess was observed from Cygnus X-3 in 1985 and 1987 so the NUSEX and Frèjus results are not contradictory. The NUSEX update showed that in 1987-1988 the flux returned to the 1982-1984 level. The second negative report came from the Kamioka group (Oyama et al. 1986) operating a detector in Japan at 2400m water equivalent between July 1983 and September 1984. Using a 10°x10° bin centred on Cygnus X-3 they obtain upper limits of $2{\cdot}2\times10^{-12}$ cm^{-2}s^{-1} for E>760GeV and $1{\cdot}7\times10^{-12}$ cm^{-2}s^{-1} for >3TeV. The upper limit for muons of energy 760GeV and above is ~30 times lower than the flux claimed by the Soudan-1 group at similar energies. However, the periods of observation of the two groups overlap for only a few months. Corbató et al. (1990) reported an upper limit to the muon flux above 2·7TeV of $2{\cdot}6\times10^{-13}$ cm^{-2}s^{-1} derived from data recorded between January 1985 and May 1987 at the Homestake Gold Mine (4200m equivalent water depth).

If genuine, the observations of underground muons seriously confuse current ideas about air showers and the nature of the initiating entities. If the primaries are gamma-rays then the flux implied by the underground experiments is much greater than the flux measured by ground based detectors. The muons in the Soudan-1 and NUSEX detectors cannot be the secondaries of neutrinos interacting in the rock above the detectors as the observed zenith angle distributions indicates atmospherically produced muons. Because of these problems new particles have been put forward to explain the flux, including dibaryons and photinos (see Weekes 1988 for review). However, the experimental evidence is as yet not sufficiently conclusive to warrant the invoking of such exotic effects.

4·6 Models of the Cygnus X-3 System

Cygnus X-3 is thought to be a close (~$5x10^8$m) binary system consisting of a neutron star and a companion star. This is the most plausible explanation for the 4·8hr X-ray periodicity observed. However, the lack of an easily observable optical counterpart means that the binary nature of Cygnus X-3 cannot be confirmed. Numerous different models have been proposed to explain the exact method of X-ray modulation. Milgrom (1976) suggested that the binary system is surrounded by a thick (~1gcm^{-2}), hollow shell of matter evaporated from the companion by X-ray heating. X-ray and IR photons are scattered in the surrounding cocoon. The modulation is caused by the rotation shadow of the binary system on the cocoon. The asymmetry of the modulation is explained by invoking an eccentric orbit. A second model, proposed by Pringle (1974), has the X-ray modulation caused by material in a stellar wind from the companion scattering the X-rays. The motion of the compact X-ray source in the material of the stellar wind results in varying amounts of scattering material between the source and the observer. However, this model fails to explain the IR modulation. A third model (White and Holt 1982) has the X-ray source surrounded by an optically

thick cloud of gas evaporated off the surface of an accretion disc. X-rays are scattered within this cloud which is not expected to be exactly spherical. It is the bulges in the cloud that produce the modulation.

During the 1983 radio flare the radio source was seen to expand symmetrically about the position of Cygnus X-3 (Spencer et al. 1986). The flares are therefore thought to be caused by synchrotron radiation from a rapidly expanding cloud of relativistic electrons.

The production of PeV gamma-rays is thought to be a two stage process. Most models assume the presence of a pulsar near which protons are accelerated to high energies.Chanmugam and Brecher (1985) have suggested that an accretion disc with an embedded magnetic field, $\underline{B}$, orbiting the neutron star with an orbital velocity $\underline{v}$ would produce an electric field $\underline{E} = \underline{B} \times \underline{v}$. A potential drop of up to 100PeV could develop. A second method has acceleration in the electric field produced by a fast spinning pulsar (Hillas 1987b). For a magnetic field of 10^{12}G and a millisecond pulsar particle energies of up to 10^{17}eV could be achieved.

The acceleration site and the gamma-ray production sites cannot be co-located. PeV gamma-rays have a pair production mean free path of less than 1km if the magnetic field strength is greater than 10^{4}G. Therefore, gamma-rays produced in the acceleration regions will be unable to escape. The generally accepted picture of gamma-ray production has the high energy protons hitting a cloud of dense gas in a region of low magnetic field. The collisions produce neutral pions (amongst other particles) which then decay to form gamma-rays. To explain the TeV and PeV light curves, with peaks in the 4·8hr period at phases 0·2 and 0·6, Vestrand and Eichler (1982) suggest that gamma-rays are produced by protons hitting the outer atmosphere of the companion star. Figure 4·7 shows schematically how the observed pre-eclipse and post-eclipse gamma-rays could be produced. The optimum thickness of intervening material is ~100gcm^{-2}. As the neutron star goes into eclipse the gamma-ray flux increases until the optimum thickness is reached. When the neutron star moves further behind the

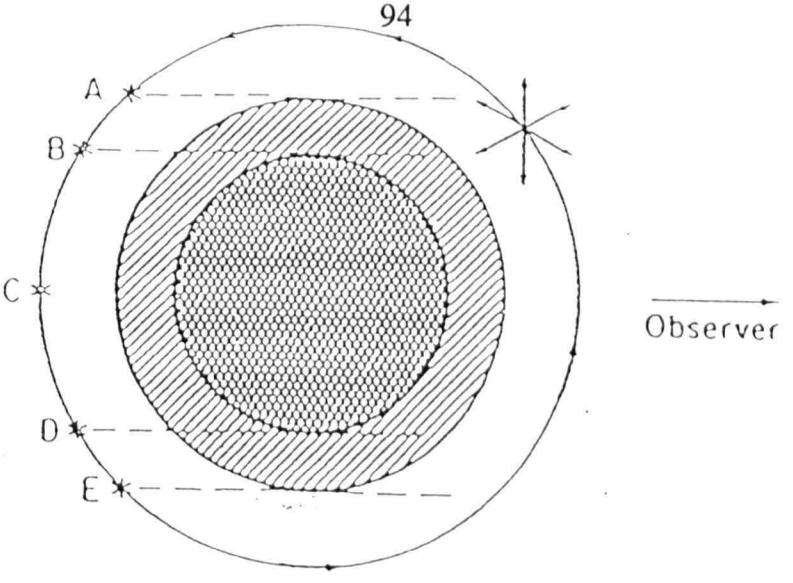

Figure 4·7 A schematic representation of the production mechanism of the UHE and VHE gamma-ray light curve from Cygnus X-3 (Vestrand and Eichler 1982). The cross-hatched region is the main body of the star with the atmosphere being the shaded region. When the atmosphere is between the observer and the source of high energy particles (i.e. when the source is between positions A and B or positions D and E) gamma-rays may be observed. C is the point of X-ray minimum.

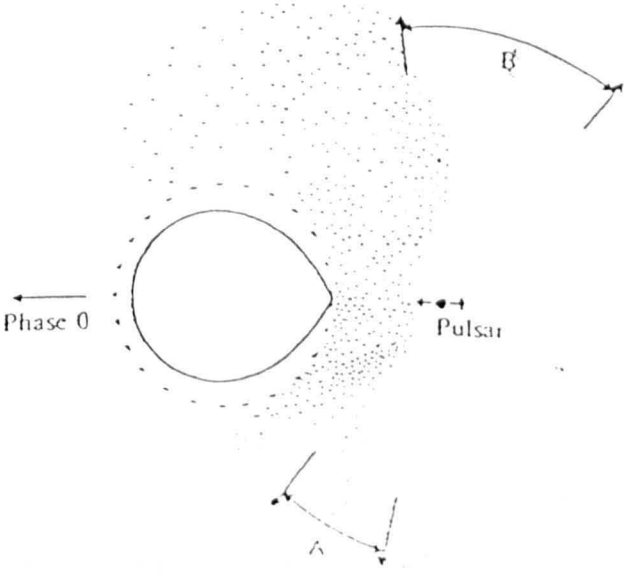

Figure 4·8 Cygnus X-3 model according to Hillas (1984). The pulsar ejects a fountain of material from the companion star. The ejected material then form a target for gamma-ray production. The approximate directions to the observer when gamma-ray burst are observed are shown (A, phase ~ 0·2, B, phase ~ 0·75).

companion the flux falls rapidly as gamma-rays are absorbed in the atmosphere.

An alternative model has been proposed by Hillas (1984). A monoenergetic beam of 10^{17}eV protons striking the companion star will lift off material from the atmosphere of the companion (see Figure 4·8). The interaction of the proton beam with this liberated material produces the gamma-rays observed. As the thickness of material increases, the initial protons can interact more than once, losing energy at each collision and so producing gamma-rays of lower energy. This model explains the observed gamma-ray spectrum from ~20PeV to ~1TeV.

4·7 Search for Cygnus X-3 in the GREX Data Set

4·7 a) Introduction

The GREX array was one of the first instruments to be built specifically to search for point sources of PeV gamma-rays. Since beginning to collect data in March 1986 the array has operated with an efficiency of almost 90%. This section will deal with a search made for PeV gamma-ray emission from Cygnus X-3 in almost five years of GREX data from 6 March 1986 to 18 December 1990.

Showers were used in the search if an arrival direction could be found by fitting a curved shower front to the detector times recorded, as described in Chapter 2. In addition, showers were only selected if the shower core fell within the array boundary, the calculated zenith angle was less than 40° and $S(50)>0{\cdot}7m^{-2}$ (equivalent to an energy of $\sim 4{\cdot}8\times10^{14}$eV for events at 20° to the zenith). The last two selection criteria were applied as the parameterisation of the array effective area breaks down for very small showers and for those at large zenith angles (see section 2·6). Knowledge of the effective area is required for flux calculations (see below).

Following these cuts over 21 million 'good' events remain available for source searches. The previous chapter described the main methods used to search the GREX data set. The azimuthal method provides a highly accurate day-by-day background

estimate and is especially useful for looking at excesses over short periods. However, as every event is weighted to the source azimuthal position, the method is sensitive to errors in the weighting. Over large periods this method may result in systematic errors. For this reason the equal exposure method is also used to provide an independent check on the cumulative background measurement. Also, if the source transits too close to the zenith the azimuthal method cannot be used.

Era	Lower S(50) limit	Vertical shower energy (10^{14}eV)	Circular bin radius (r)	Square bin ($\Delta\delta$)	($\Delta\alpha$)
Pre-ADC change	0·5	2·6	1·65	1·46	1·93
	2·0	8·0	1·31	1·16	1·54
	8·0	24·3	0·85	0·75	1.00
Unleaded	0·5	2·6	1·35	1·20	1·58
	2·0	8·0	1·10	0·97	1·29
	8·0	24·3	0·77	0·68	0·90
Leaded	0·5	2·6	1·21	1·07	1·42
	2·0	8·0	0·98	0·87	1·15
	8·0	24·3	0·67	0·59	0·79

Table 4·1 The radius of circular on-source bins and the declination and right ascension half widths for square bins as a function of shower size and array era.

Table 4·1 gives the on-source bin sizes used in the search as a function of shower size. Those for the azimuthal method are the same as are given in section 3·2c. For the equal exposure method the declination half width ($\Delta\delta$) is given by

$$(2\Delta\delta)^2 = \pi r^2$$

where r is the circular bin angular radius. The right ascension half width ($\Delta\alpha$) is given by:-

$$\Delta\alpha = \Delta\delta / \cos\delta$$

where δ is the declination of Cygnus X-3 (The coordinates of Cygnus X-3 are δ_{1988} = 40·91, α_{1988} = 307·99).

4·7 b) Steady D.C. Signal

Between the 6 March 1986 and 18 December 1990 there are 1587 sidereal days on which Cygnus X-3 was above the detector horizon (i.e. closer to the zenith than 40°) while the array was collecting data. The total exposure time to Cygnus X-3 was 11490 hours. For the azimuthal method a total of 5452 events were observed on-source with a background of 5493·2, a deficit of 0·55σ. The equal exposure method gave 5450 events on-source with a background of 5474·0 off-source, a deficit of 0·30σ. The virtually independent background estimates produced by the two methods are not significantly different. This suggests that systematic errors in the azimuthal method have been reduced to an insignificant level. Figure 4·9 shows the cumulative 'excess' from the direction of Cygnus X-3 as a function of time. Also shown are the $\pm 1\sigma$ significance levels.

As no excess is observed from Cygnus X-3 only an upper limit to the possible flux can be given. A small flux could easily be lost in a downward fluctuation of the background flux in the on-source bin. Protheroe (1984) has given the 95% confidence limit to the number of events that could have originated in the source (S_{95}) as:-

$$S_{95} = \alpha \sqrt{B}$$

where B is the mean background estimate and α the 'Protheroe Factor'. α depends on the on-source count, background count and number of off-source bins. For 5450 on-source events, a mean background of 5473·0 and 6 off-source bins the Protheroe Factor is 1·8. This gives an upper limit to the number of events recorded in the

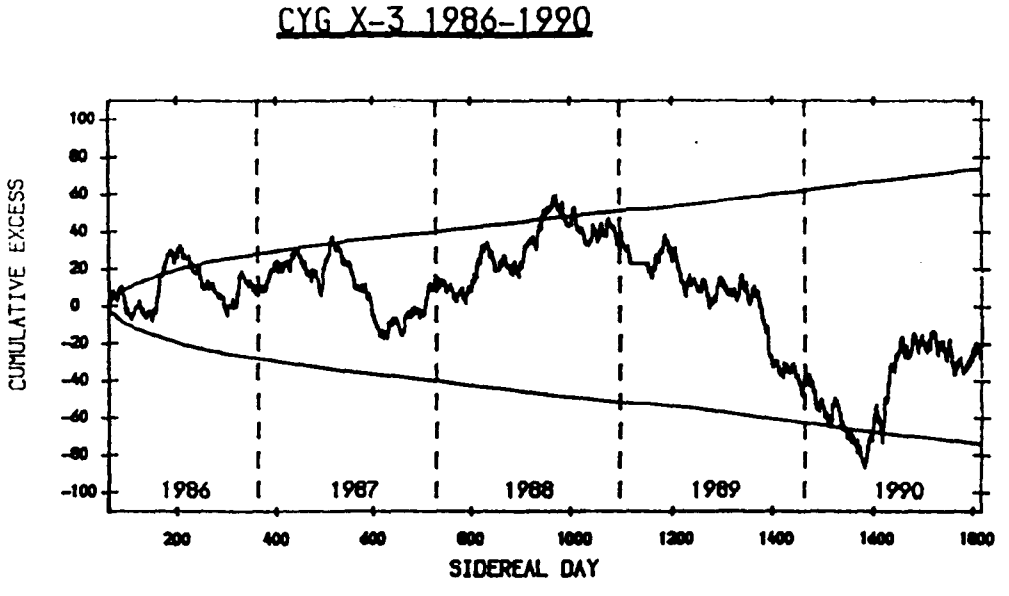

Figure 4·9 The cumulative 'excess' number of events from Cygnus X-3 as recorded by the GREX array as a function of sidereal day. Day 0 corresponds to Jan 0·0 1986. Also shown are the $\pm 1\sigma$ levels.

on-source bin that could of come from the source of 133·2.

The effective area A_i was summed for all i background showers as described in section 2·6. The off-source flux, F_B, was then determined by:-

$$F_B = \left(\frac{N_{off}}{\Sigma A_i}\right)\left(\frac{N_{off}}{T_{on}\, N_B}\right)$$

where T_{on} is the on-time, N_B the number of background bins and N_{off} the total number of off-source events. The on-time is corrected to account for the array dead-time following each event. This dead-time has decreased with faster recording electronics over the lifetime of the array.

With the mean background flux, the background count and the 95% confidence upper limit to the source count the upper limit to the flux, U_{95}, can be calculated as

$$U_{95} = F_B \frac{S_{95}}{(B \times 0{\cdot}7)}$$

As was stated in section 3·2c the on-source bins are of a size such that they will contain 70% of the signal from a point source situated at the centre of the bins. For this reason the factor of 0·7 is included in the above equation. Table 4·2 gives the 95% upper limit to the flux from Cygnus X-3 derived from almost five years of GREX data as a

Energy (eV)	On-source count	Mean off-source count	Protheroe factor	S_{95}	Flux ($cm^{-2}s^{-1}$)
$>4\times10^{14}$	5450	5474·0	1·8	133·2	$1{\cdot}93\times10^{-14}$
$>1\times10^{15}$	2353	2330·8	2·4	115·9	$1{\cdot}44\times10^{-14}$
$>4\times10^{15}$	50	62·2	1·4	11·0	$1{\cdot}35\times10^{-15}$

Table 4·2 The 95% confidence upper limits to the flux from Cygnus X-3 as a function of energy.

function of energy. These data are also plotted in Figure 4·10 together with the original Samorski and Stamm (1983a) and Haverah Park (Lloyd-Evans et al. 1983) fluxes and some recently reported upper limits from other experiments.

4·7 c) Emission Modulated With the 4·8 Hour X-ray Period

Except for the original Kiel PeV detection (Samorski and Stamm 1983a) and (possibly) the Ooty report (Tonwar et al. 1988) all claims of emission of PeV gamma-rays from Cygnus X-3 have relied on modulation of the signal by the 4·8hr X-ray period. A small signal may be lost if it is not significant compared to fluctuations in the background. However, if the source is emitting periodically the signal will be observed at a certain period (or periods) whereas the background events will be distributed randomly across the entire cycle.

The number of events (typically ~5) observed in the Cygnus X-3 bin is too small to look at emission over a single 4·8hr cycle. To obtain a phase distribution of events recorded over many cycles it is necessary to determine the phase of each event. For an event recorded at time t the number of cycles (n) that have passed since an epoch time t_0 is given by:-

$$n = \frac{t - t_0}{P} - \frac{1}{2}\dot{P}\left(\frac{t - t_0}{P}\right)^2$$

where P is the period and $\dot{P}$ the period derivative. The phase is then the fractional part of n. Obviously, if the data have been collected over a large number of cycles it is important that P and $\dot{P}$ are known as accurately as possible. Large uncertainties in P and $\dot{P}$ could lead to a peak at a certain phase being widened and, therefore, made less significant. The Cygnus X-3 4·8hr ephemeris giving the values of P and $\dot{P}$ that are most apt for the time over which the GREX data were collected is the van der Klis and Bonnet-Bidaud (1989) ephemeris. This was derived using a wide range of X-ray observations made over 15 years from 1971 and includes the EXOSAT observations of

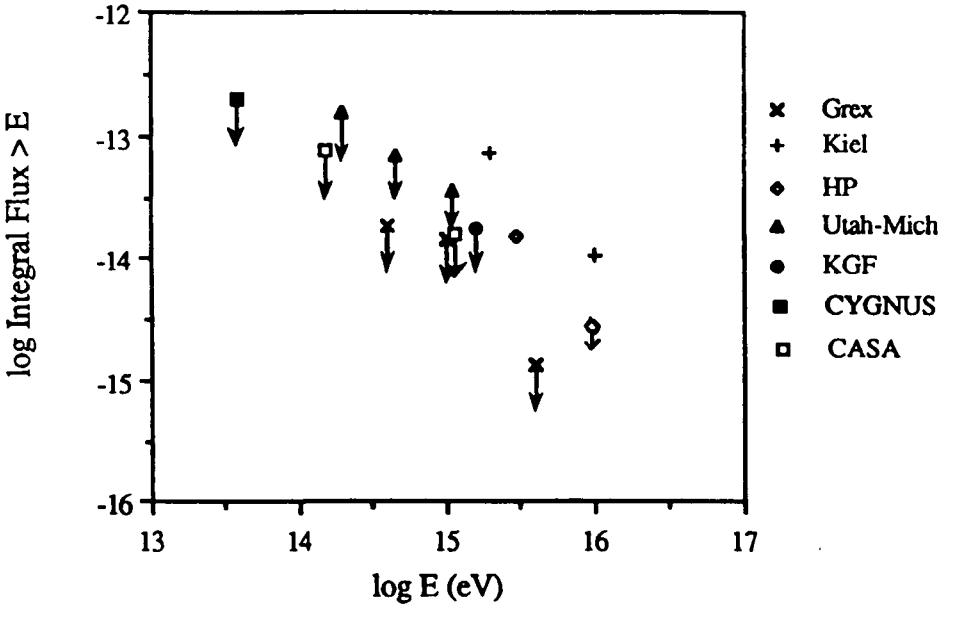

Figure 4·10 Integral flux (in $cm^{-2}s^{-1}$) of PeV gamma-rays from Cygnus X-3. The plain crosses and arrows show the upper limits set by this work. The original Samorski and Stamm (1983) fluxes are shown (+), as is the Lloyd-Evans et al. (1983) confirmation (open diamond). Also shown are the upper limits set by the Utah-Michigan group (Ciampa et al. 1990) (filled triangles), the KGF group (Sinha et al. 1991)(filled circle), the CYGNUS group (Alexandreas et al. 1991)(filled box) and the CASA group (Ong 1991)(open box).

1983-1985. As such, the data from which the ephemeris was derived were recorded before the commissioning of the GREX array. However, it is the most up to date ephemeris available. The parameters of the ephemeris are:-

t_0 = HJD 2 440 949·896 22 ± 0·000 94

P = 0·199 683 54 ± 0·000 000 15d

$\dot{P}$ = $(0{\cdot}904 \pm 0{\cdot}048) \times 10^{-9}$

van der Klis and Bonnet-Bidaud claim that the formal uncertainties of the ephemeris should be less than 1% of an orbital cycle (i.e. less than 3 minutes) until 1991.

Before calculating the phase of an event the arrival time must be corrected for the motion of the Earth round the Sun. It takes light approximately 17 minutes to travel the diameter of the Earth's orbit. If not compensated for this motion could obscure any source signal. For Cygnus X-3, which is at an ecliptic latitude of 56·9°, the maximum modulation is just under 11 minutes or 4% of a cycle. To avoid widening a potential peak the arrival times are corrected to the heliocentre. The correction (Δt_H) is given by (Lambert 1985):-

$$\Delta t_H = \frac{D}{c} \cos\beta \cos\left(2\pi\left[\left(\frac{t - t_\gamma}{T_E}\right) - \left(\frac{\lambda - 180}{360}\right)\right]\right)$$

where D = mean Sun-Earth distance

c = speed of light

T_E = Earth orbit duration 365·24 days

t = Julian Date (JD) of terrestrial observation

t_γ = JD 2 439 205·578 5 :1966 March 21 1·53hr UT (date of vernal equinox)

β, λ = source ecliptic latitude and longitude (56·90°, 328·41° for Cygnus X-3)

Although this correction assumes that the Earth's orbit is circular it gives heliocentric times accurate to better than 10s.

Figure 4·11 is the 4·8hr phasogram for Cygnus X-3 for the entire data set between 6 March 1986 and 18 December 1990. The on-source and off-source events are those found using the azimuthal method. This method has the advantage of recording on-source and off-source events simultaneously. The closeness of the 4·8hr period to 0·2 of a day means that care must be taken to avoid accidental harmonics. Collecting the on-source and off-source at the same time avoids this problem. As can be seen there are no outstanding features in the phasogram. A Rayleigh test on the phasogram produces a first harmonic with a 66% probability of occurring by chance.

4·7 d) Search for Sporadic Emission of Unknown Duration

All the evidence of TeV and PeV observations point to Cygnus X-3 being highly variable and sporadic. Owing to the low count rate it is not reasonable to look for sporadic emission on time scales less than one source transit i.e. ~7·7hr. In Figure 4·12 the differential distribution of the daily excess number of counts in the Cygnus X-3 bin is shown for all days on which Cygnus X-3 was observed. Once again the azimuthal search method has been used in this analysis as it provides a background measurement less susceptible to statistical fluctuations than the equal exposure method. Also shown is the distribution expected from Poissonian fluctuations. The most significant excesses are listed in Table 4·3. Considering the trials involved in looking at 1587 days the days listed do not provide evidence for emission on time scales of a few hours.

One of the major problems in searching a data set for sporadic emission of unknown duration is evaluating the significance of any observed effect. A very large number of statistical trials will be used if there is no a priori timescale over which to search and any excess will have to be large to produce a significant result. A technique has been developed by J. Lloyd-Evans and applied to the GREX data to attempt to avoid these problems (Beaman et al. 1991).

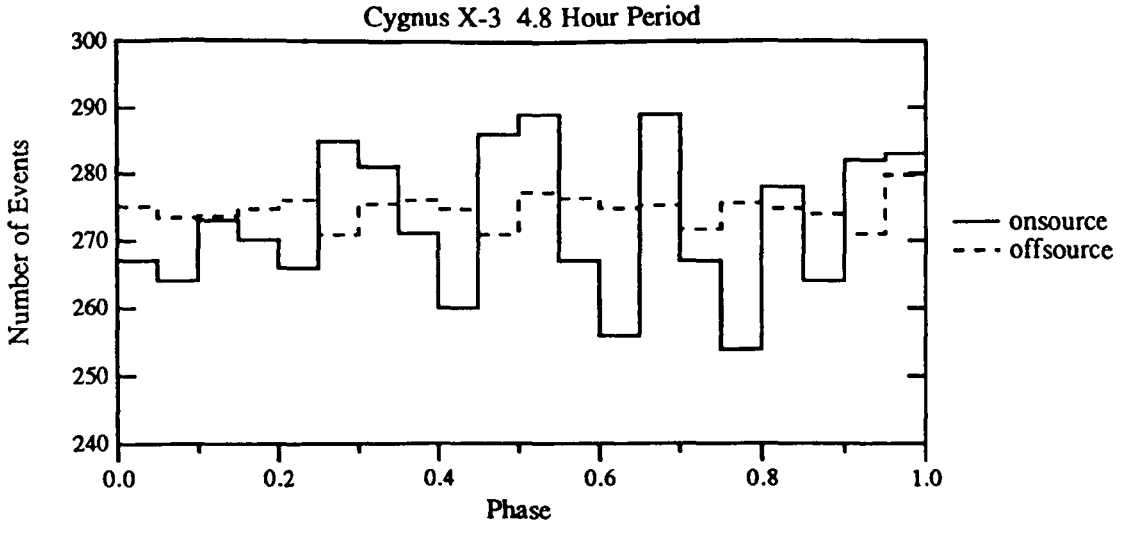

Figure 4·11 4·8hr phasogram of all events in the Cygnus X-3 on-source bins for the entire GREX data set (solid line). The events have been analysed using the van der Klis and Bonnet-Bidaud (1989) X-ray ephemeris. The background estimate (dotted line) is derived from ~50 times the number of on-source events.

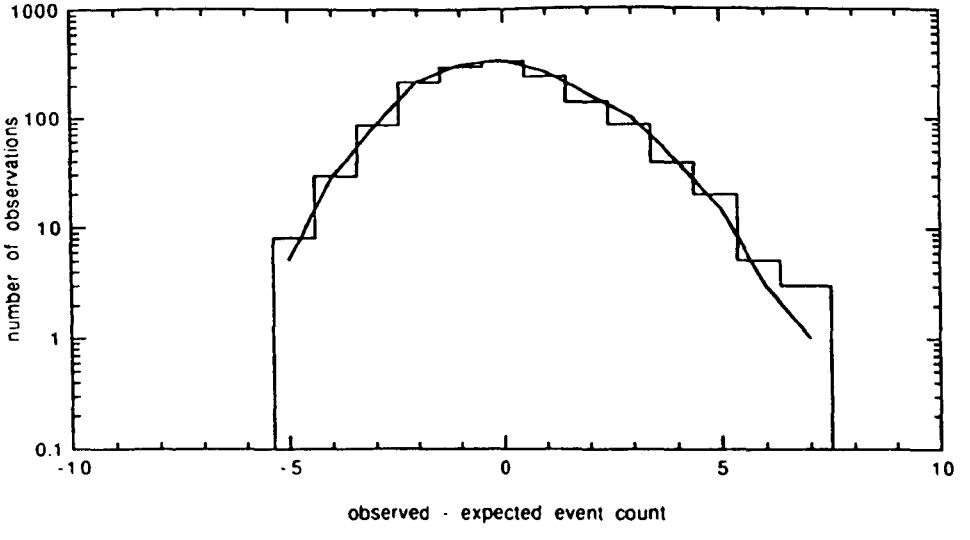

Figure 4·12 The differential distribution of daily excesses from Cygnus X-3. The histogram is the on-source data and the line the expected curve expected from Poissonian fluctuations.

On-time (hours)	Date	On	Off	Poissonian Probability (%)
7·6	14/05/87	9	3·4	0·8
4·6	16/11/87	6	1·7	0·8
7·7	13/12/87	9	3·4	0·8
4·6	29/09/89	2	0·1	0·5
7·7	24/02/90	12	4·8	0·4
7·7	16/06/90	11	4·2	0·4
7·7	08/09/90	11	4·6	0·8

Table 4·3 The set of days on which the Poisson probability of seeing at least the observed number of count was less than 1%. The background estimates are derived from the azimuthal method.

The entire data set was split into two halves, A and B, with alternate preselected events being placed into the halves. The events in A and B were then analysed in the usual manner. Set A was scanned for evidence of emission by sliding windows of duration T = 2, 4, 8, 16, 32, 64, 128 and 256 days across the complete set. A window was considered a candidate period if the Poisson probability of observing the on-source counts was less than 5% (after accounting for trials). This probability is then ignored and the probability of emission is obtained from the blind set B. The process was then repeated with set B being searched and set A as the blind set. Obviously, if the candidate window corresponds to a period of emission then an excess will be observed in the second set.

One window was discovered of 256 days duration from 26/10/87 to 06/06/88 when 381 events were observed on a background of 322 for the scanned data set. During the same period 305 events were observed on-source on a background of 321 in the blind set. There is therefore no evidence of sporadic emission from Cygnus X-3.

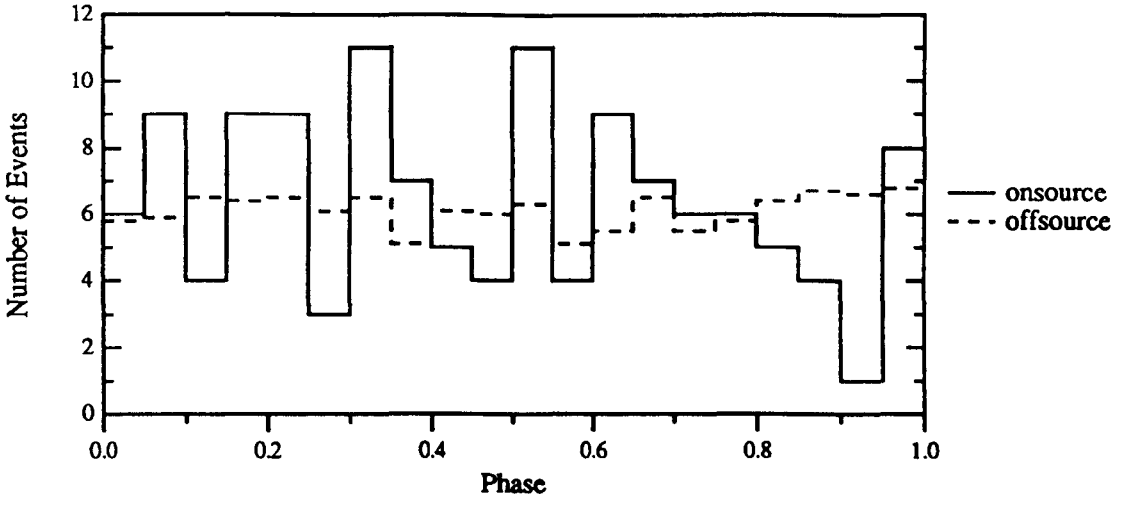

Figure 4·13 4·8hr phasogram of all events in the Cygnus X-3 recorded by the GREX array in the 45 days following 17 April 1986 (solid line). The events have been analysed using the Mason (1986) X-ray ephemeris. The background estimate (dotted line) is derived from ~50 times the number of on-source events.

4·7 e) May 1986 - Period of Baksan / Los Alamos Excess

As stated in section 4·4a the Baksan group observed in 1986 an excess from Cygnus X-3 of ~2·8σ which was modulated with the 4·8hr period (Alexeenko et al. 1987). The majority of the signal was seen in May and September-November. The CYGNUS experiment also claimed evidence for a burst lasting for 45 days starting on 17 April 1986 (Dingus et al. 1988b). Analysis of the same 45 day period shows no evidence of emission in the GREX data set with 128 events on-source and a mean background of 121·8. If the period is restricted to just May 1986, 72 events are seen on-source on a background of 77·1.

When the Baksan group phase analysed the events in their excess a peak was observed in the range 0·5-0·8 (see Figure 4·5g). The Los Alamos group saw a peak between 0·65 and 0·85 (Figure 4·5h). The GREX events in the Cygnus X-3 bin for the 45 days following 17 April were analysed using the Mason (1986) ephemeris. This is the ephemeris that was used by the Los Alamos group (the ephemeris used by the Baksan group is not given). As can be seen from Figure 4·13 there is no evidence of phase enhanced emission in the GREX data at either the Baksan or Los Alamos phases.

4·7 f) Correlation with Large Radio Flares

Since the first detected flare in 1972 large radio flares have been observed from Cygnus X-3 roughly once a year. There have been claims linking the emission of TeV and PeV gamma-rays with these flares (see sections 4·3a and 4·4a). The first flare following the commissioning of the GREX array was in June 1989. Over two days the radio flux at 8·08GHz rose from the quiescent level to a peak of 18Jy on 2 June (Waltman et al. 1989a). The flux then gradually fell over the next 17 days with 4 smaller flares of between 1 and 4Jy being observed. A second major flare was then observed on the 21st July when the flux again reached 18Jy (Waltman et al. 1989b).

Figure 4·14 shows the daily Cygnus X-3 on-source and off-source counts for the period 23/05/89 to 15/08/89. The background estimates are derived from the azimuthal

method. The dates of the 18Jy radio flares are marked. The Ōhya group claim to have detected a 4·7σ excess on 27 May and a 3·4σ excess on 16 June (Muraki et al. 1991). For these two days the GREX array observed 1 event on a background of 2·57 and 4 on a background of 3·88. It should be noted that the GREX array was not recording on 31 May and 1 June due to power failure.

A year later Cygnus X-3 again underwent a large radio flare. This was not as violent as the 1989 flares with the flux reaching 8Jy at 8·3GHz on 15 August 1990 (Waltman et al. 1990). Figure 4·15 is similar to Figure 4·14 but here the data come from 10 August to 10 September 1990. Once again there does not appear to be any obvious enhancement following the flare.

4·8 Conclusions

If it is assumed that the effects reported by Samorski and Stamm (1983a) and Lloyd-Evans et al. (1983) were genuine observations of PeV gamma-rays it must be concluded that Cygnus X-3 has either stopped emitting or is emitting with a greatly reduced flux. The extensive air shower arrays that have been purpose built to search for sources of PeV gamma-rays have much improved sensitivity compared to the original instruments of the late seventies and early eighties. Therefore, if Cygnus X-3 was still emitting at the flux originally reported there would now be many unambiguous observations. However, there have been no statistically reliable claims of emission made in the past 5 years.

The work described in the second part of this chapter places upper limits to the flux from Cygnus X-3 that are more than an order of magnitude lower than the original claimed fluxes. This is in agreement with the results from most other groups working in the late 1980's. The early promise of Cygnus X-3 to provide a PeV 'standard candle' has not been fulfilled.

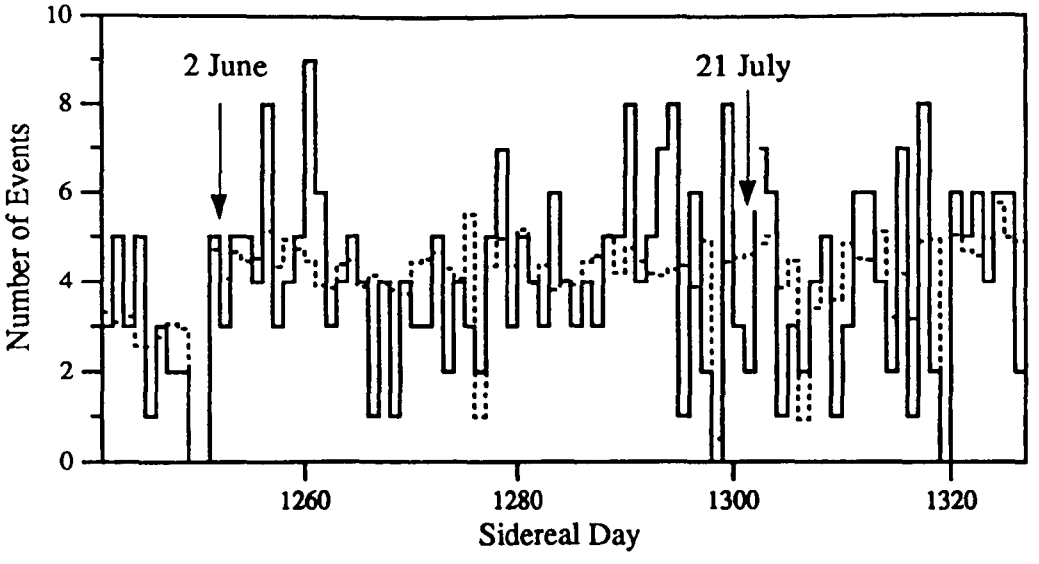

Figure 4·14 The Cygnus X-3 on-source count (solid line) and mean background count (dashed line) as recorded by the GREX array covering the period of 23 May 1989 to 15 August 1989. The dates of maximum radio flux are shown for the flares in June and July.

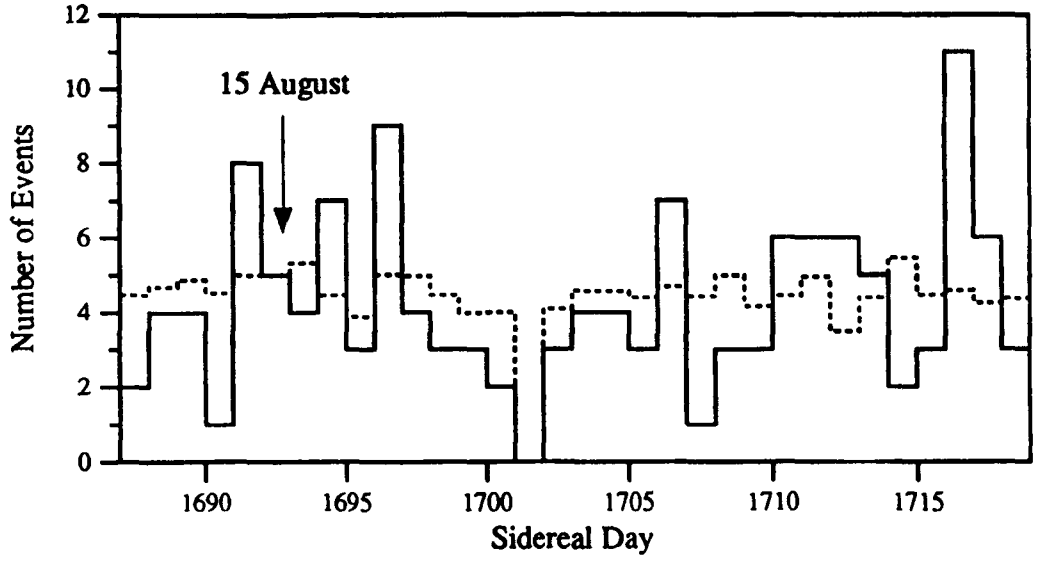

Figure 4·15 The Cygnus X-3 on-source count (solid line) and mean background count (dashed line) as recorded by the GREX array covering the period of 10 August 1990 to 10 September 1990. The date of the maximum radio flux is shown for the August 1990 flare.

CHAPTER 5

CYGNUS X-3 AT ENERGIES ABOVE $5x10^{17}$eV

5·1 Introduction

The 1980s saw the emergence of compact systems such as Cygnus X-3 as the main candidates for the production sites of PeV cosmic rays. Following experimental observations models were produced in which particles could acquire energies up to 10^{17}eV (see Chapter 4). However, the cosmic ray energy spectrum continues upwards for at least an additional three orders of magnitude and the mechanisms for producing particles with such energies still remain unknown.

In 1989 the Fly's Eye group from the University of Utah reported the detection of Cygnus X-3 at energies greater than $5x10^{17}$eV (Cassiday et al. 1989). Observations made between November 1981 and May 1988 resulted in a flux of $(2{\cdot}0\pm0{\cdot}6)x10^{-17}$ particles $cm^{-2}s^{-1}$. Following the publication of the search made of the Haverah Park $12km^2$ data set (Lawrence et al. 1989), the Akeno group claimed confirmation of the Fly's Eye result (Teshima et al. 1990) obtaining a flux of $(1{\cdot}8\pm0{\cdot}7)x10^{-17}$ particles $cm^{-2}s^{-1}$ for data collected between December 1984 and July 1989.

The $12km^2$ extensive air shower array had been operated at Haverah Park and a large data set exists of events with energies greater than 10^{17}eV recorded from 1974 until the array shut down in 1987. The major objectives of the $12km^2$ array were to determine the primary cosmic ray spectrum and mass composition and to search for large scale anisotropy at high energies, in particular to determine whether the highest energy particles were galactic or extragalactic in origin. Previous relatively crude searches for cosmic ray point sources had been made (Blake et al. 1967, Lapikens 1974) without any deviations greater than expected through statistical fluctuations from isotropy being found. Despite this it was felt that at the flux claimed by the Fly's Eye group Cygnus X-3 could be seen in the Haverah Park data.

This chapter describes a search performed by the author for evidence of Cygnus X-3 as a point source of neutral particles above $5x10^{17}$eV using the Haverah Park data set. Also the claimed detections of Fly's Eye and Akeno groups are critically compared.

5·2 The Haverah Park 12km^2 Array

The Haverah Park 12km^2 extensive air shower array (more fully described in Lawrence et al. 1991a) underwent many modifications during its long operational life. For the purpose of this work it can be thought of as consisting of two components. The first component was made up of four 34m^2 deep water-Čerenkov detectors. Three of these detectors were equally spaced around the circumference of a circle of 500m radius centred on the fourth (A1) (Figure 5·1). The array was triggered when signals were seen in the central and any two other 500m detectors. The second component was composed of six groups of four 13·5m^2 detectors, with the groups being equally spaced 2km from A1. Each detector was built up from water-Čerenkov modules made of galvanised iron tanks 1·2m deep and 2·29m^2 in area and viewed with a 5 inch diameter photomultiplier.

An arrival direction for each shower was found by fitting a plane to the relative arrival times recorded at the triggered 500m detectors. Information from all the triggered detectors was then used to find the position of the shower core using a χ^2 minimisation technique similar to that described for the GREX array in Chapter 2. It was found (Hillas et al. 1971) that the relationship between the density at 600m ($\rho(600)$) and primary energy was almost linear and only weakly dependent on models of particle interactions within air showers. The primary energy (E) is given by:-

$$E = 7{\cdot}04x10^{17}\,\rho(600)^{1{\cdot}018}\ eV$$

Fitting a plane to the triggered 500m detectors resulted in reconstructed primary

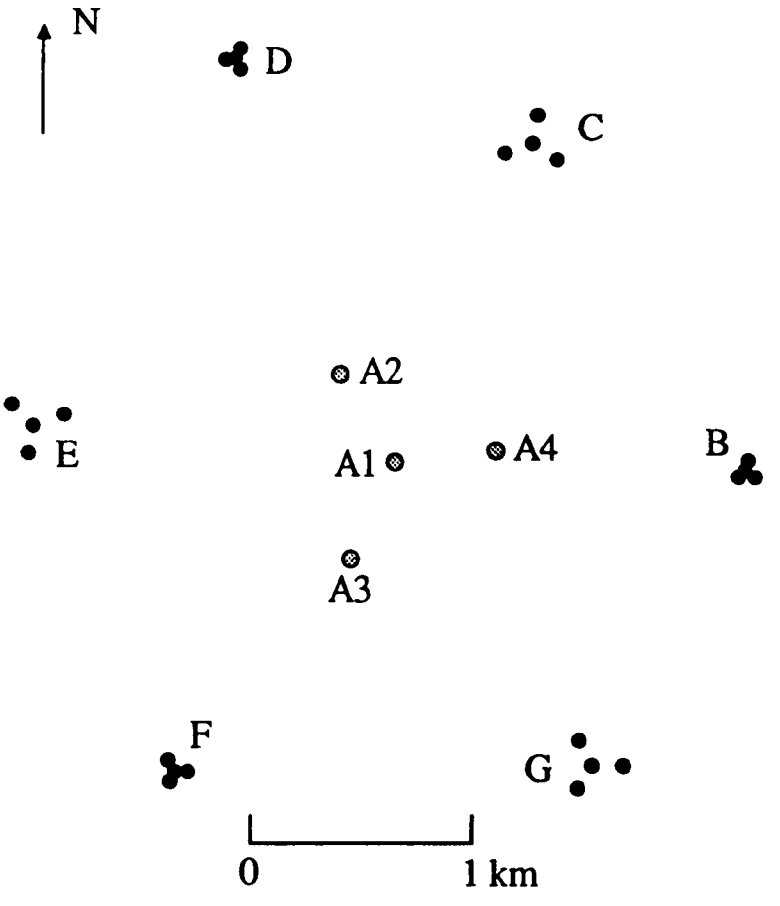

Figure 5·1 The major components of the Haverah Park 12km^2 extensive air shower array. The lightly shaded circles are the four 34m^2 triggering detectors. The sub-arrays B-G are six groups of four detectors which gave information on the shower size and core position.

arrival directions that were accurate enough (angular resolution ~4°) for energy spectrum and anisotropy work, particularly as anisotropies in the form of significant first and second harmonics were sought. However, it is well known that the shower front of an extensive air shower is curved and for optimum point source searches the arrival directions must be corrected for this curvature. Corrections can be made to the original plane fit zenith and azimuth angles (θ,ϕ) to give corrected angles (θ_c,ϕ_c) which take account of the curvature. The corrected angles are given by (Dennis 1964) :-

$$\tan\phi_c = (R \sin\theta \sin\phi - X)/(R \sin\theta \cos\phi - Y)$$
$$\tan\theta_c = (R \sin\theta \sin\phi - X)/(R \cos\theta \sin\phi_c)$$

where X and Y are the co-ordinates of the shower core on the ground measured from the centre of the array (0,0). R is the radius of curvature assigned to a shower. To describe the curved shower front all the secondary particles can be thought of as originating from one point on the shower axis; the distance from this point to the shower front at the detectors being the radius of curvature. Lapikens (1974) gives the radius of curvature as

$$R\,(km) = [\, 1{\cdot}9 + 3 \log_{10} (10\, \rho(600)) \,] \, (\sec\theta)^{1{\cdot}5} \qquad \text{eq. 5·1.}$$

The values obtained for the radius of curvature are unique to Haverah Park 12km^2 array, as is the usefulness of $\rho(600)$ in determining the primary energy, and are not applicable to extensive air shower arrays in general.

Lapikens (1974) found that the shower front was not simply described by a curve of constant radius. For vertical showers split into bins of similar $\rho(600)$ the radius of curvature varied along the shower front with distance from the shower core. For example, for a $\rho(600)$ of 5·5m^{-2} (= 4x10^{18}eV) the radius of curvature varied from 6·0km at a core distance of 500m to 7·5km at 1100m. Equation 5·1 gives a radius of curvature of 7·1km for a vertical shower of the same size. The radius of curvature was

taken to be approximately independent of distance and a single radius used to describe the curvature for a given $\rho(600)$ and zenith angle. However, disregarding the change in radius of curvature with core distance will lead to a source of error in calculating arrival directions which needs to be considered when determining the angular resolution of the array. In addition, for the zenith angle power relation in eq. 5·1 the index is only known to ±20% and this uncertainty will lead to further errors in the radius of curvature (up to ±8% at 40°) and therefore in the angular resolution.

To assess these errors in the calculation of the radius of curvature the r.m.s space angle difference (ψ_{rms}) between uncorrected (plane fit) and curvature corrected directions was plotted against radius of curvature (Figure 5·2) for events with $E > 5x10^{17}eV$ and $\theta_c < 60°$. In addition for each shower two further directions were found, one using a radius of curvature 20% smaller than the value given by eq. 5·1 for that shower and the other using a radius 20% larger. The space angle differences between the new directions found with altered radii of curvature and the plane fit direction were also plotted.

The median radius of curvature for the 23587 events that fell within the array boundary, had energy greater than $5x10^{17}eV$ and zenith angle less than 60° was 7km, with less than 20 events having a radius of curvature of greater than 19km. The decrease in ψ_{rms} at high values of radius of curvature is due to the limit placed on the shower core distance. For any event where the distance (r) from the shower core to the centre of the array is greater than 2km (i.e. the shower falls without the array) the accuracy with which the arrival direction and the primary energy can be determined is greatly reduced and so the event is discarded. The maximum possible space angle difference between a corrected and uncorrected direction is $\psi_{max} = r / 2R$ and so a limit on the shower core distance of 2km will limit ψ for showers with radius of curvature greater than 20km to less than 2·9°.

From Figure 5·2 a value of 0·7° was taken as being the typical uncertainty in the arrival direction due to uncertainties in the radius of curvature assigned to the shower

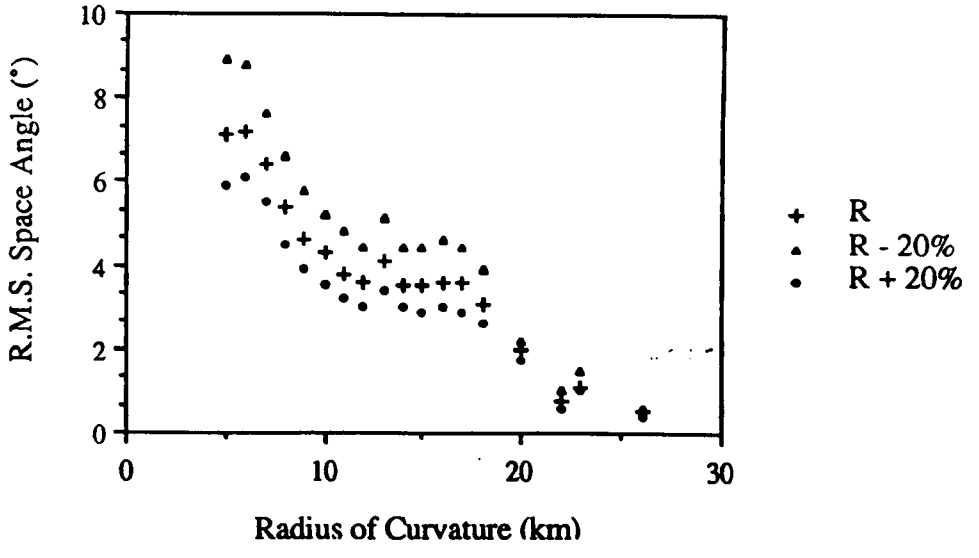

Figure 5·2 The r.m.s. space angle difference between curvature corrected and uncorrected 12km^2 directions as a function of radius of curvature. The space angle difference is also shown for values of radius of curvature that are 20% too large and 20% too small .

front.

5·3 Angular Resolution of the 12km^2 Array

As described in Chapter 3, high energy cosmic ray studies lack a strong point source that can be used as a standard candle. This means that to derive the angular resolution of an array indirect methods must be used. The angular resolution of the 12km^2 was initially estimated by considering the possible sources of random errors inherent in detecting and recording extensive air showers e.g. timing fluctuations, resolution of instruments used for recording times, etc. Lapikens (1974) gave the average angular resolution of curvature corrected showers as 2·5°.

During three periods of the lifetime of the 12km^2 array it ran concurrently with other instruments located at Haverah Park designed for detecting extensive air showers. These additional instruments have provided independent assessments of the estimate given by Lapikens.

In 1968 Durham University operated a magnet spectrograph to investigate the properties of the muon component of extensive air showers (Earnshaw et al. 1968). Comparison of the arrival directions obtained from the 12km^2 array with those from the muon spectrograph suggested that the uncertainty in the plane fit zenith angle was 2·7°. A second University of Durham experiment consisted of an array of air-Čerenkov detectors placed next to several of the central water-Čerenkov detectors (Craig et al. 1979). This array confirmed the above estimate of the zenith angle uncertainty.

The third instrument has already been described. Between the commissioning of the GREX array and the shut down of the 12km^2 array the two instruments ran simultaneously for 17 months. GREX is located at the centre of the 12km^2 array and so it was expected that some showers would be recorded by both instruments. The GREX array was designed to look at showers of much lower energy than the 12km^2 array and so the number of events common to both was low: 196 with energy greater than

$1x10^{17}$eV and only 13 with energies in excess of $5x10^{17}$eV.

The r.m.s. space angle difference between directions assigned to showers by the $12km^2$ and GREX arrays (having accounted for the shower front curvature as seen by both arrays) was 2·4°±0·2°. The 13 events with energies above $5x10^{17}$eV had an r.m.s. space angle difference of 2·2°±0·4°. The angular point spread width of the scintillator array is less than 1° at these energies which gives an angular resolution for the $12km^2$ array of 2·2°. This comparison was made before the inaccuracy in the co-ordinates of detector 12 in GREX was known (see Chapter 2). However, all the comparison events are of high energy for GREX and so high detector multiplicity. Therefore, the effect of the position of one detector being wrong on the arrival directions obtained from the GREX array should be small. All the common events fell within the boundary of the GREX array (i.e. close to the centre of the water-Čerenkov array) and so are expected to have been reconstructed by the $12km^2$ array with better than average accuracy. Therefore, the comparison with GREX gives results that are compatible with Lapikens' estimate of the angular resolution or the $12km^2$ array of 2·5°.

In addition there are no systematic differences between the arrival directions obtained by the $12km^2$ array and those obtained by the other three independent instruments. In the absence of an astronomical source this is the most reassuring indication that the pointing direction of the array is known.

Taking an angular resolution of 2·6° (Lapikens' 2·5° added in quadrature with the 0·7° from uncertainties in the radius of curvature) for the $12km^2$ array gives the optimum bin size for point source searching at the declination of Cygnus X-3 (+40°) to be 6° in declination and 8° in right ascension. It is expected that a bin of this size centred on a point source will contain ~70% of the source signal. It should be noted that an angular resolution of 2·6° gives a solid angle uncertainty in the arrival direction of $6·5x10^{-3}$sr which is of the same order as that of the Fly's Eye group who confine the shower arrival direction to a box 2° by 9° which corresponds to a solid angle uncertainty of $5·5x10^{-3}$sr (Cassiday et al. 1989).

5·4 Distribution of Events in Galactic Longitude

The most direct comparison between the Haverah Park and Fly's Eye results on Cygnus X-3 is the distribution of events in galactic longitude. In the paper describing their results Cassiday et al. (1989) show the distribution of showers with $E>5x10^{17}eV$ against galactic longitude for a strip of galactic latitude 10° wide centred on the latitude of Cygnus X-3 (+1°) for the period November 1981 to May 1988 (excluding June to October 1985) (Figure 5·3). They state that the number of counts in the bin centred on longitude +80° (the longitude of Cygnus X-3) is greater than can be explained by the expected smooth variation of number with longitude. Also shown in Figure 5·3 is the equivalent plot for showers recorded at Haverah Park. As can be seen the Haverah Park data (for January 1982 to July 1987) show no such peak in the Cygnus X-3 bin. The difference in longitudinal distribution for the two arrays is indicative of their different terrestrial latitudes: Haverah Park at 54°N is 13° more northerly than Fly's Eye.

The Haverah Park array operated at an efficiency in excess of 90% whereas the Fly's Eye instrument, which detects the fluorescence of nitrogen atoms excited by charged secondary particles produced in shower cascades, is restricted to operating only on clear, moonless nights. However, the Fly's Eye has an extremely high acceptance of $70km^2sr$ compared to Haverah Park's $5.5km^2sr$ which means that when it is operational the Fly's Eye will record many more events. The combination of on-time and acceptance results in approximately twice as many showers being recorded in the region shown in Figure 5·3 by the Haverah Park array as by the Fly's Eye during the period that the instruments operated concurrently.

Figure 5·4 shows a similar number verses galactic longitude plot for Haverah Park data from the full 13·5 years available from 1974. (Data exists from the period 1966 to 1974 but it is stored in a highly inaccessible form). Once again the number of showers in the bin containing Cygnus X-3 is no greater than might be expected. In both these plots the arrival directions of the primaries recorded by the $12km^2$ array have been

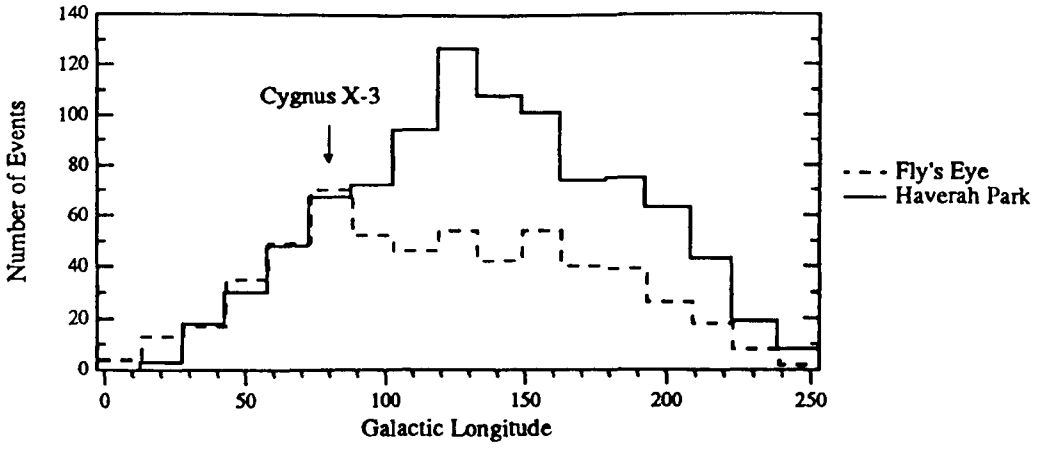

Figure 5·3 The number of showers recorded against galactic longitude for both Haverah Park (solid line) and Fly's Eye (dashed line) data from 1982 to 1987. Each bin is 15° wide in galactic longitude and 10° in galactic latitude centred on +1 (the latitude of Cygnus X-3).

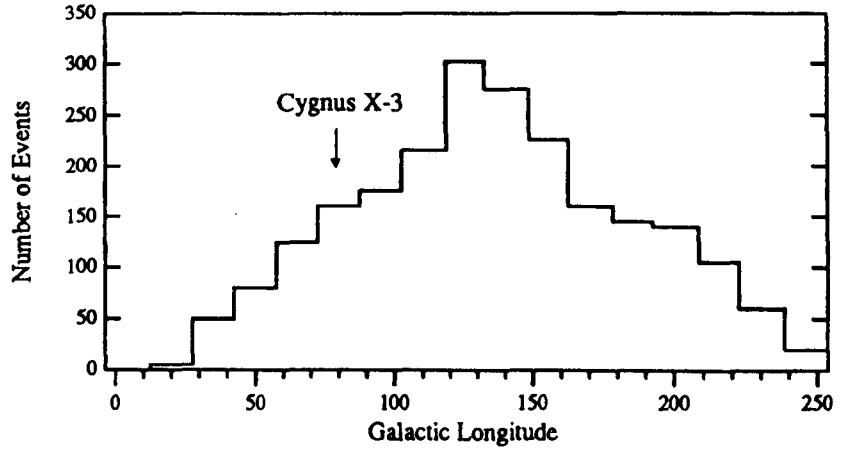

Figure 5·4 The number of showers recorded against galactic longitude for Haverah Park data from 1974 to 1987 (the full period for which data were available). The bin size is the same as for Figure 5·3

corrected for the curvature of the shower front (see section 5·2). Showers with zenith angle (θ) greater than 60° have been rejected as geomagnetic distortions of the shower front become important limitations to the accuracy with which primary arrival directions can be reconstructed at θ>60° (Andrews et al. 1971).

Owing to the high efficiency and long running of the 12km^2 array the exposure in right ascension is approximately constant and so it is more convenient to think of arrival directions in terms of right ascension (α) and declination (δ) than in galactic longitude and latitude. Therefore, the data were analysed fully in right ascension and declination.

5·5 Upper Limit to the Flux from Cygnus X-3

During the period January 1974 to July 1987 the Haverah Park 12km^2 array recorded 23587 events which fell within the array boundary and had energy greater than 5×10^{17}eV and zenith angle less than 60°. These events were binned, each bin being 8° in α and 6° in δ for reasons given above. The array of bins was centred on Cygnus X-3 (α=308°, δ=40.75°).

Figure 5·5 shows the distribution of events in 120° of right ascension. For the upper plot the declination strip is 6° wide and the bin centred on Cygnus X-3 is marked. This bin does not contain an exceptional number of events (40 on-source with a mean background of 46·1). Although only 14 off-source bins are shown the mean number of background events is calculated from all 44 off-source bins in the Cygnus X-3 declination strip. In lower plot all events with declination greater than -6° are shown. Owing to the rejection of showers with $\theta_c > 60°$ and the latitude of Haverah Park no showers of declination less than -6° are observed. The distribution of events in right ascension is consistent with the large scale anisotropies previously found (Eames et al. 1987b) with a first harmonic amplitude of ~1%, as would be expected from the array's long run-time and high efficiency.

Table 5·1 shows the number of counts in the Cygnus X-3 bin and the mean

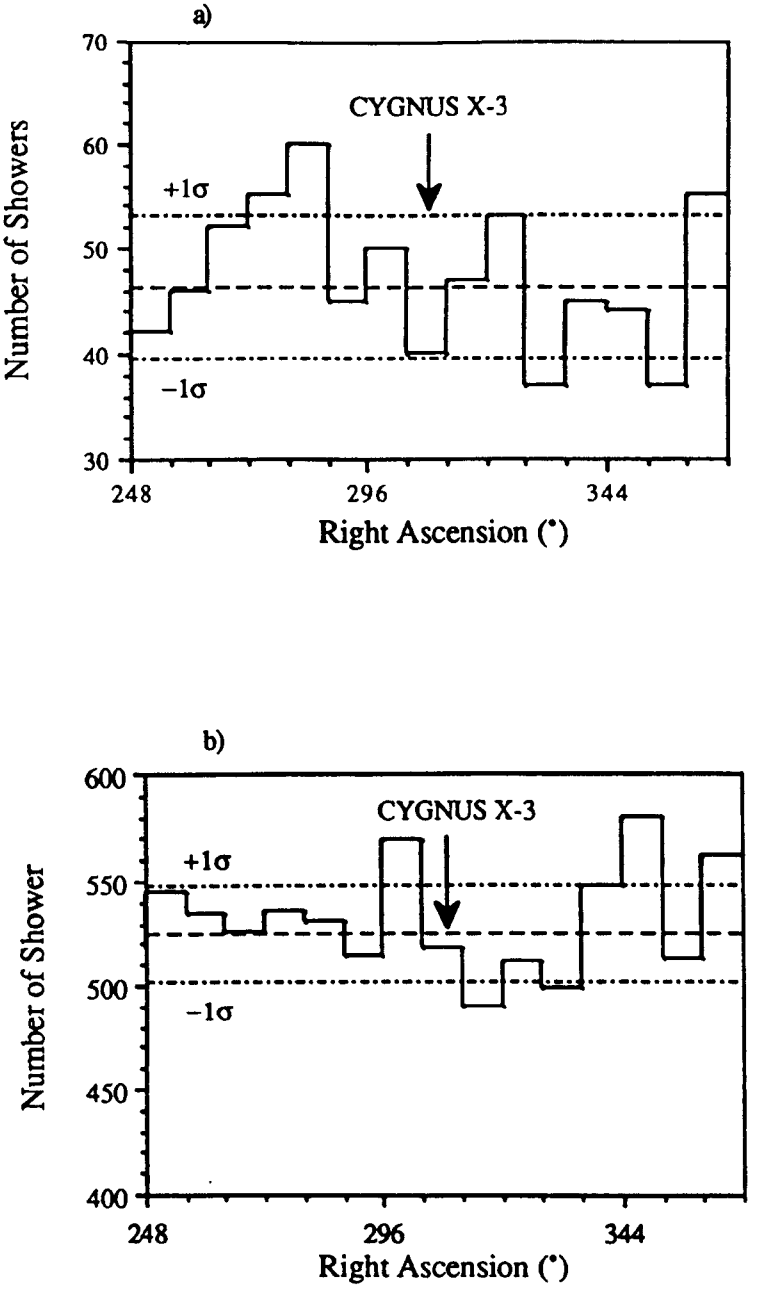

Figure 5-5 The number of showers recorded as a function of right ascension for 15 bins, 8° wide, centred on Cygnus X-3. The upper histogram (a) is for bins which are 6° wide in declination while the lower histogram (b) shows the number of events for declinations above -6°.

background as a function of energy for both the period of overlap with the Fly's Eye observations and the total Haverah Park observing period.

	1982 - 1987		1974 - 1987	
Energy (eV)	N	B	N	B
$> 5 \times 10^{17}$	11	20·0	40	46·1
$> 1 \times 10^{18}$	8	7·6	18	17·3
$> 2 \times 10^{18}$	3	2·6	9	5·8
$> 4 \times 10^{18}$	2	0·8	6	1·9

Table 5·1 The number of events, N, seen in the 8°x6° bin centred on Cygnus X-3 given with the mean background, B, calculated from the 44 off-source bins in the same declination strip.

For energies greater than 2×10^{18}eV 15 events were seen in the on-source bin during the full observing period when the background was only 7·5. This is the highest signal to noise ratio seen and the Poissonian probability of seeing 15 or more showers is 0·010. Unfortunately, there are too few showers to say whether this is an actual effect and with the 12km^2 array shut down there seems no prospect of accumulating more data.

As an excess signal is not seen only an upper limit can be placed on the flux from Cygnus X-3. If, owing to random fluctuations, the background in the source bin was low a small signal would not stand out. Protheroe (1984) gives the 95% upper limit, S_{95}, to the signal as :-

$$S_{95} = 1.6\sqrt{B}$$

where B is the mean background and 1·6 the 'Protheroe Factor' that applies in this case. (The Protheroe Factor depends on the number of on-source and off-source events). A mean background of 46·1 events gives S_{95}=10·9 which is effectively the maximum number (at the 95% level) of events that could have come from the source. The integral cosmic ray intensity above $5x10^{17}$eV is $8{\cdot}2x10^{-16}$ particles $cm^{-2}s^{-1}sr^{-1}$ (Lawrence et al. 1991a) and so the integral flux from a box 8°x6° (i.e. $1{\cdot}46x10^{-2}$sr) is $1{\cdot}2x10^{-17}$ particles $cm^{-2}s^{-1}$. Assuming that the energy spectrum of the neutral primaries from the possible source is the same as that of cosmic rays this flux corresponds to the 46·1 background showers seen in the period of interest. The 95% upper limit to the flux in the bin, F_{95bin}, is now given by :-

$$F_{95bin} = (10.9 / 46.1) \times 1.2x10^{-17} = 2.8x10^{-18} \text{ particles } cm^{-2}s^{-1}.$$

As was stated earlier a bin of size 8°x6° is expected to contain 70% of the signal from the source and so the flux in the bin must be divided by 0·7 to give a limit to the flux from Cygnus X-3 of $4x10^{-18}$ particles $cm^{-2}s^{-1}$. For the overlap period an upper limit to the flux of $5x10^{-18}$ particles $cm^{-2}s^{-1}$ is obtained.

At a flux of $(2{\cdot}0\pm0{\cdot}6)x10^{-17}$ particles $cm^{-2}s^{-1}$ as reported by the Fly's Eye group it would be expected that the Haverah Park 12km^2 array should have recorded an excess of 52±15 events in the bin centred on Cygnus X-3. However, the actual observed number was 40 on 46·1. For the overlap period (1982-1987) an excess of 23±7 is expected (compared with the 11 on 20·0 observed).

In calculating the above fluxes the assumption that the primaries are hadron-like has been made. This is not an unreasonable assumption. The preferred production mechanism of high energy gamma-rays is the decay of neutral pions produced when accelerated hadrons collide with matter close to the acceleration site. However, neutrons are also produced in these collisions and Jones (1990) has noted that at energies in excess of ~$5x10^{17}$eV the flux of neutrons from Cygnus X-3 at Earth will be greater

than the flux of gamma-rays. At these high energies the neutrons have such high Lorentz factors (~10^9 at 10^{18}eV) that they can travel the distance from Cygnus X-3 to Earth (~10kpc) with only a small probability of decaying.

However, an alternative production mechanism may be in operation and the flux observed by the Fly's Eye group could consist of gamma-rays rather than neutrons. This affects the Haverah Park upper limits. The nature of the water-Čerenkov detectors and the fact that detectors often sampled the shower front at large distances from the shower core means that the 12km^2 array was less sensitive to gamma-ray initiated showers (assuming that these showers have a lower muon component). The efficiency of the array at detecting gamma-ray initiated showers is 62% of that at detecting hadronic showers (Garmston 1976). If the signal from Cygnus X-3 consists of gamma-rays the upper limit to the flux must be increased to 7×10^{-18} particles cm^{-2}s^{-1} for the full observing period.

5·6 Temporal Distribution

Cygnus X-3 has an X-ray period of 4·8 hours and many groups have seen this periodicity in the neutral particle emission of Cygnus X-3 at energies up to 10^{16}eV. Using the Molnar ephemeris (Cassiday et al. 1989) the Fly's Eye group have analysed their data at energies greater than 5×10^{17}eV and find evidence for emission at a phase of 0. The Haverah Park data were also period analysed using the same ephemeris. Figure 5·6 shows this data binned in both 0·1 and 0·05 phase intervals. As can be seen there is no enhancement of emission at phase zero or at any other phase. The background is the mean in each phase bin calculated from the 44 similar bins in the Cygnus X-3 declination strip.

As was stated in the previous chapter Cygnus X-3 undergoes occasional burst of radio emission when the flux increases from the quiescent level of a few hundred mJy to as much as 20Jy (Johnston et al. 1986). Some groups have claimed an association

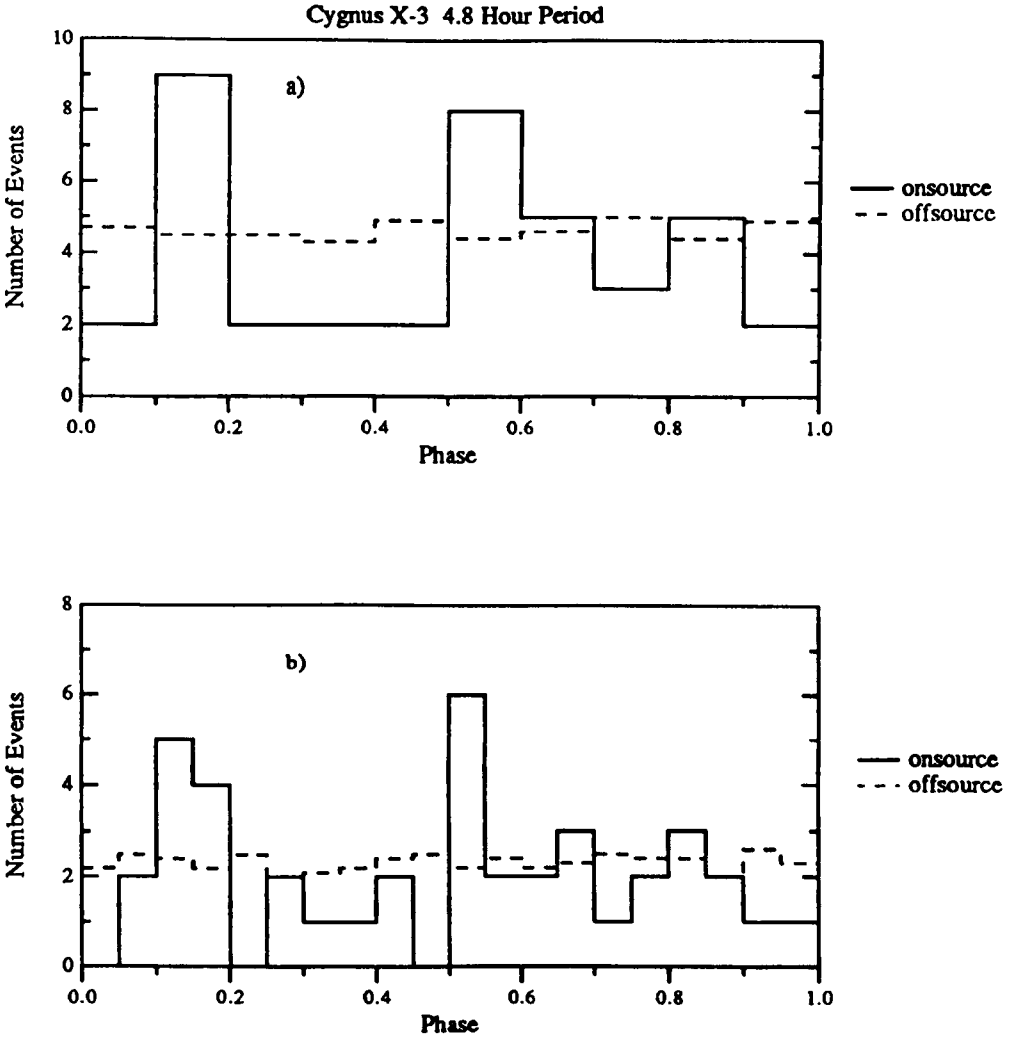

Figure 5·6 The 40 on-source events seen in the full observing period binned in 0·1 (a) and 0·05 (b) phase intervals using the Molnar ephemeris. The background is calculated from the 44 identical off-source bins in he same declination strip.

between these period of radio emission and observations of TeV and PeV gamma-rays from Cygnus X-3. Therefore, a possible correlation between radio flares and neutral particle emission was investigated. Figure 5·7 shows the time distribution of all radio flares with flux greater than 1Jy between 1974 and 1987. Also shown are the arrival times of the 40 events recorded by the 12km^2 array of energy greater than 5x10^{17}eV in the bin centred on Cygnus X-3 for the same period. There is no evidence of a correlation between the occurrence of radio flares and the highest energy cosmic rays.

5·7 Contour Plots

Neither the Fly's Eye nor Akeno groups have used a simple event binning procedure to search for Cygnus X-3. In both cases the events are replaced with a probability distribution centred on the event arrival direction and of a width given by the angular resolution of the instrument. Summing the probabilities at a given point in the sky gives the shower density at that point. It is claimed that this method optimises sensitivity to point sources as it circumvents the problem of sources falling on bin boundaries. A similar method has been developed for the 12km^2 data set.

Each event falling within a box of 40° square centred on Cygnus X-3 was replaced by a Gaussian probability function. The probability that a shower came from a given position a distance x in right ascension (measured in true degrees) and y in declination from the nominal shower position is given by (Lyons 1986):-

$$P(x,y) = \frac{1}{2\pi\sigma_x\sigma_y} \exp\left(-\frac{1}{2}\left(\frac{x^2}{\sigma_x^2} + \frac{y^2}{\sigma_y^2}\right)\right)$$

The 12km^2 had an average angular resolution of 2·6° which results in σ_x and σ_y of 1·84°. The probability function was then summed over the whole of the 40°x40° box at intervals of 1°.

An estimate of the background was obtained at each point from simulations. The

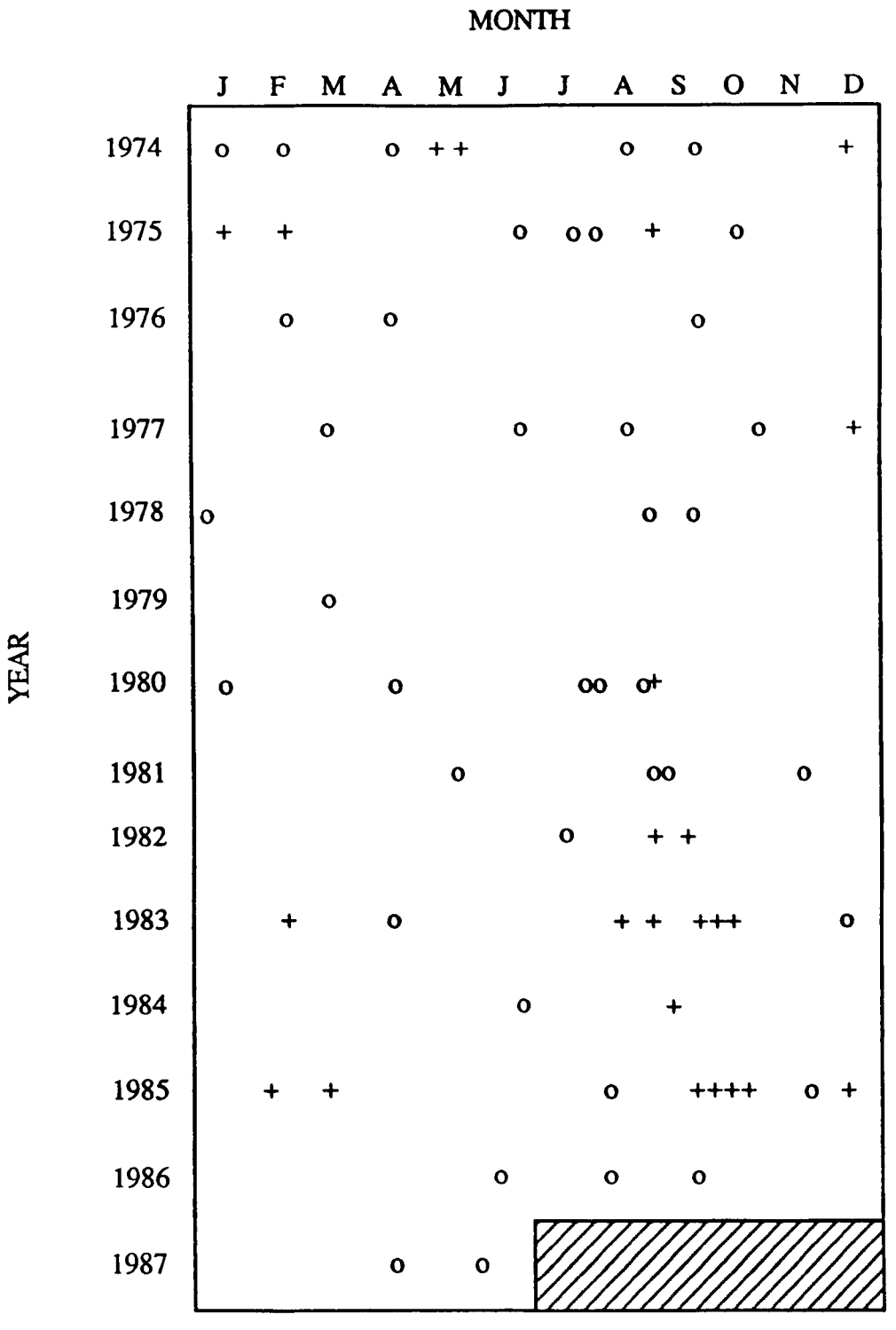

Figure 5·7 The arrival times of the 40 on-source events (depicted by circles, o) seen by the 12km^2 array from the direction of Cygnus X-3. Also shown are the times of Cygnus X-3 radio flares above 1Jy (depicted by crosses, +, and taken from Johnston et al. 1986)

right ascension of each event in the entire data set was randomised (between 0° and 360°) and then selected if it fell within the 40° box. The 'smearing' and summing procedure was then performed. This was done 10 times and at each point in the box an average was taken. The sum of the probability function for showers that originally fell in the 40° box centred on Cygnus X-3 could then be compared to the expected sum.

Figure 5·8 shows the contour plot of the observed probability density compared to the expected density. The width of the contours is 0·25 standard deviations from the expected density with red contours showing an excess and black a deficit. As can be seen there are two excess of ~2·25σ, one 8° from the position of Cygnus X-3 (i.e. from the centre of the plot) and the other 16° away. At the position of Cygnus X-3 there is a 0·5σ deficit. As will be described in the next section, one of the Fly's Eye reports showed that the peak observed was 4° from the source, which may have been the result of systematic errors in the arrival directions or mapping procedure. The presence of a peak near the source position in the Haverah Park data could also suggest similar systematic errors. However, the presence of a second peak of the same magnitude would tend to suggest that both peaks are statistical fluctuations. As an example of the types of fluctuations observed Figure 5·9 shows a similar plot, but in this case the mean background is compared to a randomised set of directions. Here can be seen a 2σ deficit 9° from Cygnus X-3. Simulations have shown that 2σ deviations from the expected density are not uncommon in an area of sky 40°x40°.

Therefore, it is not believed that there is any evidence of emission from Cygnus X-3 in the Haverah Park 12km^2 array data set, even when similar search methods that appear to have been successful for other groups are used.

5·8 Critical Comparison of the Fly's Eye and Akeno Results

As has been shown there is no evidence in the Haverah Park 12km^2 array data set that Cygnus X-3 is a source of neutral particles of energies above 5x10^{17}eV. This is in

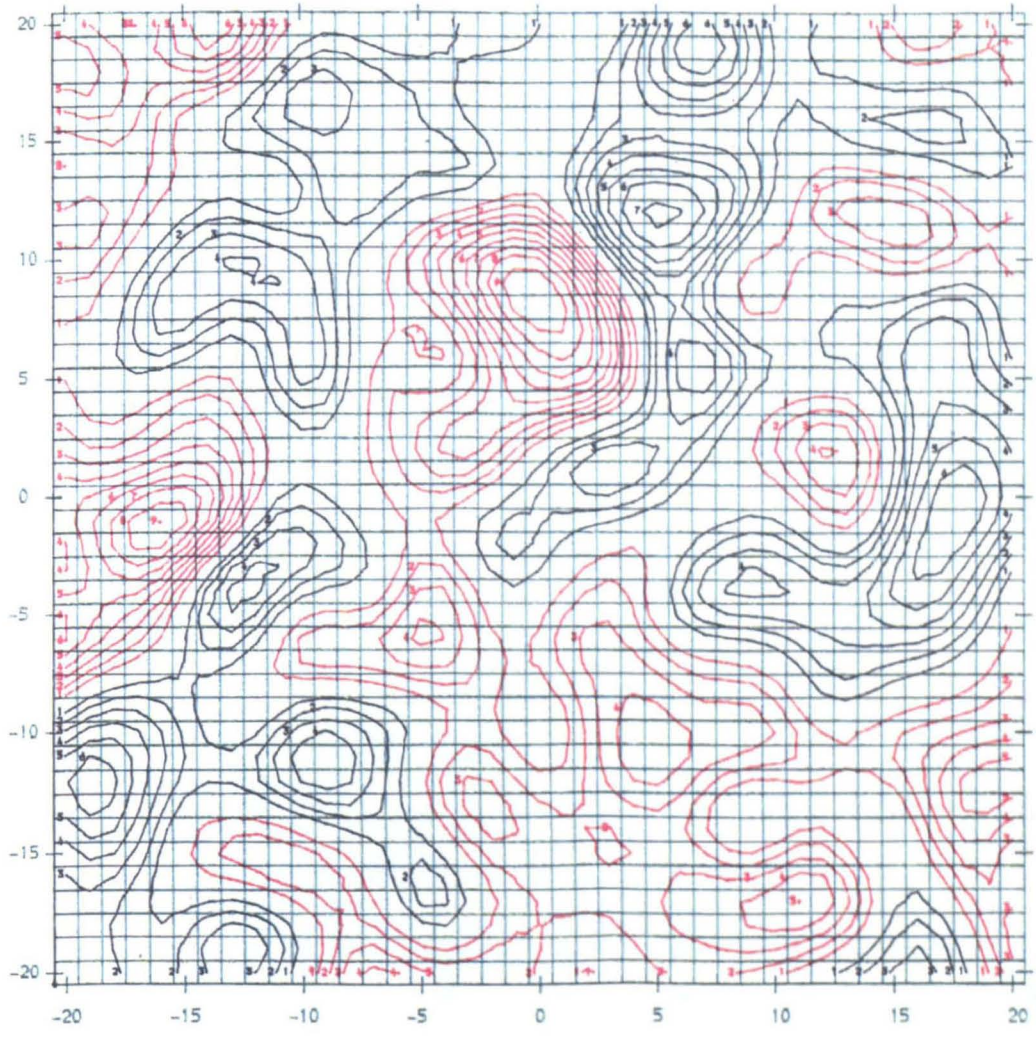

Figure 5·8 A contour plot of the Cygnus X-3 region. Cygnus X-3 is at the centre of the plot which covers ±20° in declination (vertically) and ±20° in right ascension (measured in true degrees horizontally). The contour width is 0·25 standard deviations from the background with red contours showing an excess compared to the background and black contours a deficit. The peak at (0,8) is therefore +2·25σ.

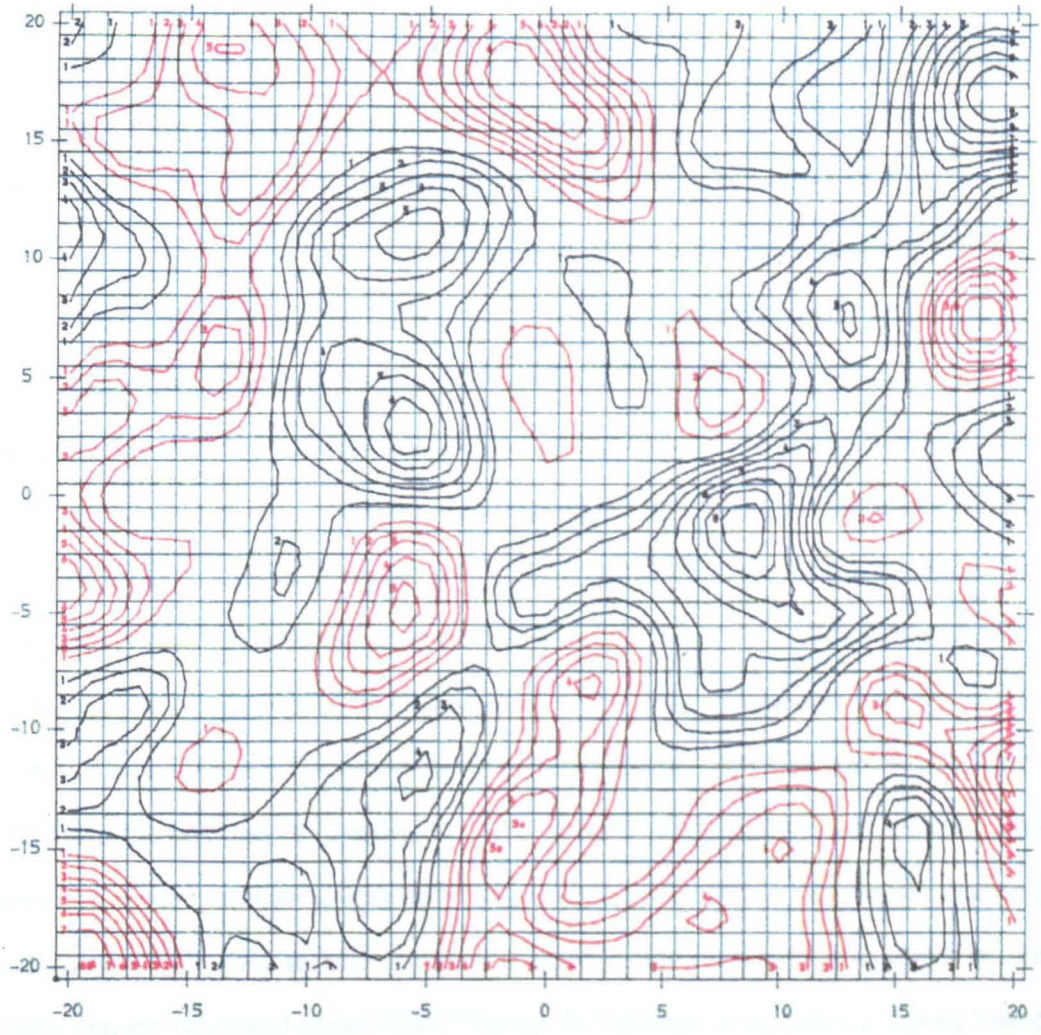

Figure 5·9 As in Figure 5·8 but with a random set of directions compared to the mean background. The contour width is 0·25 standard deviations from the background with red contours showing an excess compared to the background and black contours a deficit. The trough at (9,-1) is -2·0σ.

direct contradiction with the observations of the Fly's Eye and Akeno groups. The upper limit to the flux derived in this work is significantly lower than the signal strengths claimed, even during periods of simultaneous observations. Therefore, in this section the claims made for Cygnus X-3 at high energies will be critically examined.

The original Fly's Eye report (Cassiday et al. 1989) was based on data recorded from November 1981 to May 1988. Using their method of replacing each shower arrival direction with a Gaussian probability distribution of width 3·8° and summing the probabilities they observed a 4σ peak centred on the position of Cygnus X-3. The statistical significance of the signal was not reduced at high energies - in fact the most significant result was seen at energies greater than $4x10^{18}$eV. A search for the 4·8hr periodicity of Cygnus X-3 showed an excess of events around zero phase.

These results were updated (Cassiday et al. 1990) with additional data up to July 1989. The same analysis methods were used but the contour peak (reduced to 3·8σ) was displaced from the position of Cygnus X-3 by 4°. From simulations it was believed that a point source would produce a peak with a Gaussian width of 5·4°: the peak observed had a width of ~7·6°. This second paper also gave a year by year break down of the probability that the observed signal from Cygnus X-3 occurred by chance. It was found that Cygnus X-3 was most active during 1987 with the probability of the observed excess occurring by chance being 0·48%.

The Akeno group in their confirmation (Teshima et al. 1990) used a similar method of 'smearing' each arrival direction with an error function and then summing the probabilities to produce a contour plot. This resulted in a peak of 3·5σ for data recorded from December 1984 to July 1989. In a similar way to the Fly's Eye result this peak was displaced from the position of Cygnus X-3 by 2·4°, giving a significance at Cygnus X-3 of 2·7σ. However this shift was in the opposite direction to that of Fly's Eye and the two peaks are separated by 5·6°.

The energy distribution of the events from the direction of Cygnus X-3 shows that the signal observed at Akeno is mainly at low energies. Above $3x10^{18}$eV no events

were recorded when 5 would have been expected from the extrapolation of the observed flux at lower energies. A search for the 4·8hr periodicity showed no significant modulation.

It was also found that the time distribution of events from Cygnus X-3 was not uniform but that there appeared to be two periods, each of ~40 days duration, when the signal was enhanced. During these periods (17/4/86 to 26/5/86 when 6 events were observed with 1·7 expected and 11/3/89 to 20/4/89 when 7 events were observed with again 1·7 expected) ~40% of the excess number of showers recorded in the 4·5 years were observed. Unfortunately, the Haverah Park 12km^2 array had been shut down by 1989, but it was still in full operation in April/May 1986. Between 17/4/86 and 26/5/86 the 12km^2 array recorded no events from the direction of Cygnus X-3. If the bursts observed by the Akeno group are real then the flux from Cygnus X-3 at these times would be ~1·8x10^{-16} particles cm^{-2}s^{-1}. At this flux ~4 events should have been recorded by the 12km^2 array in 40 day period.

To summarise there are four main areas of conflict between the Fly's Eye and Akeno reports of neutral particles from Cygnus X-3 above 5x10^{17}eV:-

1) Although both groups observe peaks in their probability density maps the peaks in both cases are displaced from the position of Cygnus X-3. In addition they are 5·6° from each other. This could be indicative of systematic errors, either in the methods used to reconstruct the primary arrival directions or in the mapping procedures.
2) The Fly's Eye group observed a signal enhancement at zero phase of the Cygnus X-3 4·8hr modulation whereas the Akeno group finds no evidence for periodicity.
3) The Fly's Eye signal is at its strongest above 2x10^{18}eV but Akeno observe no events with energy greater than 3x10^{18}eV.
4) There is no evidence in the Fly's Eye data for periods of particle outbursts, although they do note that the strongest period of emission was in 1987. The

Akeno group find almost half their signal in two 40 day periods in 1986 and 1989.

Of these discrepancies 2) and 3) would appear to be the most serious as the claims are in direct contradiction and appear unreconcilable. The fourth problem may be explained by considering the modes of operation of the two instruments. Whereas the Akeno array can observe Cygnus X-3 through out the year, Fly's Eye is limited to observing on moonless nights, with the maximum exposure to Cygnus X-3 during June and July. The Fly's Eye would therefore not be expected to be able to observe Cygnus X-3 during the Akeno burst period of March/April 1989 and so would be unable to confirm the Akeno report. Even in April/May conditions are not ideal for observing Cygnus X-3 at the Fly's Eye and so it is possible that the 1986 burst was missed. However, it is surprising that Akeno group do not observe any enhanced emission from Cygnus X-3 during 1987 as this was when the Fly's Eye group observed their most significant effect.

Subsequent to the publication of these reports the Akeno array was extended from $20km^2$ to $\sim 100km^2$. The Akeno group have searched for Cygnus X-3 in data recorded by the extended array between February 1990 and July 1991. The number of showers recorded in this period is approximately the same as recorded by the smaller array between December 1984 and July 1989. A peak of $3{\cdot}4\sigma$ is seen in the new data set at the position of Cygnus X-3 with 130 events seen within 6° of the source when 93·0 were expected (Hayashida et al. 1991). No evidence is found for phase enhanced emission in the 4·8hr period of Cygnus X-3. However, half of the total excess is observed in the 50 days following the radio flare of 21 January 1991 (27 on-source, 10·2 expected).

The results from the two independent Akeno data sets do show a general consistency:- the reported fluxes are comparable, there is no evidence for phase dependence and a large fraction of the signal comes from burst periods. There have been no further claims of emission made by the Fly's Eye group.

Mention should also be made of the report (Glushkov et al. 1990) of a search made

for Cygnus X-3 using data from the Yakutsk array. For the period 1984-1986 an excess of 3·4σ was observed in the energy range (2·37-3·16)x10^{17}eV. No evidence for phase enhanced emission was found. To obtain this result an all sky survey was performed using 10°x10° bins, one of which was centred on Cygnus X-3. The data set was then split into energy and time bands. The 3·4σ result quoted above does not appear to take account of the trials involved in looking at 2025 bins on the sky, 24 energy bins and at least 3 time periods. With 2025 bins one bin of 3·5σ or more is expected by chance. Therefore, the 3·4σ result is statistically insignificant.

5·9 Clustering of the Higher Energy Cosmic Rays

The claims that Cygnus X-3 may be emitting gamma-rays with energies greater than 5x10^{17}eV draws attention to the problem of determining the origin of the highest energy cosmic rays. As these cosmic rays have extremely large Larmor radii it was felt in the 1960's that study of arrival direction anisotropies would give clues to their origins. At the very least it was thought that the question of whether these particles were galactic or extragalactic could be answered. Unfortunately, no significant anisotropies were found and the problem of the origin of the highest energy cosmic rays remained.

A recent attempt to solve this problem has been made by the Durham group. Chi et al. (1990) took the catalogues listing the arrival directions of the highest energy cosmic rays recorded at four very large extensive air shower arrays (Volcano Ranch, Haverah Park, Sydney and Yakutsk). Showers with energy greater than 3x10^{19}eV were considered marker events and the number of events with energy above 10^{19}eV within 6° of the marker event was found. When the distribution of clusters containing 5 or more events was investigated it was found that there was a concentration about the galactic plane in the direction of the outer Galaxy. 12 events with E>10^{19}eV were observed within ±6° of the galactic plane when 4·7 were expected. There was also some grouping in the direction of the Virgo cluster. The Durham group felt that each cluster could be

associated with a discrete source.

Additional events recorded by the Haverah Park group but not contained in the catalogue have been analysed for clustering (Lawrence et al. 1991b). There is no evidence for there being more clusters than is expected from Monte Carlo simulations. In addition, simulations show that the probability of getting the observed number of clusters within $\pm 6^{\circ}$ of the galactic plane is 4%. The Haverah Park group therefore believe that few, if any, of the clusters actually point to discrete sources.

5·10 Conclusions

In his rapporteur paper on gamma-ray astronomy above 0·3TeV Fegan (1990) produced a short catalogue of objects for which he felt there was compelling statistical evidence to believe them to be gamma-ray sources. In this catalogue he includes Cygnus X-3 at energies above 5×10^{17}eV (noting the possibility that the flux observed could in fact be neutrons). This chapter has shown that there is no evidence for such emission in data recorded over a 13 year period by the Haverah Park 12km^2 extensive air shower array. Even during periods of simultaneous operation with the Fly's Eye and Akeno instruments the upper limit obtained by the 12km^2 array is significantly lower than the flux claimed. In addition it has also been shown that many differences exist between the claims of the Fly's Eye and Akeno groups.

These contradictions bring into question the inclusion of Cygnus X-3 at high energies in any catalogue of sources. The continual operation of both the Fly's Eye and the Akeno array may resolve some of the contradictions but until then the emission of neutral particles from Cygnus X-3 remains unproven.

CHAPTER 6

A SEARCH FOR PeV EMISSION FROM OBJECTS OTHER THAN CYGNUS X-3

6·1 Introduction

Despite being one of the most widely studied objects at TeV and PeV energies Cygnus X-3 is by no means the only object which has been claimed as an emitter of very high or ultra high energy gamma-rays. A wide range of galactic pulsars and X-ray binaries have been studied in addition to some extragalactic objects. This chapter will describe searches made in the GREX data set for evidence of emission from 8 candidate sources.

As each new energy and wavelength range has been opened up in astronomy new types of objects have been discovered e.g. pulsars in radio wavelengths. It is therefore possible that unknown objects exist that could be emitters of PeV gamma-rays. For this reason a simple all-sky survey has been performed using the GREX data set and is described in this chapter.

6·2 Previous Observations of Candidate Sources

6·2 a) 1E 2259+586

1E 2259+586 is an interesting object in that it is one of a very small number of pulsars to be found within a supernova remnant (SNR). The system was discovered in 1979 using the Einstein X-ray observatory (Gregory and Fahlman 1980). A semicircle of emission was observed which was taken to be the shell of the SNR, G109·1-1·0, which had first been observed during a radio survey (Wilson and Bolton 1960). A strong compact X-ray source was seen at the exact centre of curvature of the shell. Connecting the central source and the shell was a curved, jet-like structure. The remnant

is at a distance of between 3.6 and 5.2 kpc and the age is estimated to be $(1{\cdot}2\text{-}1{\cdot}7)\times10^4$ years.

Analysis of the X-ray photon arrival times from 1E 2259+586 showed a period of 3·489s (Fahlman and Gregory 1981). However, it was later found that the true period was 6·978s with a strong interpulse at phase 0·5. Measurements were made with the EXOSAT observatory five years after the Einstein observations (Hanson et al. 1988 and Morini et al. 1988) and the ~7s periodicity was confirmed, although the period was now slightly longer. A slow spin down of $(5{\cdot}9\pm0{\cdot}3)\times10^{-13}ss^{-1}$ has been confirmed by the TENMA and GINGA satellites (respectively Koyama et al. 1987 and Makino et al. 1987).

1E 2259+586 has been studied at other energies. There is no point radio signal (Fahlman and Gregory 1981), but a very faint (magnitude < 22) optical companion has been suggested (Fahlman et al. 1982) and there is some evidence of 3·5s pulses in the infrared (Middleditch et al. 1983). However, the infrared period is larger than the nominal X-ray second harmonic period by 1 part in 1000.

The faintness of the possible companion star has led to the idea that the pulsar is isolated, similar to the Crab pulsar. This is supported by the spin down observed. However, the power available from the slowing down of the pulsar is not great enough (by ~4 orders of magnitude) to explain the X-ray luminosity. A detailed theoretical consideration of the accretion of matter onto a magnetised neutron star (Ghosh and Lamb 1979) has shown that for certain conditions a slow spin down is not inconsistent with an accreting binary system. If 1E 2259+586 is a binary system then a consequence of the low luminosity of the companion is that it must be of low mass. This means that stellar wind accretion is excluded and mass transfer must take place by Roche lobe overflow.

The conditions of Roche lobe overflow and low mass dictate a short orbital period: down to 10 minutes. Fahlman and Gregory (1983) reported a 2300s period in the Einstein data but this has not been confirmed by other observations. Close binary pairs

are thought to take a long time to evolve and the comparative youth of the 1E 2259+586 system (determined by considering the size of the SNR shell) suggests that the system was close prior to the supernova. One possibility is that the supernova was caused by the accretion induced collapse of a white dwarf.

There is controversy at TeV energies. The Durham group claim to have observed 1E 2259+586 on 4-11 October 1988 (Brazier et al. 1990b). Evidence was found for pulsed emission with a period of 3·489s in data taken over 13 hours. After accounting for trials the probability of the observed signal occurring by chance was 5×10^{-5}. This result is in direct contradiction with that of the Whipple group (Cawley et al. 1991). An upper limit more than 8 times lower than the Durham flux was obtained from data collected over the same period as the Durham observation. There was no evidence of emission at either the first or second harmonics. In addition, Whipple data showed no evidence of emission in 80 hours of data collected between November 1985 and November 1988.

The CYGNUS group found no evidence of emission at PeV energies in data collected between April 1986 and November 1990 (Lu et al. 1990).

The Soudan-1 group has looked for underground muons from 1E 2259+586 in data recorded in 1985. A scan of periods around the X-ray period showed a peak at the 2% chance level at a period of 6·9786s (Ruddick 1987)

6·2 b) Hercules X-1

Hercules X-1, which was discovered by the UHURU satellite (Schreier et al. 1972, Tananbaum et al. 1972), is at distance of 5kpc and has three periodicities associated with it. The X-ray flux is modulated with periods of 1·24s, 1·7 days and 35 days. The accepted picture of Hercules X-1 has a 1·24s neutron star pulsar in an orbit of 1·7 day duration with a Roche lobe filled A type companion (HZ Her). Material from the companion forms an accretion disk around the neutron star and is then funnelled onto the pole of the neutron star producing the X-rays observed. The 35 day period is

marked by two X-ray on states, the second of which has a maximum flux a third of that of the first on state. This is thought to be the result of a wobbling accretion disc which periodically obscures the pulsar (Petterson 1977). The three periods have been observed at optical and infrared wavelengths (respectively Middleditch and Nelson 1976 and Middleditch et al. 1983).

In 1984 the Durham group reported that Hercules X-1 was a TeV gamma-ray pulsar (Dowthwaite et al. 1984a). A 3 minute burst at the 3σ level was observed in 160 minutes of observing on 17 April 1983. The arrival times of the events recorded in the burst were corrected to the solar system barycentre and binary system centre. A periodicity was found (at the X-ray pulsar period) with a probability of occurring by chance of 4×10^{-4}. A broad peak was seen with a width of approximately a third of a cycle. The time average photon flux was given as $(3{\cdot}0\pm1{\cdot}5)\times10^{-11}$ cm^{-2}s^{-1} above 1TeV.

During 10-14 July 1983 the Fly's Eye detector, triggering on air-Čerenkov flashes, observed a marginal, $1{\cdot}8\sigma$, excess (Baltrusaitis et al. 1985b). However, when the data from the first half of the 11 July run were phase analysed a narrow peak (10% of a cycle) was found with 15 events on a background of ~3. This peak, after accounting for trials, had a probability of arising by chance of 2×10^{-4}. The flux was $(3{\cdot}3\pm1{\cdot}1)\times10^{-12}$ cm^{-2}s^{-1} above 500TeV. The Durham group were operating their TeV detector at Dugway which is near the Fly's Eye detector during July 1983. They saw no evidence of emission during 11 July (Chadwick et al. 1985b).

Further detections at the 1·24s X-ray period were claimed by the Whipple group for E>250GeV (Gorham et al. 1987) and the Haleakala group (Resvanis et al. 1987) for E>300GeV.

In 1988 the Haleakala group reported a burst from Hercules X-1 on 13 May 1986 lasting for 15 minutes (Resvanis et al. 1988). The events were observed to be phase modulated with a period of $1{\cdot}23593\pm0{\cdot}00018$s. This is significantly lower (by 0·15%) than the value of the period predicted by the X-ray ephemeris (see Figure 6·1a). Serious doubt would have been cast on this result if it were not for similar claims made by two

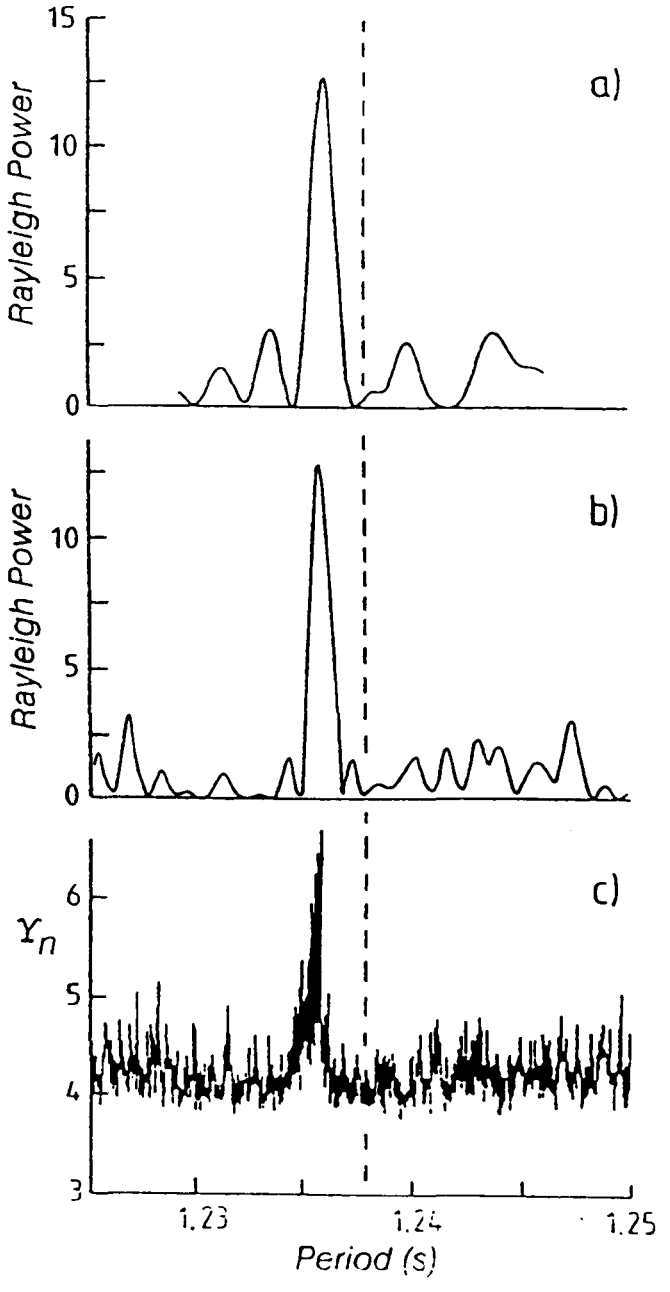

Figure 6·1 The anomalous phase distribution of events from Hercules X-1. The most probable periods around 1·24s are shown from observations made by Haleakala (a), Whipple (b) and Los Alamos (c) groups. The X-ray period is shown by the dotted line. Taken from Protheroe (1987).

other groups. Lamb et al. (1988) reported a 25 minute burst recorded using the Whipple telescope on 11 June 1986. The most favourable period found was 1·23579s with a probability of occurring by chance of 1% (Figure 6·1b). The CYGNUS group reported two bursts (with E>50TeV) on 24 July 1986 (Dingus et al. 1988a). A period of 1·23568s was found with a chance probability of occurring from random fluctuations of $2x10^{-5}$ (Figure 6·1c). The CYGNUS group also found that the muon content of the burst showers was on average higher than for background showers.

6·2 c) AM Herculis

AM Herculis is a cataclysmic variable system comprising of a magnetised white dwarf accreting matter from a Roche lobe-filling, late type main sequence star. A 3·1hr periodicity is observed in the optical and X-ray regions with measurements of polarised light shower a weak inter-pulse (Piirola et al. 1985).

AM Herculis was observed at TeV energies with one bank of the Gulmarg gamma-ray telescope in April-July 1987 (Bhat et al. 1991). When the data from 50 hours of observations were phase analysed to search for the 3·1hr periodicity two broad peaks were seen at phases (0·1±0·2) and (0·6±0·2) with the peak at 0·1 being larger. The shape of the TeV light curve closely matched the shape and phase modulation of the polarised light curve.

The cataclysmic variable AE Aqr, visible from the Southern hemisphere has been observed by the Potchefstroom group (Brink et al. 1990). They report a detection of this object, which is similar to AM Herculis, at the 1% chance level.

6·2 d) 2CG 135+01

After the publication of the COS-B catalogue of high energy (E>100MeV) gamma-ray sources (Hermsen et al. 1977) an attempt was made to identify the sources with known astronomical objects at other wavelengths. Unambiguous identification is rendered difficult by the low angular resolution of COS-B in comparison with

observations at longer wavelengths. One of the COS-B sources that has aroused a large amount of interest at a wide variety of energies is 2CG 135+01.

The main candidate put forward as the counterpart to this source is the binary system LSI +61°303. It was first discovered as a highly variable radio source at a distance of 2.3kpc (Gregory and Taylor 1978). A 26·496 day period was discovered for the radio outbursts with the amplitude of the bursts being modulated with a 1458 day period (Gregory et al. 1989). The radio source was identified with an optical object LSI +61°303 which spectrographic measurements show to be a B0 type star with a high rotational velocity undergoing mass loss through an equatorial disk (Hutchings and Crampton 1981). An observation was made in soft X-rays (0·2→5·0 keV) by the Einstein observatory with a source being found <1" from the best measured position of LSI +61°303 (Bignami et al. 1981).

Further observations have been made in hard X-rays (260→1230 keV) by Ariel 5 (Coe et al. 1978) and low energy gamma-rays by the balloon borne MISO telescope (Perotti et al. 1980). These experiments suffer from comparatively low resolution and there is no certainty that LSI +61°303 is the source. However, consideration of the Ariel 5 and MISO spectral data suggest that the X-ray and gamma-ray emission is from a common source. No evidence for the 26·496 day periodicity has been found in the optical or COS-B data although the scarcity of COS-B events makes a period search difficult. Also, the two Einstein X-ray measurements were made at phase 0·4 and 0·6 of the radio period and show no appreciable difference in flux, whereas the radio activity at these two phases is very different.

The Kiel group performed an all-sky survey on their data recorded from March 1976 to January 1980 (Samorski and Stamm 1984). One of the most significant excesses was observed at $\delta = 61{\cdot}1^\circ$ and $\alpha = 36{\cdot}2^\circ$ which is within the 1° error box of 2CG 135+01. The effect is of low significance when the number of points on the sky looked at taken into account so the association is only tentative.

The CYGNUS group have looked for steady emission of PeV gamma-rays

between April 1986 and November 1990 at three points in the region of 2CG 135+01, including the Kiel position and the centre of the COS-B error box (Lu et al. 1990). There is no evidence of emission from any of the three positions.

6·2 e) 4U 2129+47

4U 2129+47 is thought to be a 5·2hr X-ray binary. It is similar to Hercules X-1 in that the optical modulation is rather large (1·5 magnitudes) and the neutron star is of low mass (Garcia et al. 1989). In 1983 the X-ray flux and large optical variations ceased and the object has since been in an 'off' state in a manner similar to that observed in optical records of Hercules X-1 (Pietsch et al. 1986). Garcia et al. (1989) suggest that there is some evidence for 4U 2129+47 being a triple system with a third object orbiting the close binary system with a period of ~30 days. They also predict that if the on/off states are periodic then the system should have switched on in around January 1989.

6·2 f) Crab Nebula and Pulsar (PSR 0531+21)

The Crab pulsar lies at the centre of the Crab nebula, a SNR 937 years old. The pulsar, with a period of 33ms, is one of the fastest known. This periodicity is seen in radio, optical, X-ray and 100MeV gamma-ray energies with a main pulse and a weaker interpulse separated by ~0·5 of a cycle (see Weekes 1988 for a review). The emission from the nebula is thought to be due to synchrotron radiation from electrons with energies up to 1TeV. These electrons are probably accelerated in the region of the pulsar. Owing to the poor resolution of TeV and PeV telescopes there is no way of separating the nebula and pulsar spatially and so the 33ms period is used.

At TeV energies claims have been made for both steady and transient emission from the pulsar. The Durham group in 1981 (Gibson et al. 1982) and the Tata group in 1985 (Bhat et al. 1986b) saw emission on time scales of less than 15 minutes. Steady emission was observed by the Durham group in 1982-83 (Dowthwaithe et al. 1984b) and the University of California group (Tümer et al. 1985) in autumn 1984. In all cases

where the absolute phase is known the peak in emission is seen at the radio peak, although the width of the TeV peak varies between <0·4ms to 13ms depending on the group making the claim.

One of the most impressive observations of any source at TeV energies is that of the Whipple group's detection of the Crab nebula. Data collected in 1988-89 showed a raw 5·1σ excess (Vacanti et al. 1991). A method had been developed, following extensive simulations, of using the differences in the shape of the Čerenkov images of gamma-ray and proton initiated showers to reject a large part of the hadronic background. Using this method 97% of events were rejected and an excess of 20σ was seen from the direction of the nebula. No evidence was found for the pulsar 33ms periodicity and so it was assumed that the emission emanated from the nebula.

At PeV energies one of the most interesting observations of the Crab nebula/pulsar is that of a transient burst on 23 February 1989. The Tata, Baksan and Gran-Sasso groups all claimed to have observed the burst, which appears to have lasted ~8hr (Fegan 1990). Individually the claims are not particularly significant, but the overall chance probability of the three groups observing an effect has been put at 10^{-6}. The HEGRA group, observing later on the same day, failed to observe any enhanced emission.

6·2 g) M92

Globular clusters are observed to contain large numbers of compact X-ray binaries (Grindlay 1984). M92 is a relatively close cluster at 7·9kpc and at a declination of +43° it is easily observable with the GREX array.

6·2 h) PSR 0355+54

PSR 0355+54 is an old (~one million years), isolated, radio pulsar with a period of 156ms. Although generally stable, the pulsar underwent a timing glitch in 1986 in which the period changed by 1 part in 2×10^5, the largest jump recorded for any pulsar

(Lyne 1987).

The Tata group observed PSR 0355+54 in mid December 1987 with the air-Čerenkov telescope at Pachmarhi, India. When phase analysed with the 156ms period a 4·7σ excess was seen at phase 0·5 with a $3x10^{-4}$ probability of occurring by chance. The main radio peak is seen at phase 0·0. Further data recorded between October 1989 and January 1990 failed to provide evidence for either pulsed or steady emission (Acharya et al. 1990). The Whipple group searched for PSR 0355+54 in September to December 1989 and produced upper limits to the flux consistent with those of the Tata group for the same period (Lamb et al. 1990).

At PeV energies the CYGNUS group find no evidence of continual emission from PSR 0355+54 in their data recorded between April 1986 and November 1990 (Lu et al. 1990).

6·3 Search for Steady Emission from 8 Candidate Sources

The GREX data set was searched for evidence of steady emission from each of the 8 candidate sources described above. The method used was that described in section 4·7a with both the azimuthal and equal exposure methods being utilised. The bin sizes in each search were those given in Table 4·1, with the exception of the right ascension half width ($\Delta\alpha$) which is given by:-

$$\Delta\alpha = \Delta\delta / \cos\delta$$

where $\Delta\delta$ is the declination half width (from Table 4·1) and δ is the candidate source declination.

Only the equal exposure method was used for PSR 0355+54 as it passes too close to the zenith to be analysed with the azimuthal method. If the angular distance between the source position and the zenith is less than the bin radius the background area in the

azimuthal method goes to zero. This leads to a systematic underestimate of the background.

Owing to the fact that there is no unambiguous association between the COS-B source 2CG 135+01, the Kiel source and the star LSI +61°303 two regions of this area of sky have been investigated. One (A), centred on $\alpha = 39{\cdot}0^{\circ}$, $\delta = 61{\cdot}0^{\circ}$ (1950), takes in LSI +61°303, which, with it its radio variability and X-ray flux has many properties in common with X-ray binaries, and the other (B), centred on $\alpha = 36{\cdot}0^{\circ}$, $\delta = 61{\cdot}0^{\circ}$ (1950), which covers the Kiel region. Owing to the closeness in right ascension of the two points upon which the searches are centred and the angular resolution of the GREX array there will be showers that fall within the on-source bin for each point and so the searches are not totally independent.

Source	Total observation time, Hours	Azimuthal method			Equal exposure method		
		on	off	σ	on	off	σ
1E 2259+586	15304	8354	8133	+2·45	8311	8163	+1·54
Hercules X-1	9947	3912	3967	-1·34	3950	4019	-1·03
AM Herculis	13653	7355	7352	+0·04	7383	7349	+0·37
2CG 135+01 (A)	15298	7684	7796	-1·26	7738	7831	-0·99
2CG 135+01 (B)	15325	7883	7800	+0·94	7914	7824	+0·96
4U 2129+47	13617	7281	7286	-0·06	7226	7313	-0·96
Crab	6056	1088	1053	+1·09	1090	1087	+0·09
M92	12208	5953	5933	+0·27	5937	5931	+0·07
PSR 0355+54	14010	---	---	---	7481	7454	+0·29

Table 6·1 The cumulative on-source counts and background estimates for 8 candidate sources searched for in the GREX data set. For each source both the azimuthal and equal exposure search methods have been used (with the exception of PSR 0355+54).

Table 6·1 shows the cumulative on-source counts and background estimates for each of the sources. The lack of significant differences between the background estimates derived from the two search methods suggests that any systematic errors in the azimuthal method have been reduced to a tolerable level. Figure 6·2 shows the cumulative excess as a function of time for two of the candidate sources. 1E 2259+586, the source which has the largest final cumulative excess is shown in a) and Hercules X-1 is shown in b).

As can be seen from Table 6·1 there is no evidence for continuous emission from any of the candidate sources. For this reason upper limits to the flux from each of the objects for energies greater than $4x10^{14}$eV have been calculated using the methods described in section 4·7b. Table 6·2 shows these upper limits. The upper limit derived for Cygnus X-3 has been included for comparison.

Source	On-source count	Mean off-source count	Protheroe factor	S_{95}	Flux ($cm^{-2}s^{-1}$)
1E 2259+586	8311	8163	3·3	298·2	3.38×10^{-14}
Hercules X-1	3950	4019	1·5	95·1	1.74×10^{-14}
AM Herculis	7383	7349	2·4	205·7	2.63×10^{-14}
2CG 135+01 (A)	7738	7831	1·5	132·7	1.54×10^{-14}
2CG 135+01 (B)	7914	7824	2·8	256·6	2.99×10^{-14}
4U 2129+47	7226	7313	1·5	128·3	1.64×10^{-14}
Crab	1090	1087	2·3	75·8	2.44×10^{-14}
M92	5937	5931	2·2	169·4	2.17×10^{-14}
PSR 0355+54	7481	7454	2·5	215·8	1.64×10^{-14}
Cygnus X-3	5450	5474	1·8	133·2	1.93×10^{-14}

Table 6·2 The 95% confidence upper limits to the integral flux above an energy of $4x10^{14}$eV for the 8 candidate sources studied. Cygnus X-3 is included for comparison (see Chapter 4).

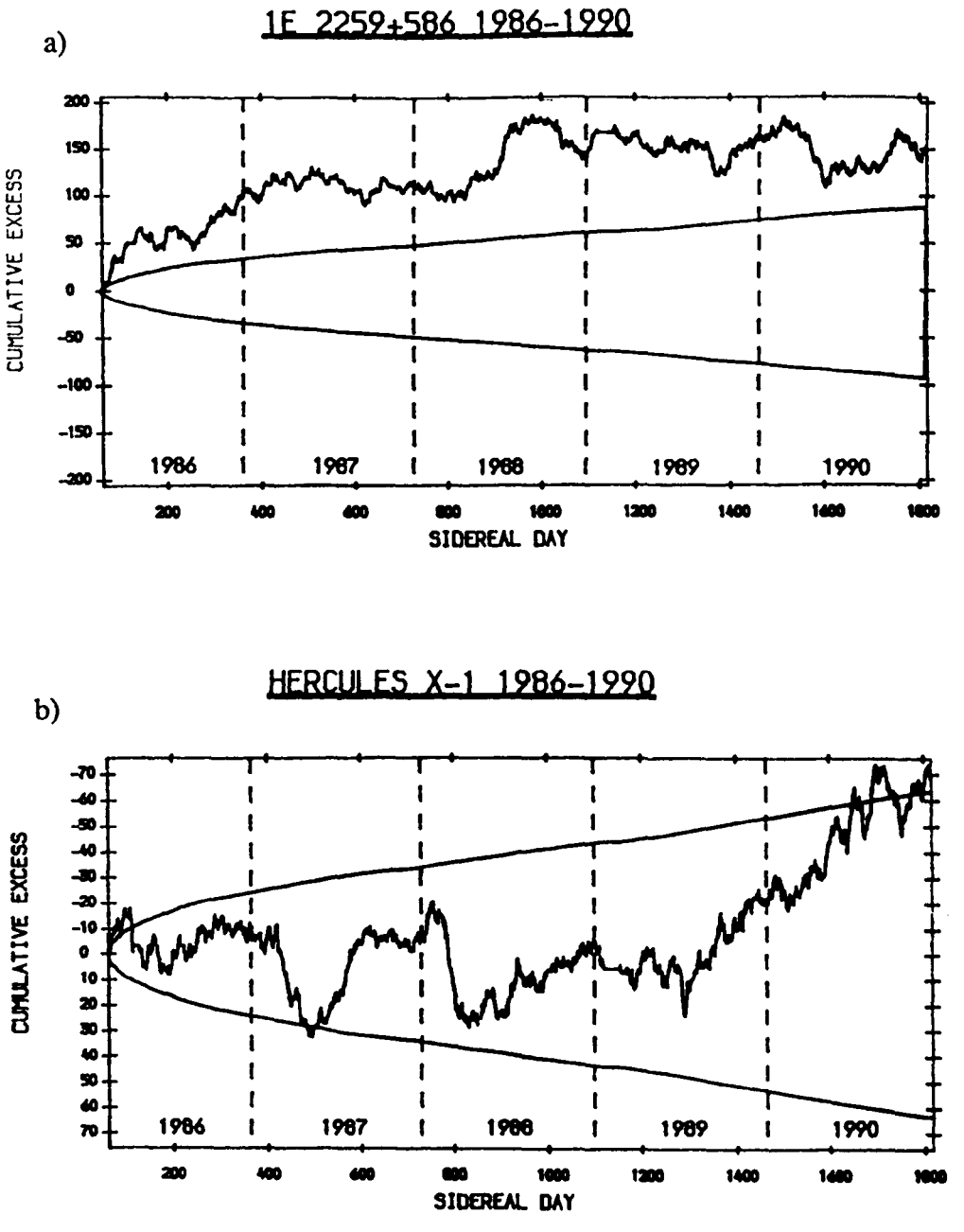

Figure 6·2 The cumulative excess number of events recorded by the GREX array as a function of time for two typical candidate sources. 1E 2259+586 is shown in a) and Hercules X-1 in b). Day 0 corresponds to Jan 0·0 1986. The $\pm 1\sigma$ levels are shown.

6·4 Phase Modulated Emission

Some of the candidate sources looked at have periodicities associated with them. Specifically, the 1·7d period of Hercules X-1, 3·1hr period of AM Herculis and the 5·2hr period of 4U 2129+47 are thought to be the orbital periods of binary systems in which one of the stars is a compact object (e.g. white dwarf of neutron star). These periodicities have been searched for using the methods described in section 4·7c. The ephemerides used were those of Deeter et al. (1981) for Hercules X-1, Priedhorsky et al. (1978) for AM Herculis and McClintock et al. (1982) for 4U 2129+47. The phasograms for these objects are given in Figures 6·3, 6·4 and 6·5 respectively. There is no evidence for phase modulated emission. The Gulmarg group claim to have detected pulsed emission from AM Herculis at TeV energies in April-July 1987 (Bhat et al. 1991). During this period the GREX array observed 367 events from the direction of AM Herculis when 376·7 were expected from the background estimate. When phase analysed with the 3·1hr period these events show no evidence of phase modulation.

The 26·496 day period of the radio object LSI +61°303 (associated with 2CG 135+01) is also thought to be due to the orbit of a binary system. Of the two regions in the area of 2CG 135+01 searched for it is region A which contains LSI +61°303. Figure 6·6 shows the 26·496d phase analysis of events in the bin containing LSI +61°303. Owing to the large period the background estimates are not as uniform as is the case for searches on time scales of a few hours. After correcting for the variations in the background estimates the amplitude of the first harmonic of the distribution is 0·3%.

6·5 Search for Sporadic Emission

As described in section 6·2f three extensive air shower array groups claimed to have detected a burst from the Crab nebula/pulsar on 23 February 1989. At the time of

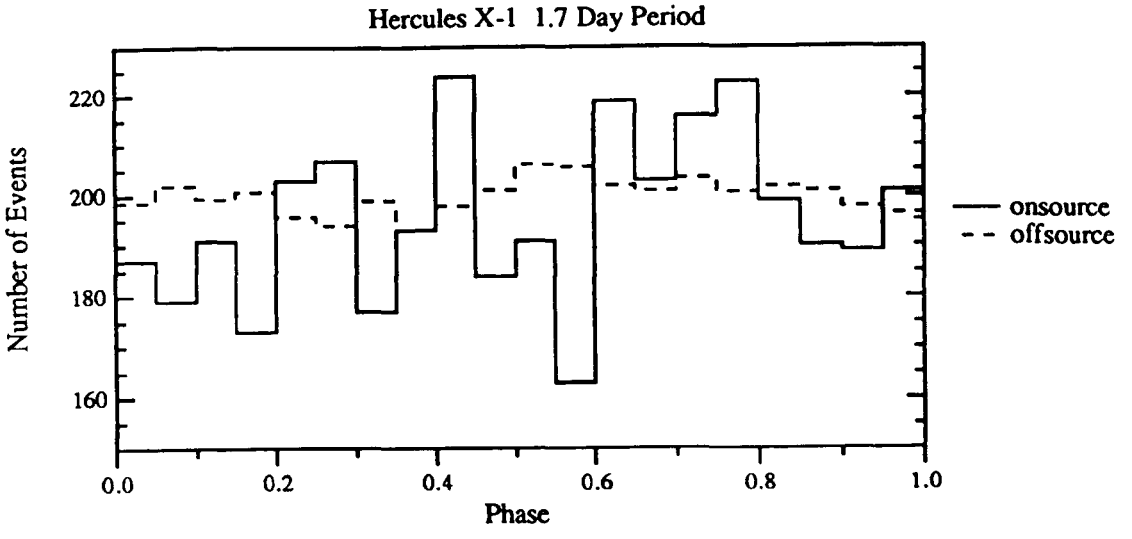

Figure 6·3 1·7 day phasogram of all events recorded by the GREX array from the direction of Hercules X-1. The ephemeris used is that of Deeter et al. (1981). The background estimate (dotted line) is derived from the azimuthal method.

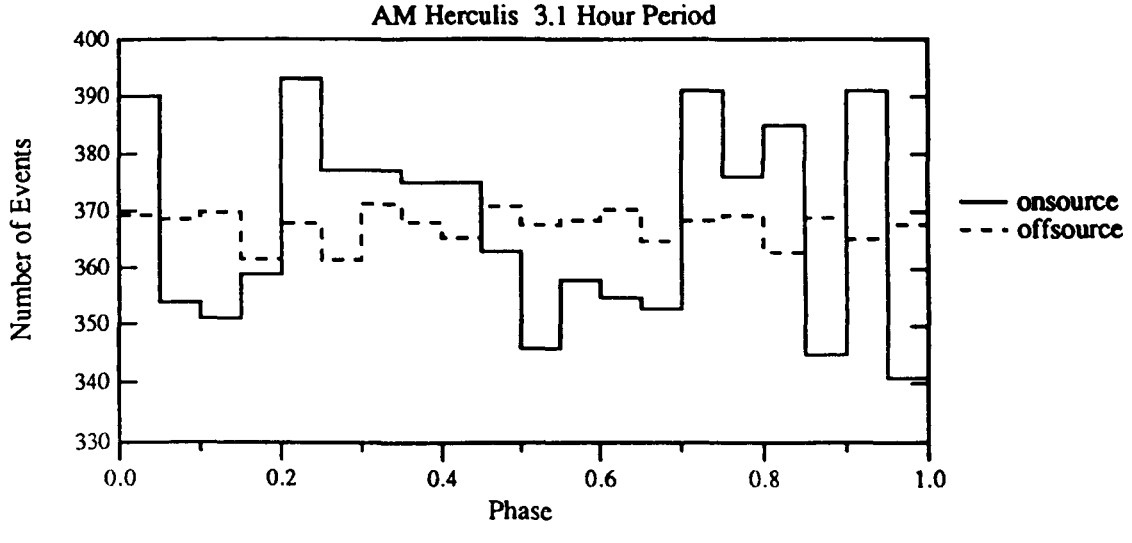

Figure 6·4 3·1hr phasogram of all events recorded by the GREX array from the direction of AM Herculis. The ephemeris used is that of Priedhosky et al. (1978). The background estimate (dotted line) is derived from the azimuthal method.

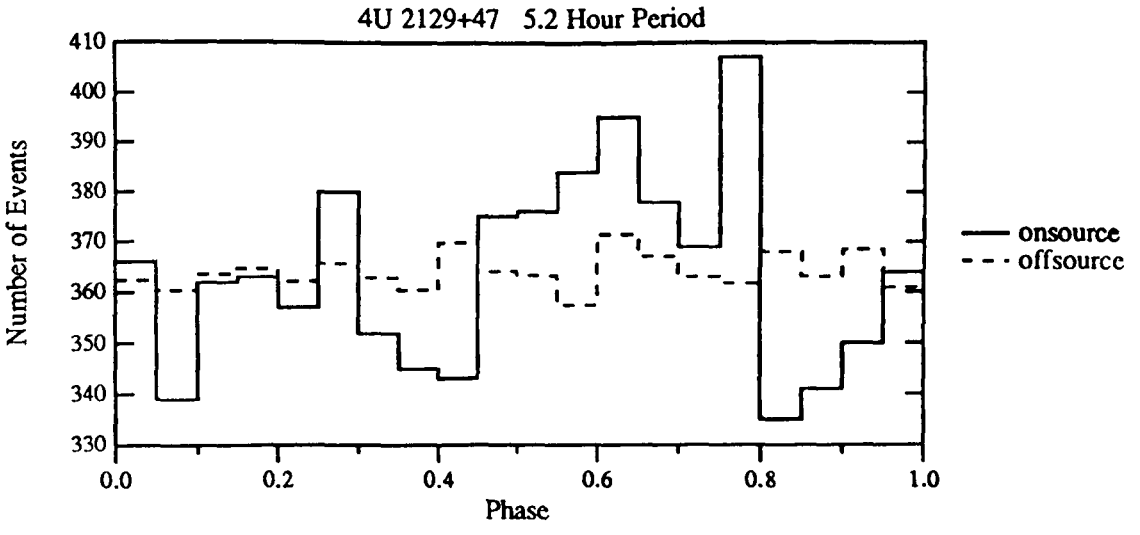

Figure 6·5 5·2hr phasogram of all events recorded by the GREX array from the direction of 4U 2129+47. The ephemeris used is that of McClintock et al. (1982). The background estimate (dotted line) is derived from the azimuthal method.

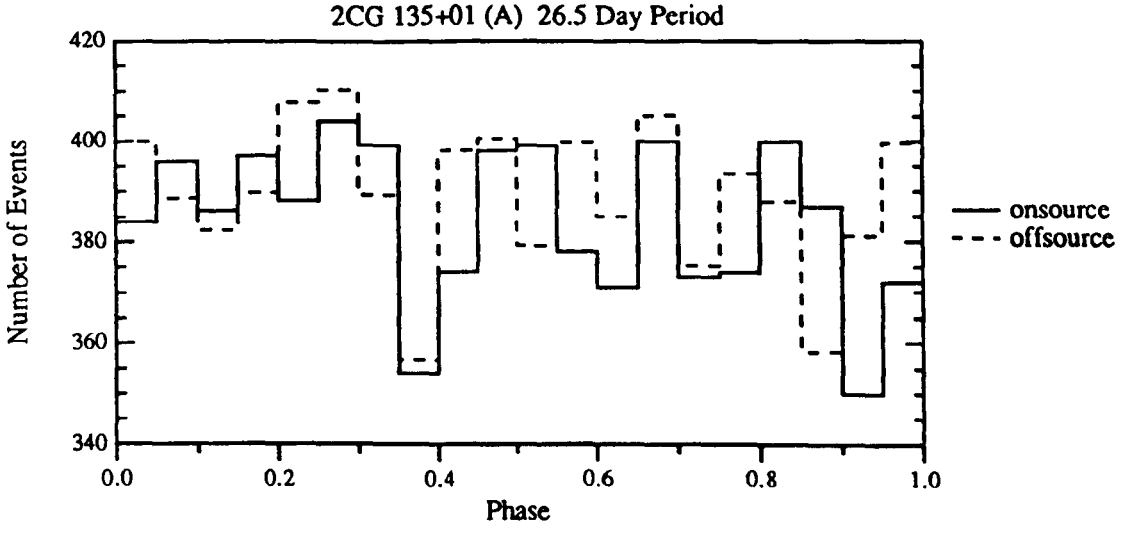

Figure 6·6 26·496 day phasogram of all events recorded by the GREX array from the direction of 2CG 135+01 (A). The ephemeris used is that of Gregory et al. (1989). The background estimate (dotted line) is derived from the azimuthal method.

the EAS-Top array observations the Crab, as seen at Haverah Park, was rising in the sky. Unfortunately, during February 1989 the GREX array control system underwent a major change and testing resulted in the array being off for long periods. No data were recorded during the Crab transit of 23 February and so no information on the possible burst is available.

On a day-by-day basis the observed distribution of excess counts (i.e. number on-source - mean background from the azimuthal method) is entirely consistent with Poissonian statistics. The most significant daily excess seen for any source is 14 on-source when 3·96 were expected for 4U 2129+47 on 1 August 1988. The probability of observing 14 or more events when 3·96 are expected is 8×10^{-5}. However, this is not significant when the number of days and sources looked at are considered.

The problems in searching large data sets for sporadic emission of unknown duration were described in section 4·7d. Also described was a method developed by J. Lloyd-Evans in an attempt to avoid these problems. The proposed method consists of splitting the data set in two and searching for sporadic emission over varying time scales in one of the halves. A candidate period of time is one in which a significant excess number of on-source events is seen compared to the background estimate (i.e. the probability of the excess occurring by chance is less than 5%). These candidate periods are then searched for in the other half of the data. Any signal from a source should be split roughly equally into the two halves and so an excess seen in one half will be seen in the second. Two candidate periods were found. In the first, 28 June 1986 to 10 March 1987, 557 events were observed from 1E 2259+586 when 480 were expected. When the blind data set was examined 482 events were seen on-source with a background of 481. In the second candidate period, 1-4 December 1988, 14 events were seen from M92 on a background of 3·21. The blind set had 2 events on 3·00. In both cases the excesses from the second data set fail to confirm those of the first data set.

6·6 All-Sky Survey

Groups working at TeV and PeV energies have claimed to detect signals from many astronomical objects. These claims have led to evidence being sought in the GREX data set for emission of PeV gamma-rays from Cygnus X-3 and the objects described in this chapter. No such evidence has been found. However, it is possible that objects that have not as yet been looked at are emitting PeV gamma-rays. To search for unknown emitters an all-sky survey has been performed.

Any all-sky survey will involve looking at a large number of regions in the sky. This means that a correspondingly large number of statistical trials are invoked and so increases the minimum signal strength required for a source to stand out. To try and reduce the number of trials the search was, initially, restricted to the galactic plane. The all pervasive 3K background radiation attenuates PeV gamma-rays (at 2·5PeV the attenuation length is ~7kpc) and so extra-galactic sources cannot be observed. The vast majority of claimed sources lie on the galactic plane (the major exception is Hercules X-1) and so the galactic plane is probably the richest region of unknown sources.

The terrestrial latitude of the GREX array and the condition that only events with zenith angles less than 40° are used result in a strip of the galactic plane with galactic longitude greater than 50° and less than 200° being visible. The exposure of the array to each part of this strip varies greatly along the strip. The simplest possible search method was employed. The sky was split into declination strips of width 2·24°. Each strip was then divided into bins where the right ascension length of the bin was given by:-

$$2{\cdot}24 / \cos\delta$$

(δ being the centre declination of the strip). If the centre of a bin was within 3° of the galactic plane then the bin was (a priori) considered a bin of interest. For each

declination strip the background estimate was obtained from the bins that were not on-source. The right ascension coverage of the GREX array is not uniform and so the background estimates must be corrected. This was done in a similar way to that described in section 3·4a for the azimuthal search method. The first and second harmonics of the right ascension distributions were calculated and then each event corrected so that the distribution becomes uniform.

Using this method the bin boundaries are placed arbitrarily and it is possible that a source could fall on the boundary of two or more bins and so be missed. For this reason the above procedure is performed three times with the bins shifted in declination and right ascension by a third of a bin size after each search. The three searches gave a total of 602 on-source bins. The distribution of significance of the excess in these bins is given in Figure 6·7a. The most significant excess observed (8661 on a background of 8388 at $\alpha = 2^{\circ}$, $\delta = 62^{\circ}$) has a probability of occurring in one of 602 bins of ~40%.

As there was no evidence for an unknown steady emitter lying on the galactic plane the search was extended to the entire sky above $\delta = 10^{\circ}$. The significances of the excesses observed in the 10485 bins are shown in Figure 6·7b. Once again there is no evidence for any bin having an excess number of counts inconsistent with statistical fluctuations.

6·7 Conclusions

In the mid 1980's there were many unanswered questions and problems regarding PeV gamma-ray astronomy. Were there many sources like Cygnus X-3? Was Cygnus X-3 variable? The lateral distribution (i.e. the age) and muon content of signal showers differed depending on the group making the observation and in many cases differed from what was expected of gamma-ray initiated showers. A large amount of effort was put into answering these questions and reconciling the differences. Instruments were built that had much improved sensitivity compared to the instruments

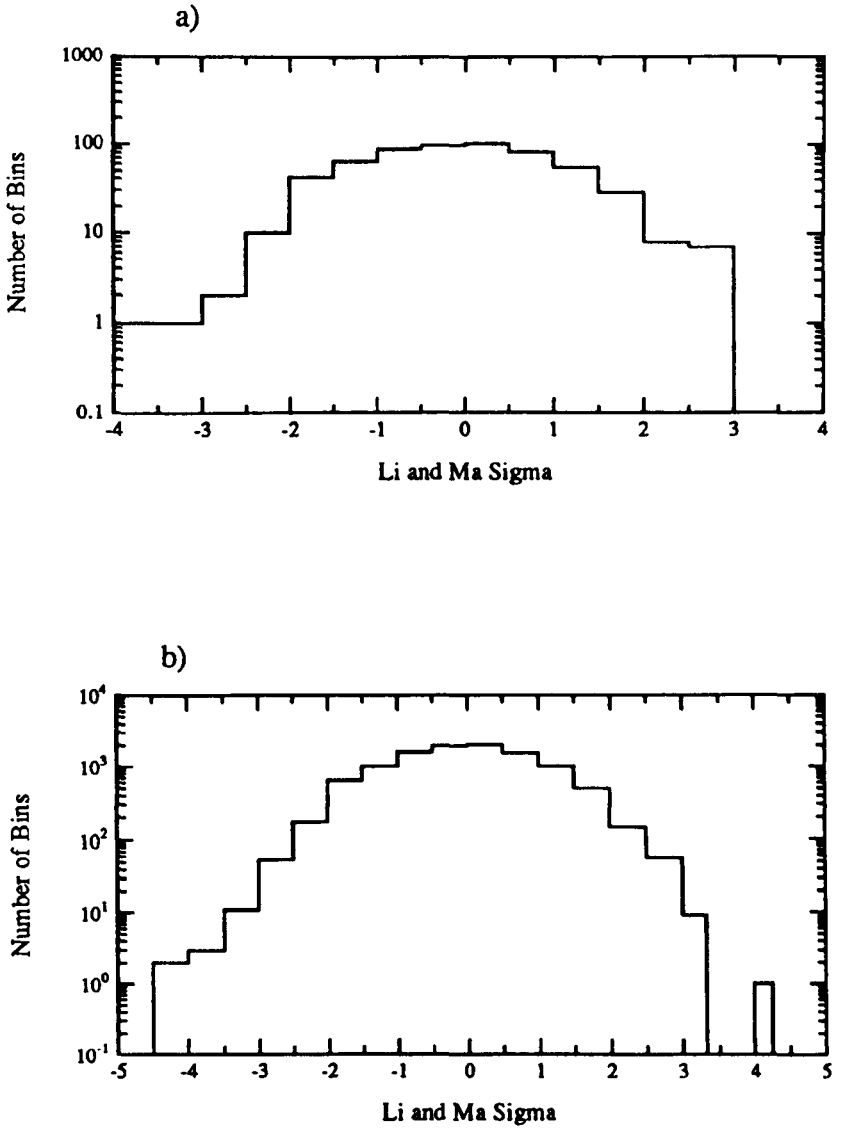

Figure 6·7 The distribution of excesses observed in a survey for unknown point sources. The distribution for 602 bins along the galactic plane is shown in a) and for 10485 bins over the whole sky (d>10°) in b).

with which the original detections of Cygnus X-3 had been made. However, there are still no definite answers to the questions posed above.

The GREX array was commissioned in March 1986 and was one of the first instruments purpose built for detecting point sources of PeV gamma-rays. The high efficiency with which it has been operated has resulted in a large data set being amassed. Chapter 4 showed that there was no evidence in this data set for the emission of PeV gamma-rays from Cygnus X-3. This chapter has shown that there is in fact no evidence for emission from any region of the sky visible at the latitude of GREX (δ>+10°). This is very much in agreement with observations made by other groups as there has been no overwhelmingly statistically significant observation of any Northern hemisphere object in the past 5 years.

REFERENCES

Acharya B.S. et al. (1990), Proc. Int. Conf. on High Energy Gamma Ray Astron., (Ann Arbor), p87

Aglietta M. et al. (1990), Proc. 21st ICRC (Adelaide), 9, 388

Alexandreas D.E. et al. (1991a), Proc. 22nd ICRC (Dublin), OG 10-4-4

Alexandreas D.E. et al (1991b), Submitted to Ap. J. Letts.

Alexeenko V. et al. (1985), Proc. 19th ICRC (La Jolla), 1, 91

Alexeenko V. et al. (1987a), Proc. 20th ICRC (Moscow), 1, 229

Alexeenko V. et al. (1987b), Proc. 20th ICRC (Moscow), 1, 219

Aller H.D. and Hodge P.E. (1972), Nature: Phys. Sci., 245, 40

Alvarez L.W. and Compton A.H. (1933), Phys. Rev., 43, 835

Andrews D. et al. (1971), Proc. 12th ICRC (Hobart), 3, 995

Auger P. et al. (1939), Rev. Mod. Phys., 11, 288

Baltrusaitis R.M. et al. (1985a), Ap. J., 297, 145

Baltrusaitis R.M. et al. (1985b), Ap. J., 293, L69

Baltrusaitis R.M. et al. (1987), Ap. J., 323, 685

Barley S.K. et al. (1990), Proc. 21st ICRC (Adelaide), 2, 43

Battistoni G. et al. (1985), Phys. Letts., 155B, No. 5+6, 465

Beaman J. et al. (1991), Proc. 22nd ICRC (Dublin), OG 4-6-2

Becklin E.E et al. (1974), Ap. J., 192, L119

Berger C. et al. (1986), Phys. Letts. B, 174, No. 1, 118

Bhat C.L. et al. (1986a), Ap. J., 306, 587

Bhat C.L. et al. (1990), Proc. 21st ICRC (Adelaide), 2, 10

Bhat C.L. et al. (1991), Ap. J., 369, 475

Bhat P.N. et al. (1986b), Nature, 319, 127

Bignami G.F. et al. (1981), Ap. J., 247, L85

Blake P. et al. (1967), Proc. 10th ICRC (Calgary), Can. J. Phys., 46, No. 10, Part 2, 782

Bloomer S.D. et al. (1990a), Proc. 21st ICRC (Adelaide), 4, 314

Bloomer S.D. et al. (1990b), Proc. 21st ICRC (Adelaide), 4, 326

Bloomer S.D. (1990), Ph.D. Thesis, Leeds University

Bonnet-Bidaud J.M. and van der Klis M. (1985), Cataclysmic Variables and Low-Mass X-Ray Binaries, Eds. Lamb D.Q. and Patterson J.R. (Reidel), p147

Bonnet-Bidaud J.M. and Chardin G. (1988), Phys. Rep., 170, No. 6, 375

Braes L.L.E. and Miley G.K. (1972), Nature, 237, 506

Brazier K.T.S. et al. (1990a), Ap. J., 350, 745

Brazier K.T.S. et al. (1990b), Proc 21st ICRC (Adelaide), 2, 379

Brink C. et al. (1990), Proc. 21st ICRC (Adelaide), 2, 283

Brinkmann A. et al. (1972), IAU Circ., No. 2446

Brooke G. et al. (1985), Proc. 19th ICRC (La Jolla), 3, 426

Cassiday G.L. et al. (1989), Phys. Rev. Letts., 62, No. 4, 383

Cassiday G.L. et al. (1990), Proc. 21th ICRC (Adelaide), 2, 60

Catalano O. and Linsley J. (1991), Private communication

Cawley M.F. et al. (1985), Ap. J., 296, 185

Cawley M.F. et al. (1991), Astron. Astrophys., 243, 143

Chadwick P.M. et al. (1985a), Nature, 318, 642

Chadwick P.M. et al. (1985b), Proc. 19th ICRC (La Jolla), 1, 251

Chan J.K.W. et al. (1990), Proc. 21st ICRC (Adelaide), 4, 322

Chanmugam G. and Brecher K. (1985), Nature, 313, 767

Chardin G. and Gerbier G. (1989), Astron. Astrophys., 210, 52

Chi X. et al. (1991), Proc. ICCR Int. Symp. on 'Astrophysical Aspects of the Most Energetic Comic Rays' (Kofu), p140

Ciampa D. et al. (1990), Proc. 21st ICRC (Adelaide), 2, 35

Clark G.W. (1957), Phys. Rev., 108, 450

Clay J. (1932), Proc. Roy. Acad. Amsterdam, 35, 1282

Coe M.J. et al. (1978), Nature, 274, 343

Compton A.H. (1932), Phys. Rev., 41, 681

Corbató S.C. et al. (1990), Proc. 21st ICRC (Adelaide), 9, 398

Craig M.A.R. et al. (1979), Proc. 16th ICRC (Kyoto), 8, 180

Danaher S. et al. (1981), Nature, 289, 568

Deeter J.E. et al. (1981), Ap. J., 247, 1003

Dennis B.R. (1964), Ph.D. Thesis, University of Leeds

Dingus B.L. et al. (1988a), Phys. Rev. Letts., 61, No. 17, 1906

Dingus B.L. et al. (1988b), Phys. Rev. Letts., 60, No. 18, 1785

Dowthwaite J.C. et al. (1983), Astron. Astrophys., 126, 1

Dowthwaite J.C. et al. (1984a), Nature, 309, 691

Dowthwaite J.C. et al. (1984b), Ap. J., 286, L35

Eames P.J.V. et al. (1987a), Very High Energy Gamma-Ray Astronomy, Ed. Turver K.E., (Reidel), p179

Eames P.J.V. et al. (1987b), Proc. 19th ICRC (La Jolla), 2, 254

Earnshaw J.C. et al. (1968), Can. J. Phys., 46, S122

Elsner R.F. et al. (1980), Ap. J., 239, 335

Fahlman G.G. and Gregory P.C. (1981), Nature, 293, 202

Fahlman G.G. and Gregory P.C. (1983), IAU Symp. No. 101, (Reidel), p445

Fahlman G.G. et al. (1982), Ap. J., 261, L1

Fegan D.J. and Danaher S. (1981), Proc. 17th ICRC (Paris), 1, 31

Fegan D.J. et al. (1989), Astron. Astrophys., 211, L1

Fegan D.J. (1990), Proc. 21st ICRC (Adelaide), 11, 23

Fichtel C.E. et al. (1975), Proc. 14th ICRC (Munich), 1, 106

Fichtel C.E. et al. (1987), Ap. J., 319, 362

Fomin V.P. et al. (1981), Proc. 17th ICRC (Paris), 1, 28

Galper A.M. et al. (1975), Proc. 14th ICRC (Munich), 1, 95

Garcia R. et al. (1989), Ap. J., 341, L75

Garmston H.J. (1976), Ph.D. Thesis, University of Leeds

Garner J. and Davey P.M. (1985), GREX surveyor report, Dept. of Civil Engineering, Leeds University

Ghosh P. and Lamb F.K. (1979), Ap. J., 234, 296

Giacconi R. et al. (1967), Ap. J., 148, L119

Gibson I.A. et al. (1982), Nature, 296, 833

Gillanders G.H. et al. (1990), Proc. 21st ICRC (Adelaide), 2, 23

Glushkov A.V. et al. (1990), Proc. 21st ICRC (Adelaide), 2, 64

Gorham P.W. et al. (1987), Very High Energy Gamma-Ray Astronomy, Ed. Turver K.E., (Reidel), p125

Gregory A.A. et al. (1990), Astron. Astrophys., 237, L5

Gregory P.C. et al. (1972a), Nature, 239, 440

Gregory P.C. et al. (1972b), Nature: Phys. Sci., 239, 114

Gregory P.C. and Taylor A.R. (1978), Nature, 272, 704

Gregory P.C. and Fahlman G.G. (1980), Nature, 287, 805

Gregory P.C. et al. (1989), Ap. J., 339, 1054

Greisen K. (1956), Progress in Cosmic Ray Physics, Ed. J.G. Wilson, 3, 249 (Amsterdam: North Holland)

Grindlay J.E. (1984), IAU Symp., No. 113, (Reidel), p43

Gupta S.K. et al. (1990), Ap. J., 354, L13

Gupta S.K. and Tonwar S.C. (1991), J. Phys. G., 17, 1271

Hanson C.G. et al. (1988), Astron. Astrophys., 195, 114

Hayashida N. et al. (1991), Proc. 22nd ICRC (Dublin), OG 4·3-20

Hermsen W. et al. (1977), Nature, 269, 494

Hermsen W. et al. (1987), Astron. Astrophys., 175, 141

Hess V.K. (1912), Physik Zeitscher., 13, 1804

Hillas A.M. et al. (1971), Proc. 12th ICRC (Hobart), 3, 1001

Hillas A.M. (1984), Nature, 312, 50

Hillas A.M. (1987a), Proc. 20th ICRC (Moscow), 2, 362

Hillas A.M. (1987b), Very High Energy Gamma-Ray Astronomy,
Ed. Turver K.E., (Reidel), p71

Hjellming R.M. et al. (1972), Nature, 237, 507

Hutchings J.B. and Crampton D. (1981), Publ. Astron. Soc. Pacific, 93, 486

Idenden I.W. (1991), Ph. D. Thesis, Leeds University

Johns K. et al. (1990), Proc. 21st ICRC (Adelaide), 9, 402

Johnson P.A. (1991), Private communication

Johnson T.H. (1933), Phys. Rev., 43, 834

Johnston K.J. et al. (1986), Ap. J., 309, 707

Jones L.W. (1990), Proc. 21th ICRC (Adelaide), 2, 75

Karle A. (1991), Proc. Int. Conf. on High Energy Gamma-ray Astron.,
(Ann Arbor), p127

Kifune T. et al. (1986), Ap. J., 301, 230

Kifune T. et al. (1987), Very High Energy Gamma-Ray Astronomy,
Ed. Turver K.E., (Reidel), p173

Koyama K. et al. (1987), Pub. Astron. Soc. Japan, 39, No. 5, 801

Krimm H.A. et al. (1990), Proc. Int. Conf. on High Energy Gamma Ray Astron.,
(Ann Arbor), p122

Lamb R.C. et al. (1977), Ap. J., 212, L63

Lamb R.C. et al. (1982), Nature, 296, 543

Lamb R.C. et al. (1988), Ap. J., 328, L13

Lamb R.C. et al. (1990), Proc. Int. Conf. on High Energy Gamma Ray Astron.,
(Ann Arbor), 47

Lambert A. et al. (1985), Proc. 19th ICRC (La Jolla), 1, 71

Lambert A. and Lloyd-Evans J. (1985), Proc. 19th ICRC (La Jolla), 3, 449

Lambert A. (1985), Ph.D. Thesis, Leeds University

Lapikens J. (1974), Ph.D. Thesis, University of Leeds

Lawrence M.A. et al. (1989), Phys. Rev. Letts., 63, No. 11, 1121

Lawrence M.A. et al. (1991a), J. Phys. G., 12, 733

Lawrence M.A. et al. (1991b), Proc. 22nd ICRC (Dublin), OG 6·3-7

Li T.P. and Ma Y.Q. (1983), Ap.J., 272, 317

Lloyd-Evans J. et al. (1983), Nature, 305, 784

Lu X-Q. et al. (1990), Proc. Int. Conf. on High Energy Gamma Ray Astron., (Ann Arbor), p105

Lyne A.G. (1987), Nature, 326, 569

Lyons L. (1986), Statistics for Nuclear and Particle Physicists, Cambridge University Press

McClintock J.E. et al. (1982), Ap. J., 258, 245

McKechnie S.P. et al. (1976), Ap. J., 207, L151

Makino F. et al. (1987), IAU Circ., No. 4459

Marshak M.L. et al. (1985), Phys. Rev. Letts., 54, No. 19, 2079

Mason K.O. (1986), Unpublished. Quoted in Weekes T.C. (1988)

Mason K.O. et al. (1986), Ap.J., 309, 700

Middleditch J. and Nelson J. (1976), Ap. J., 208, 567

Middleditch J. et al. (1983), 274, 313

Milgrom M. (1976), Astron. Astrophys., 52, 215

Molnar L.A. et al. (1984), Nature, 310, 662

Morello C. et al. (1983), Proc. 18th ICRC (Bangalore), 1, 127

Morello C. et al. (1990), Il Nuovo Cimento, 13C, 453

Morini M. et al. (1988), Ap. J., 333, 777

Muraki Y. et al. (1991), Ap. J., 373, 657

Neshpor Y.I. et al. (1979), Astrophys. Space Sci., 61, 349

Nishimura J. and Kamata K. (1952), Prog. Theor. Phys., 7, 185

Ong R.A. (1991), Joint Int. Lepton-Photon Symp. and Europhys. Conf. on High Energy Phys., Geneva

Oyama Y. et al (1986), Phys. Rev. Letts., 56, No. 9, 991

Parsignault D. et al. (1972), Nature: Phys. Sci., 239, 123

Parsignault D. et al. (1976), Ap. J., 209, L73

Perotti F. et al. (1980), Ap. J., 239, L49

Petterson J.A. (1977), Ap. J., 218, 783

Pietsch W. et al. (1986), Astron. Astrophys., 157, 23

Piirola V. et al. (1985), Proc. ESA Workshop on Recent Results on Calaclysmic Variables (ESA SP-236), p245

Porter N. (1983), Nature, 305, 179

Priedhorsky W.C. et al. (1978), Ap. J., 225, 542

Pringle J.E. (1974), Nature, 247, 21

Protheroe R.J. (1984), Astron Express, 1, 33

Protheroe R.J. (1987), Proc. 20th ICRC (Moscow), 8, 21

Resvanis L.K. et al. (1987), Very High Energy Gamma-Ray Astronomy, Ed. Turver K.E., (Reidel), p131

Resvanis L.K. et al. (1988), Ap.J., 328, L9

Ruddick K. (1987), Very High Energy Gamma-Ray Astronomy, Ed. Turver K.E., (Reidel), p185

Samorski M. and Stamm W. (1983a), Ap. J., 268, L17

Samorski M. and Stamm W. (1983b), Proc. 18th ICRC (Bangalore), 11, 244

Samorski M. and Stamm W. (1984), Ap. J., 277, 897

Sandford P.W. and Hawkins F.H. (1972), Nature: Phys. Sci., 239, 135

Schönfelder V. (1990), Proc. 21st (Adelaide), 12, 177

Schreier E. et al. (1972), Ap. J., 172, L79

Sinha S. et al. (1990), Proc. 21st ICRC (Adelaide), 2, 51

Spenser M.B. (1990), M.Sc. Thesis, Auckland University

Spencer R.E. et al. (1986), Ap. J., 309, 694

Stanev T. et al. (1985), Proc. 19th ICRC (La Jolla), 7, 219

Tananbaum H. et al. (1972), Ap. J., 174, L143

Teshima M. et al. (1990), Phys. Rev. Letts., 64, No.14, 1628

Tonwar S.C. et al. (1988), Ap. J., 330, L107

Tümer O.T. et al. (1985), Proc. 19th ICRC (La Jolla), 1, 139

Vacanti G. et al. (1991), Ap. J., 377, 467

Van der Klis M. and Bonnet-Bidaud J.M. (1981), Astron. Astrophys., 95, L5

Van der Klis M. and Bonnet-Bidaud J.M. (1989), Astron. Astrophys., 214, 203

Vestrand W.T. and Eichler D. (1982), Ap. J., 261, 251

Vladimirsky B.M. et al. (1973), Proc. 13th ICRC (Denver), 1, 456

Wagner R.M. et al. (1989), Ap. J., 346, 971

Walker A. et al. (1991), Nucl. Instr. and Meth., A301, 574

Waltman E.B. et al. (1989a), IAU Circ., No. 4798

Waltman E.B. et al. (1989b), IAU Circ., No. 4817

Waltman E.B. et al. (1990), IAU Circ., No. 5075

Weekes T.C. et al. (1981), Astron. Astrophys., 104, L6

Weekes T.C. and Geary J.C. (1982), Publ. Astron. Soc. Pac., 94, 708

Weekes T.C. (1988), Phys. Rep., 160, No. 1+2, 1

West A.A. (1988), Ph.D. Thesis, Leeds University

White N.E. and Holt S.S. (1982), Ap. J., 257, 318

Wilson R.W. and Bolton J.G. (1960), Publ. Astron. Soc. Pac., 72, 231

ACKNOWLEDGEMENTS

I owe the fact that this thesis has been written at all and that I have enjoyed working on it so much to a great many people. Firstly, none of the preceding work would have been possible without the guidance, enthusiasm, insistence and (mainly constructive) criticism of my supervisor, Alan Watson. I am grateful for the time and energy that he has spent working with me during my studentship. Over the last three years I have received a large amount of help from members of the Haverah Park group. Without exception everybody has been willing to take the time to share their knowledge and expertise with me. Three people who have been especially helpful are doctors Mark Lawrence, Steve Bloomer and Jeremy Lloyd-Evans.

The thing I will remember most of my time as a postgraduate student is the friendship shown to me by people both within the group and the Physics department as a whole. I couldn't have hoped to work with a better group of people and shall miss Friday nights in the Fenton, morning coffee time and terminal room banter (although I won't miss spending nights in Welsh puddles!).

I acknowledge the basic grant provided by the SERC.

Finally, I would like to thank my parents and my sister Caroline. Despite not always knowing what I was doing or why I was doing it they have been a constant source of encouragement and support. I dedicate this thesis to them with my love.